AST4-CT-2005-012282

LAPCAT

Long-Term Advanced Propulsion Concepts and Technologies

SPECIFIC TARGETED RESEARCH PROJECT

Thematic Priority – 1.4
AERONAUTIC and SPACE

Publishable Final Activity Report

Period covered: 15th April 2005 to 14th October 2008

Date of Preparation: 1st March 2008

Start date of project: 15th April 2005

Duration: 36 months

Project coordinator: Dr J. Steelant

Project Coordinator Organisation name: ESA-ESTEC

APPROVAL

Title	**issue**	revision
Final Activity Report	1	0

Author(s)	**date**
J. Steelant (ESA-ESTEC)	*29/07/2008*
A. Bond (REL)	*27/07/2008*
A. Götz (EADS)	*20/07/2008*
K. Hannemann (DLR)	*14/07/2008*
C. Bruno (Uni Roma)	*29/07/2008*
J. Longo (DLR)	*25/07/2008*

Approved by	**Date**
Program Board	*29/07/2008*

Table of Contents

Page

Nomenclature

Acronyms

ATR	Air Turbo Rocket	
BL	Boundary Layer	
CC	Combustion Chamber	
CARS	Coherent Anti-Stokes Raman Scattering	
CG	Center of Gravity	
CFD	Computational Fluid Dynamics	
CP	Center of Pressure	
DES	Detached Eddy Simulation	
DNS	Direct Numerical Simulation	
EDC	Eddy Dissipation Concept	
EoS	Equation of State	
ER	Equivalence Ratio	
FM	Fractal Model	
GTOW	Gross Take-Off Weight	
HC	Hydrocarbons	
HEG	High Enthalpy Shock Tunnel Göttingen	
HHV	Higher Heating Value	[MJ/kg]
HPT	High Pressure Turbine	
HSCT	High Speed Civil Transport	
I_{sp}	Specific Impulse	[s]
m’	air mass flow	[kg/s]
m_f’	fuel mass flow	[kg/s]
LES	Large Eddy Simulation	
LHC	Liquid Hydrocarbons	
LHV	Lower Heating Value	[MJ/kg]
LPT	Low Pressure Turbine	
LOX	Liquid Oxygen	
MTF	Mid Tandem Fan	
NGLT	Next Generation Launcher Transportation	
OPR	Overall Pressure Ratio	
PDF	Probability Density Function	
RAMS	Reliability Availability Maintainability Safety	
RANS	Reynolds-Averaged Navier-Stokes Equations	
RBCC	Rocket-Based Combined Cycle	
ROM	Rough Order of Magnitude	
RTA	Revolutionary Turbine Accelerator	
RTD	Research and Technology Development	
Scramjet	Supersonic Combustion Ramjet	
SERN	Single Expansion Ramp Nozzle	
sfc	Specific Fuel Consumption	[kg/s/daN]
SGS	Subgrid Scale Model	
SST	Supersonic Transport	
SWBLI	Shock Wave Boundary Layer interaction	
TBCC	Turbine Based Combined Cycle	
TIT	Turbine Inlet Temperature	[K]
TN	Technical Note	
USCER	UnSwept-Compression/Expansion-Ramp	
VCE	Variable Cycle Engine	
WT	Wind Tunnel	

Roman Symbols

T	temperature	[K]
P	pressure	[Pa]
M	Mach number	[-]

Greek Symbols

α	angle of attack	[-]
λ	bypass ratio	[-]
ρ	density	[kg/m^3]
Π	pressure ratio	[-]

Superscripts and subscripts

a	ambient
cc	combustion chamber
j	jet condition
∞	cruise flight point
o	upstream reference point
sep	separation points

1. Introduction

In April 2005, the EC kicked-off a 3 years long project called LAPCAT: Long-Term Advanced Propulsion Concepts and Technologies to initiate research on propulsion concepts for sustained hypersonic flight. The project is coordinated by ESA-ESTEC and is composed of a consortium of 12 partners from industry, research institutions and universities representing 6 countries (see table below). The total cost of the project was fixed at 7.1 M€ of which 4M€ was financed by the European Commission under the Sixth Framework Programme FP6 under the priority 1.4 'Aeronautic and Space'. The present report is a synthesis of the achieved results and highlights the major conclusions drawn from this project. The project was officially ended in April 2008. However, some experimental work continued until August 2008 as some test campaigns were delayed due to technical problems of some test rigs. Related numerical work relying on the generated experimental database was therefore also delayed until the end of the summer.

The project objectives are to identify and assess critical propulsion technologies required to reduce long-distance flights, e.g. from Brussels to Sydney, to less than 2 to 4 hours. Achieving this goal intrinsically requires a new flight regime for commercial transport with Mach numbers ranging from 4 to 8. At these high speeds, classical turbo-jet engines are not feasible and need to be replaced by advanced airbreathing engines. The identification of required breakthrough technologies goes hand in hand with the assessment of innovative propulsion concepts, and with steps towards their realisation.

Two major directions on conceptual and technological level will be studied and assessed, namely ram-compression (i.e. ramjet/scramjet) and active compression (i.e. compressors/turbines). The latter has the drawback of having an upper Mach number limitation well below that of a ram-compression. However, it can accelerate a vehicle from the runway up to its cruise speed. Ram-compression engines need an additional propulsion system, e.g. a rocket engine, to achieve their minimum working speed.

Long-term objective is to secure European competitiveness for future high-speed flight by identifying potential propulsion concepts and the assessment of related critical technologies. Key objectives are hence:

1. to define and assess different propulsion cycles and concepts for high-speed flight at Mach 4 to 8 in terms of:
    - turbine based combined cycles (TBCC)
    - rocket-based combined cycles (RBCC)

2. to define, assess and develop critical technologies in:
    - external aerodynamics for integrated engine/aircraft performance
    - internal aerodynamics for engine performance including intake and nozzle
    - mass efficient turbo-compressors and heat exchangers
    - high-pressure combustion experiments, modelling and validations
    - supersonic combustion experiments, modelling and validations
    - ramjet combustion modelling and validations
    - injector technologies for high-pressure and supersonic combustion

The project is broken down into *6 main technical activities* (workpackages WP2 to WP7) and *one project management task* (WP1). Each workpackage represents a general effort and is divided into major tasks. The planned effort in manpower for each of these workpackages is given in the table below. A total of 45 Man years or 15MY/year was scheduled to perform the different tasks.

Two major advanced propulsion concepts, i.e. TBCC & RBCC, are evaluated in parallel to trade-off their technological and economic characteristics respectively, in *WP2* and *WP4* with respect to requirements. Further on, each concept is evaluated in parallel to guarantee a complete and independent perspective view. In the meanwhile, activities in the field of advanced propulsion technologies (*WP3, WP5, WP6 and WP7)* checked their feasibility and limitations in terms of experimental and numerical capabilities. As an outcome of this trade-off, critical points allowed the clear definition of breakthrough technologies for both concepts, keeping in mind the technological borders.

Critical technologies related particularly to TBCC-concepts, i.e. heat exchangers and turbo-compressors, are grouped into individual tasks within *WP3*.

Of course combustion remains the key issue for propulsion which is reflected by two dedicated workpackages. *WP5* focused extensively on experimental investigations related to ramjet/scramjet propulsion in combination with specific issues linked to propulsion assistance modes: TBCC & RBCC. This includes the evaluation of ground based facilities, the investigation of combustion at high-pressure and supersonic conditions and the characterization of both hydrogen and hydrocarbon fuels. This largest workpackage resulted in building blocks for all modes of combustion encountered in both approaches.

WP6 addressed the modelling and simulation of combustion phenomena (kinetics, chemistry, mixing, turbulence…) and is closely linked to the experimental outcome of *WP5* for validation purposes. Also here the different tasks focused on the different modes of operations.

As the internal engine flowpath needs a tightly coupled engine/airframe integration for advanced airbreathing engines, particular attention was given to aerodynamical issues. This is addressed in *WP7*. This task is also interlinked with *WP5* and *WP6*.

Nr	Participant name	State	Activity
1	ESA-ESTEC: Division of Propulsion and Aerothermodynamics	NL	Research Institute
2	SNECMA	FR	Industry
3	Von Karman Institute: Institute for Fluid Dynamics	B	Research Institute
4	EADS - Astrium	D	Industry
5	CENAERO: Centre of excellence in aeronautical research	B	Industry (SME)
6	REL: Reaction Engines Limited	UK	Industry (SME)
7	DLR: German Aerospace Center (3 institutes, 5 locations): - Institute of Aerodynamics and Flow Technology (DLR-AS-RF: Göttingen and Braunschweig; DLR-AS-WK Cologne) - Institute of Propulsion Technology (DLR-RA-TE: Lampoldshausen; DLR-SART: Cologne) - Institute of Combustion Technology (DLR-VT: Stuttgart)	D	Research Institute
8	CIRA: Aerothermodynamics and Space propulsion Laboratory	I	Research Institute
9	University of Stuttgart: Institute of Aerospace Thermodynamics	D	Higher Education
10	University of Rome: Department of Mechanics and Aeronautics (DMA)	I	Higher Education
11	University of Southampton: Aerodynamics and Flight Mechanics (AFM) group	UK	Higher Education
12	University of Oxford: Osney Laboratory	UK	Higher Education

Partners involved in LAPCAT

Work-package	Workpackage title	Lead contractor	Person-months	Rel. [%]
WP1	Project management and co-ordination	ESA-ESTEC	20	4
WP2	System Study for TBCC	REL	43	8
WP3	Critical Technologies for TBCC	REL	57	10
WP4	System Study for RBCC	EADS-ASTRIUM	20	4
WP5	Combustion Experiments	DLR-Göttingen	120	22
WP6	Combustion Modelling and Validation	Uni. Of Rome	174	32
WP7	Design and Aerodynamics of Propulsion Units	DLR-Braunschweig	112	20
	TOTAL		546	

Manpower allocation for each of the workpackages

2. Project Objectives and Major Achievements

2.1 General Project Objectives

The LAPCAT project aimed at providing a sound technological basis for the industrial introduction of innovative advanced propulsion concepts on the long-term (20-25 years), defining the most critical RTD-building blocks to achieve this goal and finally to investigate in depth these critical technologies by developing and/or applying dedicated analytical, numerical and experimental tools. The scientific and technological objectives of the project were:

1. *to evaluate two advanced airbreathing concepts:* a Turbine or Rocket Based Combined Cycle (TBCC/RBCC) capable of achieving the ultimate goal to reduce long-distance flights, e.g. from Brussels to Sydney, to less than 2 to 4 hours. To guarantee an independent, non-biased and complete view, each concept will be investigated by two different groups (i.e. a single partner or a group of partners) and based on a commonly agreed reference vehicle(s) and trajectory point(s).
2. *to assess critical technologies* for each cycle. For those already defined in the different workpackages, the conditions and parameters to be verified or investigated will be defined.
3. Specific objectives for the envisaged concepts are listed below:
   a. *Dedicated combustion experiments* are clearly needed for both concepts:
      - to evaluate the performance and achievements for specific conditions, i.e. supersonic combustion and high-pressure combustion.
      - to evaluate the performance and achievements for potential fuels, either hydrogen or hydrocarbons (HC), and potential oxidizers, either air or liquid oxygen, including the investigation of reaction products and hence the impact on emission requirements.
      - to evaluate the chemical kinetics and its interaction with the flow-field turbulence, its impact on ignition delay and flame stabilization.
      - to evaluate potential injection systems: wall and strut injections with emphasis on mixing and combustion efficiencies.
      - to set-up a database for modelling and validation purposes in these areas where detailed and dedicated experiments are lacking: e.g. supersonic combustion, turbulence interaction with high-speed combustion, etc… for both hydrogen and hydrocarbons.

   b. *Modelling and validation of numerical simulation tools for combustion physics* applicable for both concepts:
      - to define the chemical kinetics for hydrogen and hydrocarbon fuels in combination with air or oxygen as oxidizer.
      - to set-up fuel spray vaporization models for sub-, trans- and supercritical conditions
      - to set-up and validate various turbulence models affecting the combustion kinetics, including eddy-dissipation concepts, PDF-methods and Large Eddy Simulation subgrid scale models.

   c. *Aerodynamic experiments* for a wide range of Mach numbers (up to Mach 8) are needed to verify and quantify the design of overall concepts and major components of advanced airbreathing engines, such as intakes, nozzles, full engines, external aerodynamics including base flows, interaction of external aerodynamics with internal aerodynamics, in order
      - to evaluate intake designs optimised for a range of Mach numbers including effects of transition and shock-wave/boundary layer interaction.
      - to evaluate the design of a nozzle along with its interaction with the base and external flow dynamics
      - to evaluate the unsteady behaviour of a nozzle design during start-up and shut-down
      - to set-up a database for modelling and validation purposes in these areas where detailed and dedicated experiments are lacking

   d. *Evaluation and validation of computational fluid dynamic tools for advanced turbulence & transition models*
      - the use of advanced turbulence models (Detached Eddy Simulation: DES) to evaluate separated flow regimes for unsteady flow phenomena (e.g. nozzles)

- the development of engineering models to simulate the increase and overshoot of skin friction and heat transfer including start and length of transition by means of intermittency related parameters

e. Design, development and testing of particular hardware components
- design and performance characterization of wall and strut injectors for supersonic combustion chambers, both for hydrogen and hydrocarbon as a fuel
- design and performance prediction of stator-less counter-rotating turbo-compressors
- design and performance characterization of cryogenic fuel heat exchangers by means of metallic alloys and ceramics.

A *duration of 36 months* for this project is required in order to
- define the requirements and operational conditions on system level
- perform dedicated but lengthy in-depth experiments in various fields
- setting-up and validating physical models integrated into numerical simulation tools

The project is broken down into *6 main technical activities* (workpackages WP2 to WP7) and *one project management task* (WP1). Two major advanced propulsion concepts, i.e. TBCC & RBCC, are evaluated in parallel to trade-off their technological and economic characteristics respectively, in *WP2* and *WP4* with respect to requirements. Critical technologies related particularly to TBCC-concepts, i.e. heat exchangers and turbo-compressors, are grouped into individual tasks within *WP3*. Of course combustion remains the key issue for propulsion which is reflected by two dedicated workpackages. *WP5* focused extensively on experimental investigations related to ramjet/scramjet propulsion in combination with specific issues linked to propulsion assistance modes: TBCC & RBCC. *WP6* addressed the modelling and simulation of combustion phenomena (kinetics, chemistry, mixing, turbulence…) and is closely linked to the experimental outcome. Since friction drag is the major show stopper for this class of engines and vehicles, the internal engine flowpath needs a tightly coupled engine/airframe integration. Therefore, particular attention was needed for the aerothermodynamic aspects with respect to the intake, nozzle and coupling to the external flowfield. This is addressed in *WP7*.

2.2 The objectives and major achievements of individual workpackages

In order to specify realistic conditions for both the detailed experimental and numerical campaigns, several vehicle systems studies were performed. Two different designs were conceived for a Mach 4 to 5 range on the basis of turbine based combined cycles, based on hydrogen or kerosene as a fuel. This approach was taken in order to capitalise as far as possible on the vast experience now available from turbojet design and operation. For the Mach 8 range a single vehicle concept was started on the basis of a rocket based combined cycle where the airbreathing part is done consecutively by a hydrogen fuelled ejector, ramjet and finally scramjet. The poor performance during acceleration of this vehicle triggered the team to investigate an alternative design where the ejector rocket was replaced by an air turbo-rocket and the aerodynamic.

2.2.1 WP2: System Study for TBCC

The project objective was to examine two turbine based cycle (TBCC) engine concepts for high Mach number (4 – 5) flight in the context of future civilian transportation. The experience accumulated from turbojet design and operation is huge and this should obviously form the basis of the next generation of engines if at all possible.
Using the engine concepts, vehicles were defined and their aerodynamic performance optimised. These were incorporated into trajectory models together with subroutines of the engine performance to derive scaled performance and formed the basis of estimating vehicle size and mass. The nominal mission was to fly economically from Brussels to Sydney in approximately 4 hours.

Hydrogen Precooled Turbo-Ramjet
The first study focused on a precooled Mach 5 engine, named Scimitar, employing a cycle based on the Reaction Engines SABRE spaceplane engine and fuelled by liquid hydrogen **[D2.1.1]**. The Scimitar engine must have good subsonic and supersonic performance if it is to be a practical engine for a new generation of hypersonic aircraft. This would allow it to operate from normal airports and over-fly inhabited regions without the nuisance and political problems which limited Concorde's effectiveness. These characteristics have been successfully incorporated into the Scimitar design (fig. below) by incorporating a high bypass fan into the bypass duct which encloses the core engine and is otherwise needed to match the intake air capture flow to

the engine demanded flow over the supersonic Mach number range. The bypass fan is driven by a hub turbine using flow diverted from the core engine nozzle. The flow then discharges into the bypass and mixes with the bypass flow. The engine mass is roughly estimated to be 10 ton.

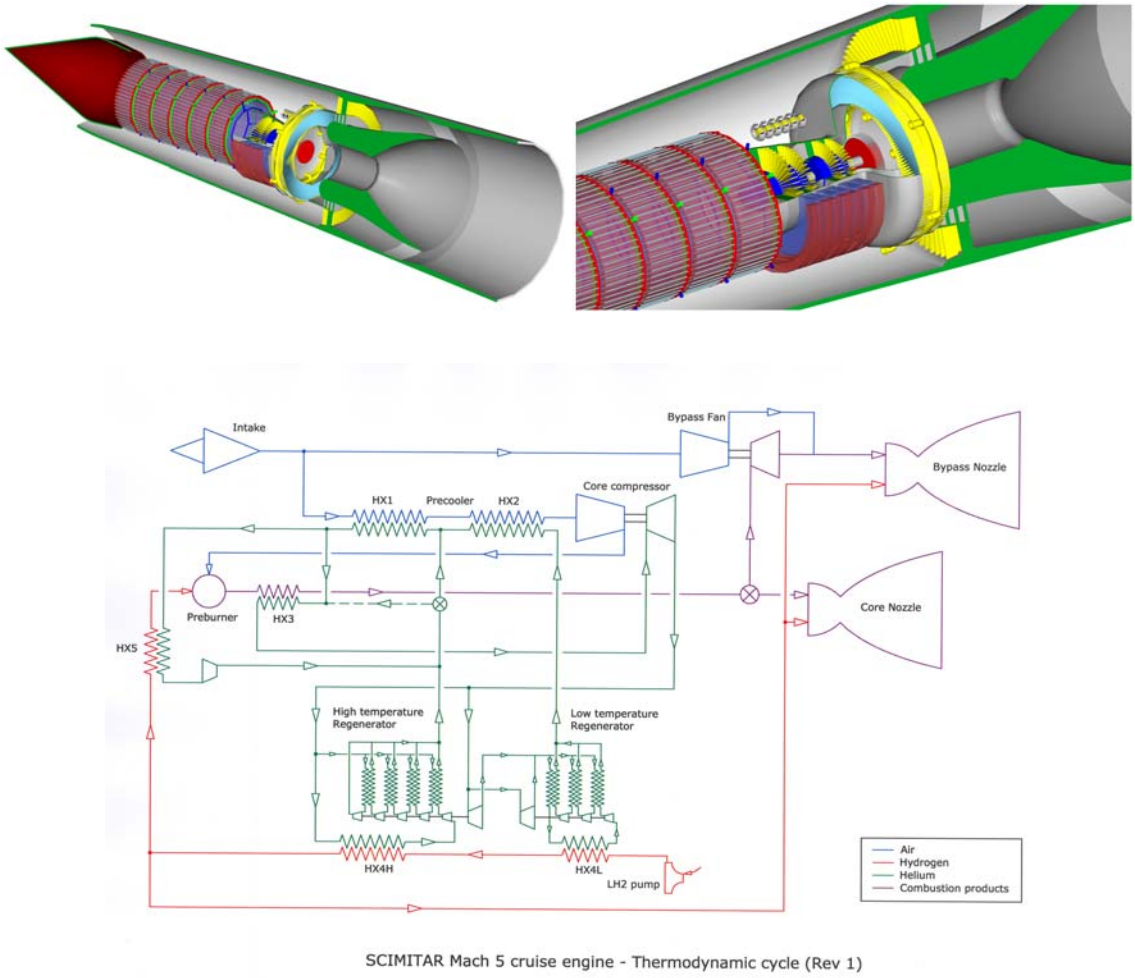

Scimitar: Precooled Turbofan-Ramjet engine for LAPCAT A2 cruiser.

Due to their central role to the concept of the precooled engine two technologies are being addressed at experimental level: a lightweight heat exchanger and a contra-rotating turbine **[D2.1.3]**. The progress obtained for these two topics are described in more detail in the next section.
The Scimitar engine analysis suggests that it can produce efficient supersonic and subsonic flight and meet the anticipated noise regulations for normal airport operation. An important side result is the critical role of environmental impacts, specifically NOx, contrails and Ozone damage **[D2.1.5]**. These may prove to be one of the most significant potential obstacles to scheduled hypersonic civil aviation and a literature search showed that they played a large part in the USA's decision in the early 1970s not to pursue a Concorde-like aircraft at that time. The Scimitar engine as configured in the current design would be unacceptable for its NOx production although some options exist for reducing the NOx at a performance penalty. Future studies need to include these problem at the outset to avoid naïve results and the expenditure of considerable resources on studying projects which are ultimately not viable. The studies in this area are complete for the current project.

Hydrogen Mach 5 Cruiser Vehicle
The LAPCAT A2 vehicle flying at Mach 5 was carried out by Reaction Engines. The preliminary results of this analysis are encouraging **[D2.0.1]**. The vehicle study is complete at initial project study level and indicates that a 400ton, 300 passenger vehicle could achieve antipodal range without marginality. The concept is particularly interesting for this mission requirement as a trajectory optimization allowed to fly almost continuously over sea and avoiding sonic boom impact when flying over land.

The proposed aircraft configuration LAPCAT-A2 is shown in the figures below. The vehicle consists of a slender fuselage with a delta wing carrying 4 engine nacelles positioned at roughly mid length. The vehicle is controlled by active foreplanes in pitch, an all moving fin in yaw and ailerons in roll. This configuration is designed to have good supersonic and subsonic lift/drag ratio and acceptable low speed handling qualities for takeoff and landing. A leading edge sweep angle of 55 deg was chosen as roughly equivalent to the Concorde value and known to be the minimum necessary to generate a stable separated vortex at high angle of attack. A thickness/chord of 3% was selected as typical of supersonic cruise vehicles. An achievable takeoff wing CL of 0.59 gives a minimum wing area of 900 m^2 for a takeoff mass of 400 tonnes. A fuselage diameter of 7.5 m was chosen to trade a small increase in drag for a saving in fuselage mass. The resulting fuselage length at 139m is much longer than any existing aircraft.

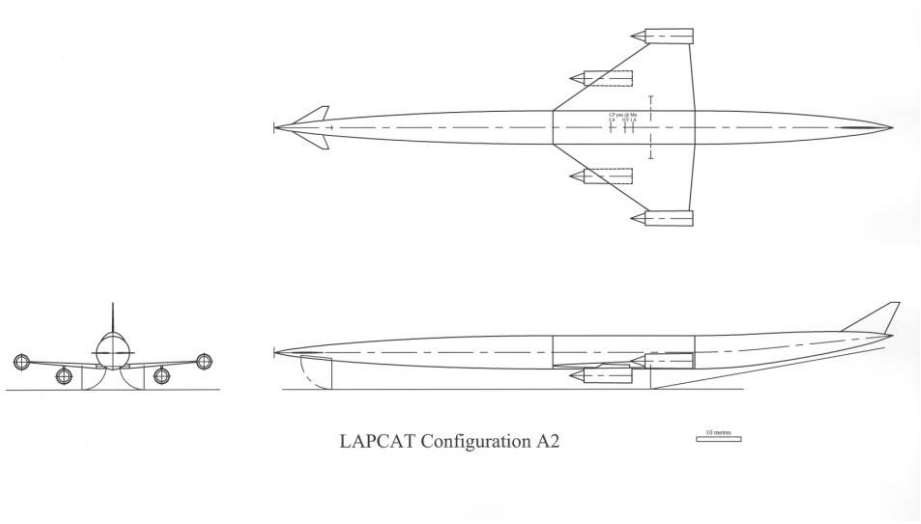

LAPCAT A2: configuration for a Mach 5 TBCC vehicle based on hydrogen

The flight deck and passenger compartment (arranged in two decks) occupies a length of about 32 m and is located over the wings on the vehicle centre of gravity. Unlike conventional airliners hydrogen storage within the wings is not feasible since the wing volume is too small. Consequently the liquid hydrogen occupies the remainder of the fuselage volume and is split into two large pressurised tanks either side of the passenger compartment. This permits circular cross section tankage which minimises insulation and pressure vessel mass.

The vehicle has 4 engines (for redundancy), which are mounted in separate axisymmetric nacelles on the wing. Currently two engines are located on the wingtips whilst the remaining two are located within inboard nacelles located under and ahead of the wing leading edge. Physically separating the nacelles reduces the possibility of a mechanical failure in one engine causing damage to the adjacent engine, and also causes less aerodynamic disruption when an engine is shutdown or unstarts. Carrying the engines on the wing gives good CP/CG matching and is structurally efficient, whilst the alternative option of mounting the engines on the fuselage incurs the penalty of a large boundary layer diverter and acoustic fatigue of the fuselage skins. Locating the engines at the rear of the fuselage would pull the vehicle centre of gravity too far back. The wing tip mounted engines generate a large yawing moment if one is shutdown however calculations indicate that the all moving fin is capable of controlling the vehicle since it is acting at a large moment arm.

Normally the engines of supersonic cruise vehicles are mounted underneath the wing towards the trailing edge which permits the designer to capitalise on precompression and allows the nozzle to discharge aft of the wing trailing edge. However at Mach 5 the wing shock wave is at an angle of only 8.9 deg relative to the wing lower surface, which would necessitate moving the nacelle aft until the intake face was behind the wing trailing edge. Therefore this approach is structurally impractical and would scrape the nacelles on the runway during takeoff rotation. Consequently the nacelles are positioned with the intake face ahead of the wing shock wave in relatively freestream conditions, which has the added advantage that no wing boundary layer has to be dealt with. The inboard nacelles are mounted underneath the wing to reduce wing skin acoustic fatigue damage. The main disadvantage of the inboard nacelle location is that the nacelle cross section is introduced ahead of the wing maximum thickness which is counter to normal area ruling practice and will increase transonic wave drag.

Routes

Commercial civil transport aircraft, flying subsonically, normally follow a “great circle” route between the airports of departure and arrival, once they are clear of local traffic. However in the case of supersonic aircraft there is the complication of the “sonic boom”, or ground overpressure produced by supersonic flight. Various tests show broad agreement that an overpressure below 50 Pa is tolerable for regular overflights of populated areas (although there appears to be no safe level which will eliminate complaints) **[D2.1.2]**. Unfortunately practical civil transports produce overpressures above this level. For example Concorde generated an overpressure of about 93 Pa, which restricted supersonic flight to over water regions only and effectively reduced its commercial viability. Current overpressure estimates for the LAPCAT configuration A2 vehicle suggest that at the start of Mach 5 cruise the overpressure will be about 85 Pa under the ground track, reducing to about 70 Pa at mid cruise. Therefore preliminary route planning for the LAPCAT vehicle has assumed that supersonic flight is only possible over regions of very low population density (oceans and the North and South Poles). The possibility of over flying desert regions (e.g.: central Australia or the Sahara) has been ignored although this may be feasible following international negotiation. This philosophy will give a “worst case scenario” for the range requirement – in the event that the vehicle will be able to fly over land the distances travelled will obviously be smaller.

The Brussels to Sydney route was adopted as the baseline mission. This was seen as a sensible starting point in that it requires extreme range and would greatly benefit from hypersonic speeds in significantly reducing flight times. Nevertheless, other potential routes of interest are evaluated in the next table. Some of the routes are depicted in the figs. below.

Route	Subsonic aircraft	Mach 5 aircraft
Brussels – Sydney	22.25 hours[1]	4.6 hours[2,6]
Brussels – Los Angeles	10.0 hours	2.5 hours[2]
Brussels – Tokyo	10.75 hours	2.5 hours[2]
Brussels - New York	7.5 hours	1.6 hours
Brussels - Beijing	8.9 hours	4.9 hours
Brussels - Delhi	7.2 hours	5.3 hours
Paris - Kourou	7.9 hours	1.7 hours
Los Angeles - Tokyo	9.75 hours	2.0 hours
Los Angeles - Sydney	13.4 hours	2.6 hours
Los Angeles - Singapore	15.7 hours	3.0 hours
Los Angeles - Delhi	14.3 hours	7.5 hours

Table: Approximate Flight Times: 1) Includes 2 hour refuelling stop; 2) Assumes supersonic overflight of the Bering Straits; 3) No wind (jet stream) effects; 4) No "airport flight stacking" (i.e. straight in approaches); 5) Nominal ascent/descent times and distances; 6) Detailed trajectory modelling indicates 4.6 hours due to longer ascent/descent times than initially forecast.

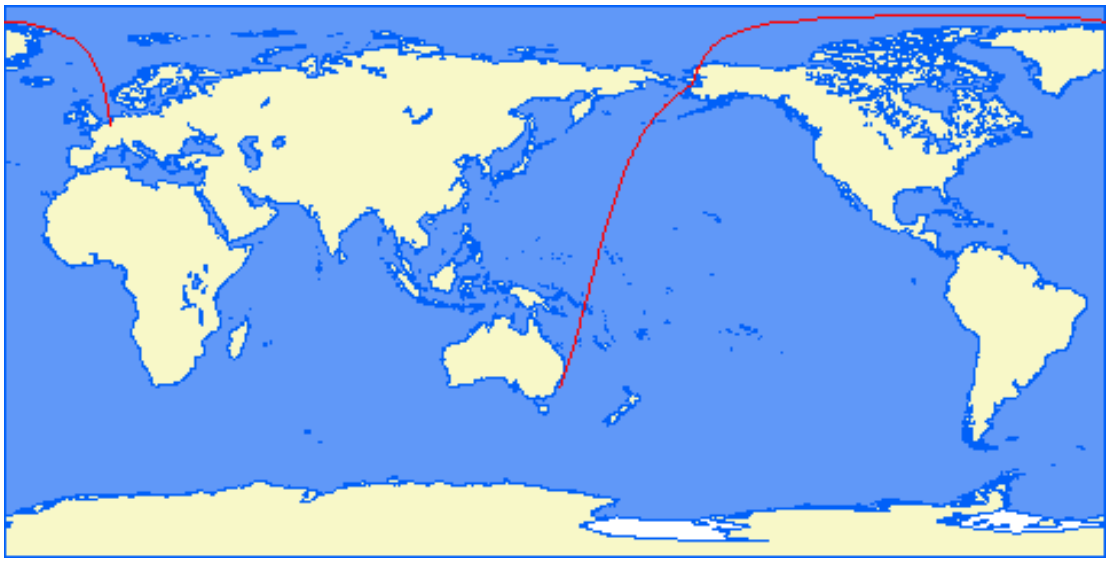

Brussels to Sydney via Bering Strait (18,728 km)

Brussels-Beijing via Nome and Tokyo (14,100 km)

Development plan and economics

To address the relatively high technical risk of this project it is proposed that the development program proceed in a step by step basis in 3 phases, namely Concept Validation (2 years), Technology Demonstration (3 years) and System Development (8 years). At the end of each program stage the project would be reviewed before deciding whether to proceed with the next stage. An arbitrary start date of 2010 has been assumed which implies an Entry Into Service date at the beginning of 2023 **[D2.1.4]**.

The predicted engine development cost in 2006 prices is 8,147M€ and vehicle development cost 14,454M€ to give a total development cost of 22,601M€. The first vehicle production cost is 979M€. Assuming an 85% learning factor and a total production run of 100 vehicles implies an average vehicle sale price of 639M€ (including full development cost recovery).

The estimated annual operating cost per vehicle is 553.8M€ of which the liquid hydrogen fuel comprises 83%. This assumes hydrogen derived from electrolysis of water however hydrogen derived from steam reforming of hydrocarbons would be about 1/3rd the cost which would roughly halve the annual operating cost.

The A2 vehicle should carry about 148,000 passengers per year assuming 2 flights per day, 90% availability and 75% load factor. This implies an average one way ticket price to Australia of 3940€ in 2006 prices. This compares with a current Business class ticket of around 4060€ and First class ticket of 5075€. Therefore in principle the A2 vehicle could capture all of the current business and first class traffic due to the greatly reduced journey time of 4.5 hours compared to the current 22 hours (assuming subsonic carriers do not drop their prices in competition). The ticket prices would roughly halve (2000€) if the hydrogen is produced by steam reforming. This analysis assumes no hydrogen subsidy, however in reality it is likely that the first generation of hydrogen fuelled aircraft would be subsidised to promote the switch to a more environmentally friendly fuel.

Unlike Concorde, the A2 vehicle has exceptional range (both subsonic and supersonic) and is therefore able to service a large number of routes whilst simultaneously avoiding supersonic overflight of populated areas. Its good subsonic performance enables it to service conventional subsonic overland routes thereby increasing its sales potential to airlines.

Kerosene Variable Cycle Engine

A parallel study carried out by DLR-Sart focuses on kerosene as a fuel in order to explore the performance of this fuel in preference to hydrogen since its supply infrastructure is well established.

It was identified that turbofans are most efficient in subsonic flight whereas turbojets are better suitable for supersonic flight as their dry thrust drops far more slowly than that of a fan with increasing vehicle airspeed. A supersonic aircraft would profit of an engine which combines both performances: one for supersonic cruise flight and the other for take-off and landing as well for subsonic cruise over densely populated areas. This demands for a Variable Cycle Engines (VCE) might offer a good compromise for such applications where the specific thrust is low at low altitude flight and subsonic cruise, but is forced high during supersonic cruise and acceleration.
DLR-SART made a comprehensive overview of VCE **[D2.2.3]**. Recently the US was aggressively pushing this technology for military and space function (RTA, Revolutionary Turbine Accelerator). The cycles are based on a suitable arrangement of the fan stages and variable by-pass flows. The MTF (Mid Tandem Fan) type VCE engine has been studied in Europe by Rolls Royce and Snecma in the early 1990ies.
Based on development work for the GE-21, the YF120 is a variable cycle engine capable of adjusting its bypass ratio to the optimum for a given flight regime. The F-120 can be seen as one of the most advanced jet engines ever flown in the YF-22 and YF-23 ATF test airplanes. Another VCE project has been the Revolutionary Turbine Accelerator (RTA) as the TBCC demonstration project in the NGLT program of NASA (fig. below). Designated as the GE57 by General Electric (GEAE), the RTA engine represents a unique variable cycle engine where internal flowpath changes allow for high Isp throughout the flight trajectory for an accelerator vehicle.

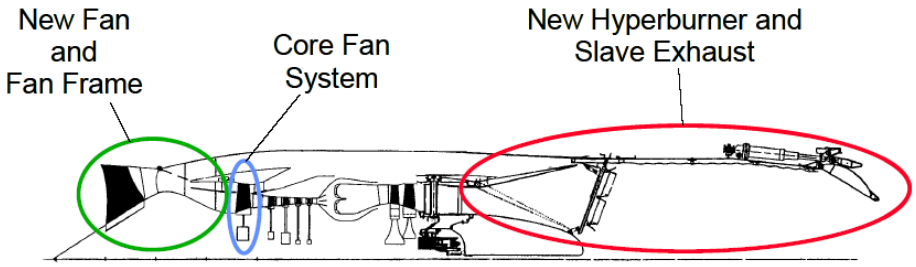

General Electric RTA-1 (GE-57) cut view

Three different variants of advanced variable cycle engines have been conceptually designed for the LAPCAT supersonic airliner. All are double bypass turbofans principally similar to the RTA-1 design, however adapted to the mission and thrust requirements of the LAPCAT-M4. The major differences of the three concepts are in the number of fan or compressor stages and their OPR. A RAM burner is integrated with the convergent divergent nozzle in all variants. The different concepts are evaluated in depth. The discussion below is however limited to the one selected as most optimal for the M=4.5 vehicle.

The LAPCAT VCE-214 is a variable cycle incorporating a two stage fan with large blades mounted on the low pressure spool. The first bypass flow is controlled by the first variable area bypass injector (VABI). This device is followed by the core section, starting again with a single stage fan (core driven fan stage CDFS). After the second VABI the four stage core compressor delivers the remaining air into the combustion chamber. A single stage HPT is followed by a single stage LPT and the bypass flow is again controlled by an aft VABI to achieve mixing with the core flow in the complete flight regime.

The more complicated lay-out of the VCE allows an adaptation of the different compressors more or less independently of each other. This feature can be used at higher supersonic Mach numbers. Around Mach 2.5 these engines are switching to an operation mode in which the first fan is transitioning to windmilling. At Mach 3 the low pressure spool is in full windmilling, thus temperature and pressure of the incoming air is no longer altered by this component. The turbofan is operating in double bypass mode with small bypass ratios λ_1 and λ_2 and still at its maximum TET of 1950K and a OPR of 28 without reaching the compressor exit temperature limitation of 1000 K. The first VABI is opened with λ_1 approaching 0.85. The VABI2 is kept slightly open. The core engines of VCE will be closed beyond the Mach 3.5 trajectory point and the complete air-flow is directed through the bypass duct to the RAM chamber. Technical solutions for the practical design of such a TBCC might become very challenging **[D2.2.4, D2.2.6]**. A thermal environment around 1050 K for the windmilling LP-Fan during the several hours of RAM cruise could raise problems. In case of the turbojet these design challenges might become even tougher and a switch to two separate flow passes might be necessary. The RAM cycle limits the maximum combustion temperature to 2100 K as for the afterburner.

This high value is used during the acceleration phase and can be significantly reduced when reaching the cruise flight. Depending on the remaining airliner weight, the combustion temperature is reduced in steady cruise to values between 1850 K and 1700 K. The lower thermal loads ease somewhat cooling concerns because no cryogenic fluid for active cooling is available. Numerical optimisation of the engine and the intake design has been performed by CENAERO **[D2.2.5]**.

Kerosene Mach 4.5 Cruiser

Vehicle

The preliminary design of the LAPCAT-M4 vehicle is based on a critical recalculation of a 1990 NASA Langley and Lockheed study of a 250-passenger, Mach 4 high-speed civil transport with a design range of 6500 nautical miles (12045.8 km) **[D2.2.1]**. The LAPCAT mission range Brussels to Sydney is highly ambitious and by almost 40 % larger than NASA's 12000 km, which requires a re-design.

The new supersonic cruise airplane has to be considerably enlarged compared to the earlier NASA design to meet its ambitious range requirement. To keep the wing loading in an acceptable range the wing size has been increased to 1600 m2 (+ 36%). The span grows almost proportionally by 16 %, while the total length reaches 102.78 m which is only slightly longer (+ 8.8 %) than the earlier HSCT proposal. The general arrangement of the generic airplane geometry is illustrated below. The LAPCAT-M4 employs similar to the NASA concept a blended wing-body with a modified nose, a highly swept inboard wing panel, and a moderately swept outboard wing panel. The inboard wing panel is swept 78°, allowing the flow component normal to its leading edge to remain subsonic even at the Mach 4.5 cruise condition. The outboard wing panel is swept 55° but its exact, possibly curved form has not been defined yet. The total wing is inclined with a positive angle of attack of approximately 2.75°. Note that this angle and the wing's airfoil are not optimized yet and might be adapted in the future, if required.

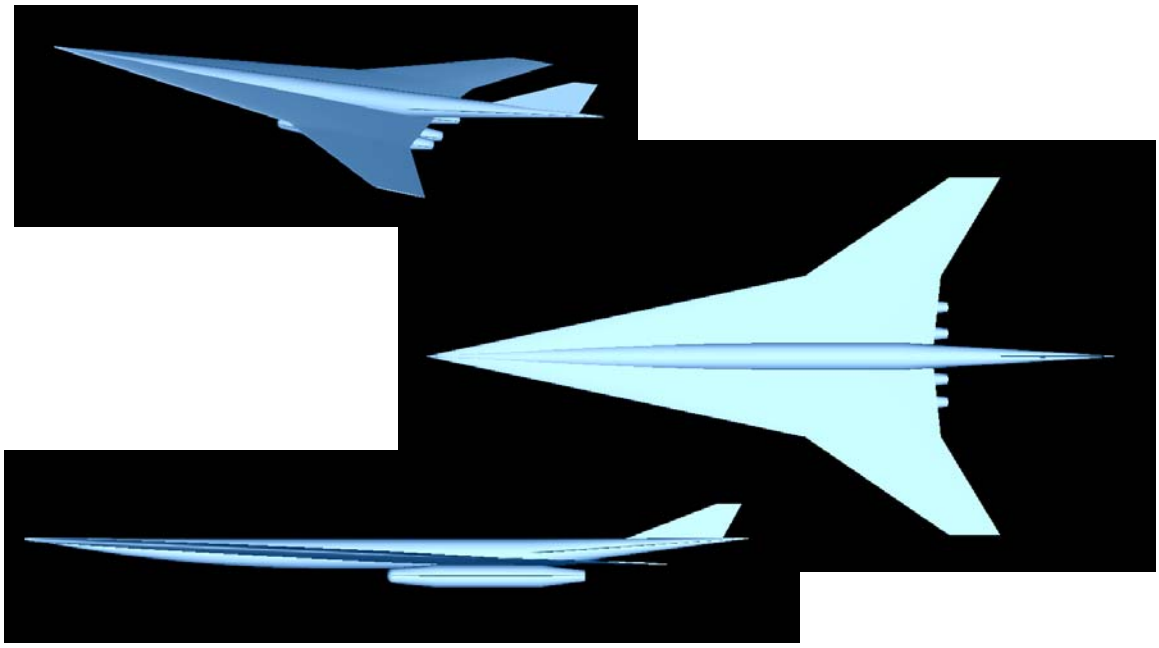

Preliminary Mach 4.5 kerosene fuelled aircraft for 200 passengers with a MTOW of 720 ton.

The forebody of the concept is slender and elliptical in cross section. The wing-mounted struts of the main landing gear should retract into the engine nacelles and are housed between the inlet ducts. The two-wheeled nose gear is mounted on the bulkhead forward of the crew station and retracts forward. The four advanced turbo-RAM-jet engines are mounted in two nacelles on the wing lower surface adjacent to the fuselage. The location of the engine and nacelles is still open for adaptation if required by trim as long as they remain under the wing. The axial-symmetric geometry and the size of the air-intakes, nacelles and

nozzles shown in the above figure are not representative of the actual LAPCAT design. A rectangular shape of the air-intake with vertical ramps is the preferred design option.
Fuel is carried in integral wing tanks and in a single aft fuselage tank. It is further assumed that the vehicle uses thermally stabilized jet fuel (TSJF) because the existing airport infrastructure is designed around conventional jet fuel. A single vertical stabilizer is attached to the upper part of the aft fuselage. The large, slightly inclined wing might help to achieve a good maximum L/D of 7.8 at a small angle of attack and cruise Mach number 4.5 according to preliminary DLR-analysis. Actually, a high L/D is essential to achieve the ambitious range requirement.
The total take-off mass of the supersonic cruise airplane has been iterated in the first loop to the huge value of 720 ton, which is well beyond any supersonic passenger aircraft built to date. The dry mass is estimated at 184.5 ton and the structural index is at a for airplanes low 25.6%. According to current data the HSCT would be able to transport about 200 passengers with their luggage. More data on the LAPCAT-M4 airliner design can be found in **[D2.2.2]**.

Routes

The complete flight trajectory of LAPCAT-M4 from take-off, via ascent, acceleration to the supersonic cruise, descent and landing approach has been simulated using control algorithms. The calculation ends after depletion of nominal propellants with descent to sea-level altitude. The vehicle follows almost the orthodrome, however, with some deviations to avoid some densely populated areas, adding about 200km to the shortest great circle route. It's no objective in LAPCAT to proof if the chosen track is actually acceptable for supersonic high altitude flight. Nevertheless, the propulsion system performance should be assessed under realistic operational conditions. Thus, a significant portion of the trajectory (from Brussels in eastern direction up to Volgograd) is assumed to be flown in subsonic cruise.

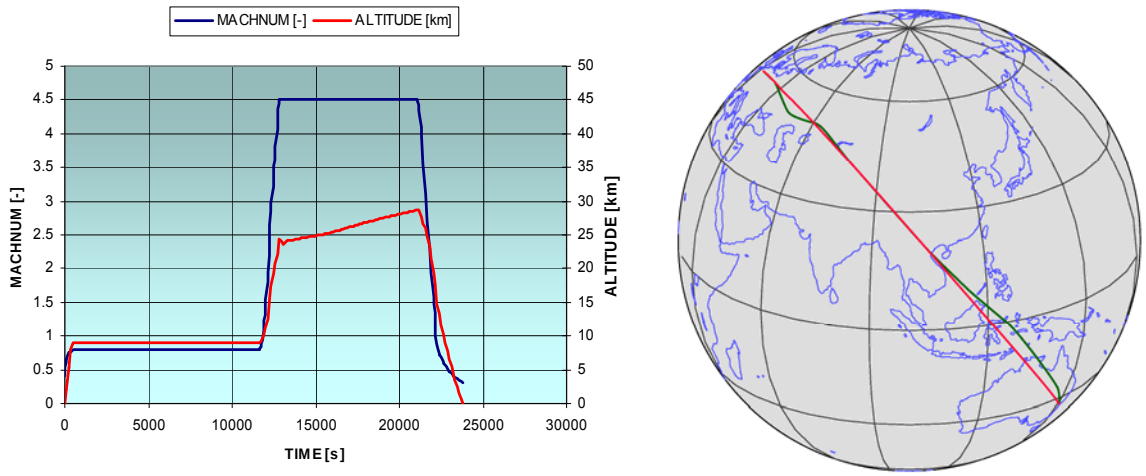

Brussels to Sydney: flight profile and route (16,700 km)

Under these hypotheses LAPCAT-M4 with the available 484.8 ton of JP-fuel does not fully reach its final destination Sydney but at least arrives after 15,989 km in central Australia (145.9° E; 26.4° S). Flight time is 23,811s (6.6h). It has not been intended to further enlarge the vehicle to finally fulfil the mission goal. Such work could be the subject of a separate study while LAPCAT focuses on propulsion system research. Simulations show that if a direct acceleration to Mach 4.5 already over the European continent would be acceptable, the HSCT could reach its final destination of Sydney.

Therefore, the obtained results demonstrate the principle feasibility of a TBCC-powered ultra long-haul supersonic airliner. The VCE-214 engine variant with relatively high OPR shows the best performance of all investigated types as long as potentially different engine masses are not taken into account.

2.2.2 WP3 Critical Technologies for TBCC

Two technologies associated with the precooled engine are being addressed at experimental level, reflecting their critical role in realising this engine. The first technology is for heat exchangers associated with the air precooler and with the preburner system while the second technology is for the high pressure helium turbine driving the turbocompressor **[D3.1.1]**.

The air precooler is a metallic tubular matrix with the captured intake air in cross flow over a helium cooled small diameter (1.0mm) tube bank. The preburner is needed to heat the helium from the precooler exit temperature up to around 1000K at low Mach numbers when the captured air enthalpy is low. The precooler heat exchanger is a smooth plate Silicon Carbide surface in order to minimise the pressure loss on the combustor gas side. The work has been performed by REL.

The heat transfer surface manufacturers were unable to supply the requirement in the time scale initially planned and this work is therefore being extended considerably relative to the initial program. The design of the tubular surface test items has been done and oxidation trials of Inconel 718 tube material have been completed. Strength problems have been identified at high temperature with the metallic materials and further manufacturing contracts have been placed to address these. The SiC technology is in the early stages of development **[D3.1.2]**.

The progress on WP3.1 was slower than planned throughout, initially due to the response of the manufacturers of the basic surface (tubes, sheets) then latterly due to internal company work pressures, with which the LAPCAT project had to compete for resources. No other work packages have been affected by this slow progress.

WP3.1 addressed two heat exchanger technologies, metallic and SiC ceramic. The metallic technology was an extension of work already being explored by REL for the SABRE engine to power a spaceplane and was therefore reasonably advanced. The SiC technology had only been addressed prior to the LAPCAT project in connection with simple tubular surfaces and through dialogue with St-Gobain in the USA.

For the LAPCAT work the tubular metallic technology is for the precooler of the Scimitar engine for the A2 aircraft configuration derived in WP2.1. The ceramic technology is for the heat exchanger which heats the helium to the top cycle temperature (HX3) prior to its entry into the turbine of the Scimitar engine.

The drawing of the metallic tube (0.98mm OD x 40μm wall in Inconel 718) was performed by High Tech Tubes Ltd. using starting stock drawn by Fine Tubes Ltd. This production route had been developed by REL, fitting in with the business preferences of the two companies. Some 1100m of tube, in nominally 1.3m lengths, was drawn. The quality however was not up to standard, having been annealed at too high a temperature, resulting in some grain-growth and loss of properties. However, the main task was a manufacturing exercise and it was decided to accept the material since it is known that the required quality can be obtained and it was not a technology issue.

In parallel with the manufacturing exercise, work was begun on the design of a test rig to test the modules under representative loading **[D3.2.1]**. As the design of this rig progressed it became obvious that it was becoming too elaborate and very expensive. A new design was embarked on which would test a specially built subscale section of the precooler and be much more manageable. However, at the same time the turbine being built under WP3.2, described later, experienced very significant cost over-runs, while WP3.1 reached its forecast expenditure limit. The testing was therefore eliminated from the LAPCAT activity and the effort and money diverted to WP3.2. The matrix testing will now be carried out by REL as part of its own program at a future date.

Two precooler modules have been built for this program. They are the correct flow length and tube dimensions, but shorter than a full engine module. They were used to demonstrate the manufacturing technology for these items. This demonstration consisted of tube surface preparation, support of the matrix in the brazing fixture and brazing of the tubes to the headers. An in-house QA failure in manufacture resulted in the first module achieving only 98% brazed joint efficiency. In addition, a thermocouple used to check the braze temperature cycle curled up at temperature and became brazed to the matrix, resulting in damage when it was removed. However this module is of sufficient quality to be subjected to a gas pressure test. The second module has completed its brazing cycle but has not yet been inspected.

This program reinforced the conclusion that precooler manufacture by this technique is practical, although some refinement of the industrial process is still needed. These refinements will be incorporated into the REL modules to be manufactured for the ongoing SABRE R&D program over the next three years.

The SiC technology program became hard going quite early in the project. Although straight SiC tubes made by sintering are available and can undoubtedly be refined, other surface shapes proved very daunting to manufacturers. CVD technology was tried by Archer Technicoat Ltd. without success and without any indication that it could become viable with expenditure of more money. The manufacture of multi-channelled plates by green state extrusion followed by siliconising showed much greater promise (Tenmat Ltd.) and probably could be made to work if the manufacturers' interest could be more successfully engaged. This route of investigation will remain ongoing beyond the LAPCAT project as an REL activity.

The SiC heat exchanger technology remains appealing but will require considerable inducement to the manufacturers to investigate manufacturing routes leading to practical components. As a consequence a future investigation will examine whether engine cycle changes could allow metallic HX3 designs to be employed.

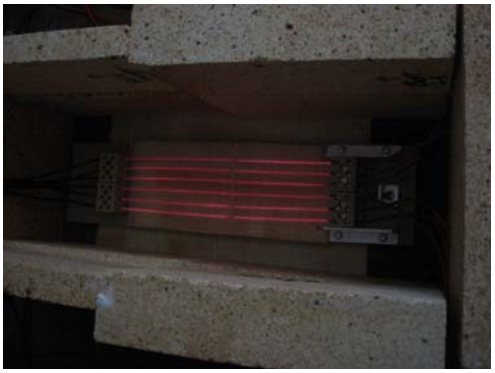

Oxidation testing of Inconel 718 tubes

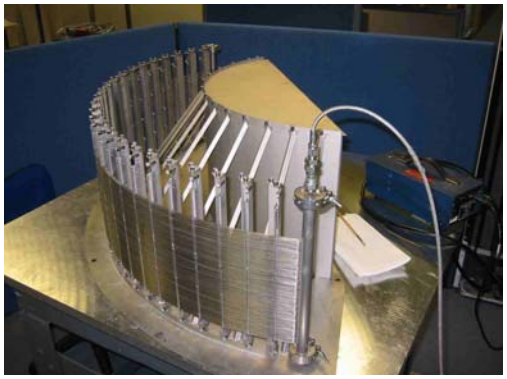

Completed precooler module in assembly fixture during pressure testing.

Close-up of precooler matrix/header brazed joint

Sintered silicon carbide tubes

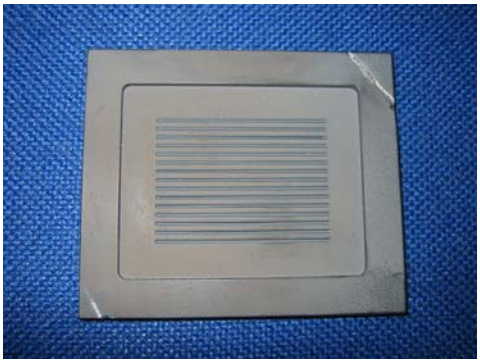

Trial SiC matrix plate manufactured by deposition onto graphite grid.

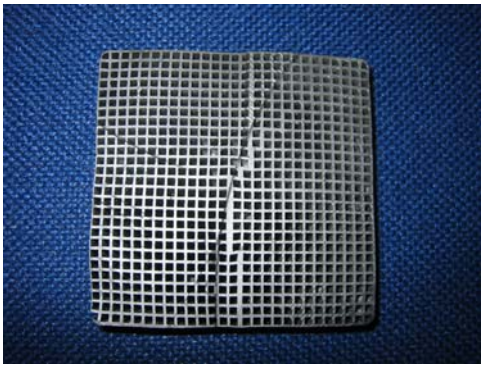

Alternative SiC manufacture route: CVD green extrusion followed by siliconising

The design, building and testing of a stator-less contra-rotating model turbine is aerodynamically similar to the real turbine for the engine concept. This will be run on a low pressure high molecular weight gas, i.e. argon, which can simulate the high pressure helium used in the engine. REL prepared an initial scoping design for the real engine **[D3.2.1]** for which VKI have optimised the aerodynamics **[D3.2.2]**. CENAERO scaled and optimised the helium aerodynamic design to the model **[D3.2.3]**.

The turbine rig design was completed in the first half of 2007 **[D3.2.4]** and the various components placed for tender. There were many unforeseen delays with subcontractors (including one company bankruptcy) and cost escalations during the latter half of 2007 and as a consequence the entire test program is now running late.

The argon system (comprised by hot water supply, boiler, super-heater, ducting and flow meter) was installed and pressure tested by the end of November 2007 but the turbine and its dynamometers were not delivered to site until mid March 2008. The turbine casing was a major cost-overrun item and as a result expenditure on other LAPCAT items (WP3.1) was not allowed to exceed their budget. The test results are reported in **[D3.2.6]**.

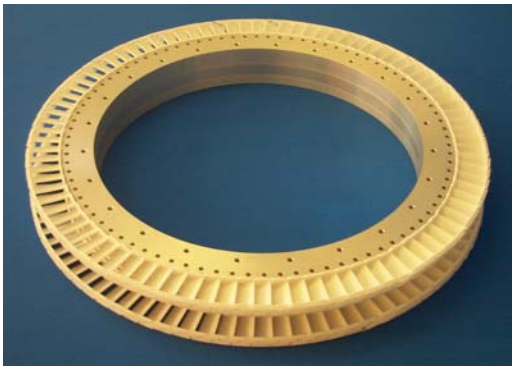

Rotors 1 and 3 [D3.2.5]

Rotors 2 and 4 [D3.2.5]

Turbine inlet casing

Turbine and Dynamometers on Bed Plate [D3.2.5]

Argon Supply System: Boiler (most remote from camera), Superheater, flow control valves. The 5tonne water supply tank is extreme right of picture.

Turbine and one of the two dynamometers. The argon inlet diffuser enters from the left of the picture.

Complete turbine test rig. In the foreground is the 5 ton hot water tank and the water feed pump. In the background is the argon supply system and to the right the turbine and dynamometers.

2.2.3 WP4 System Study for RBCC

The initial work on RBCC mainly concentrated on deriving first performance figures to be used in the context of vehicle pre-design and analysis. This was accomplished by providing net Isp figures over a wide flight Mach number range such that absolute dimensioning could be avoided in the initial absence of requirements derived from a vehicle concept **[D4.2.1, D4.4.1]**.

LAPCAT-M8 is considerably enlarged compared to other known hypersonic vehicle concepts to accommodate the passengers and to meet the ambitious LAPCAT range requirement. The configuration uses hydrogen as fuel and two complete design loops had been performed until November 2005 by DLR-SART and results are presented in deliverable [D2.2.1] and [D4.2.1]. The skipping cruise trajectory was initially proposed for LAPCAT-M8 for the reason of better thermal management. Further, a conventional cruise trajectory has been assessed on its feasibility and performance. This third loop has been performed about one year after completion of the first two sizing loops in November 2005. The geometry has been completely redesigned and the latest –M8-3 configuration is presented in the following figure. An iterative definition of the air-intake, the propulsion system, and the nozzle is included and all these parts have been investigated numerically and experimentally. Taking these data, as far as available, into account a resizing and a new vehicle mass estimation has been started followed by trajectory analyses of a conventional cruise and an innovative skipping flight.

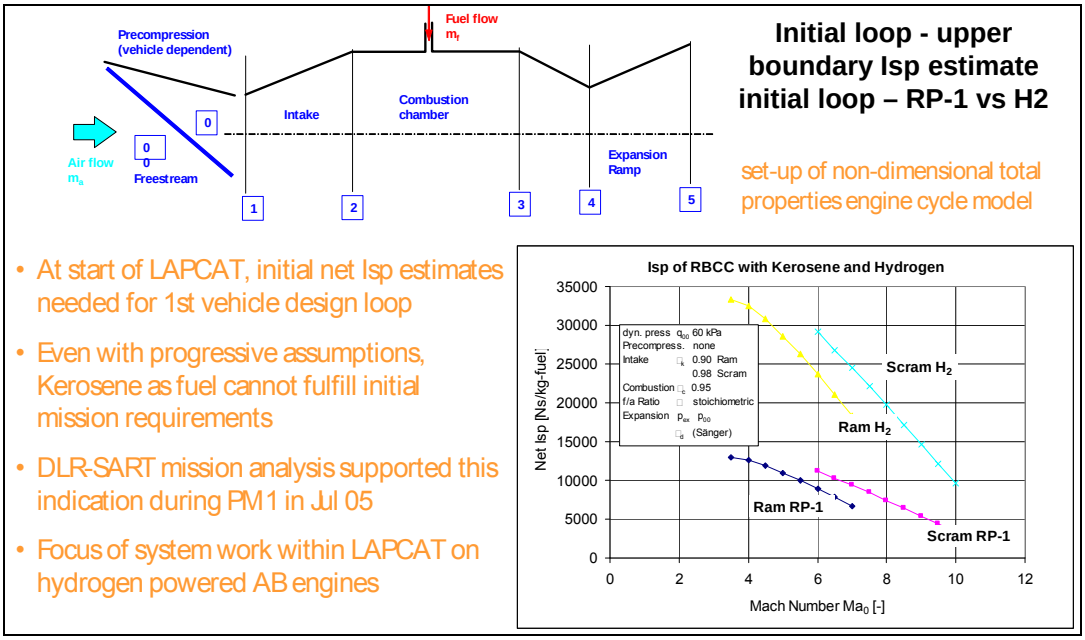

Initial upper boundary RBCC Isp estimates (sample) for RP-1(Rocket Propellant-1) and hydrogen. Note the progressive combustion efficiency and total pressure loss assumptions in the scram Isp values.

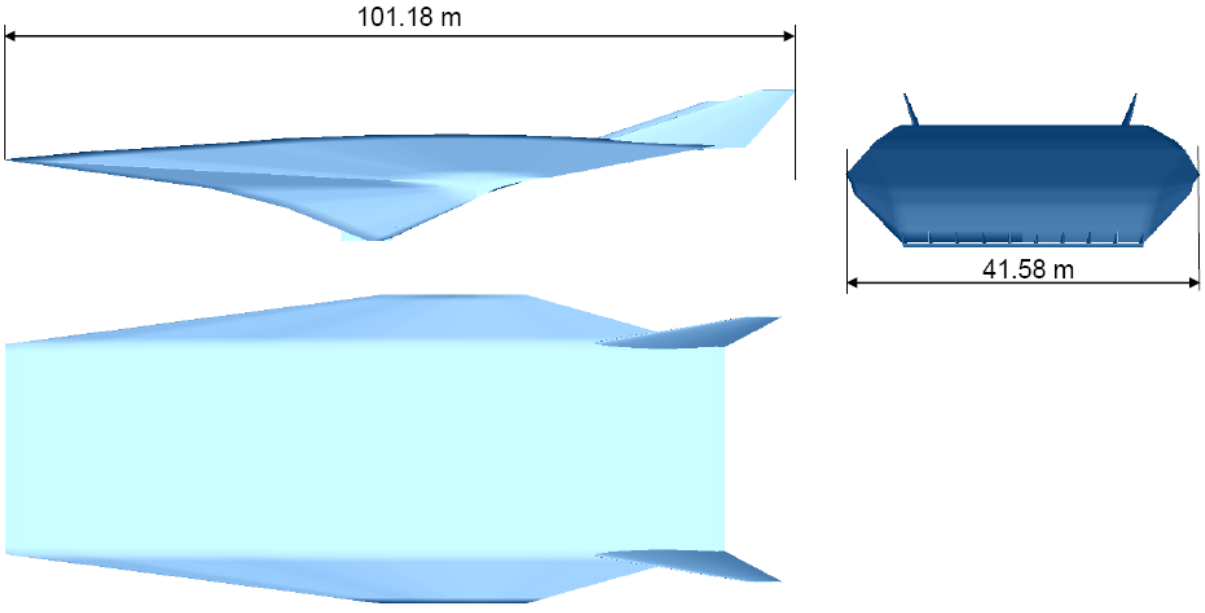

Generic Mach 8 RBCC hypersonic cruise airplane

The reduced propulsion Isp compared to the previous configuration required a considerable size growth of LAPCAT-M8. Take-off mass is almost 950 ton, however, the design is no longer aiming to fulfil the extremely ambitious LAPCAT range requirement of the Brussels to Sydney route. Under realistic conditions for vehicle mass a flown distance between 5200 and 5800 km might be achievable depending on the cruise mode and applied control algorithms.

The total take-off mass of the hypersonic cruise airplane has been iterated to 943.5 ton within the latest sizing loop, which is well beyond any aircraft built to date. This value is similar to heavy lift launch vehicles, and already about 160 ton beyond the Ariane 5 ECA launcher's lift-off mass. Although the flight performance of LAPCAT-M8 and its outsize dimensions and mass on the first look are somehow sobering, it is to be noted

that the presented trajectories and achieved range of this report are in no way based on worst case assumptions.
One of the reasons for the less than impressive performance of LAPCAT-M8-3 is its disappointing aerodynamic performance in terms of lift over drag ratio. Whereas a slim design would result in a better aerodynamic performance, the need to integrate large hydrogen volume tanks resulted in a bulky vehicle. The analyses further reveal that an RBCC without an enormous thrust excess operates too long in an unfavourable fuel consumption regime, depleting about two-thirds of the totally available fuel. The mission is flown in the ejector mode up to a Mach number of 2.5 when switching to pure airbreathing RAM-SCRAM-mode is performed. After finishing the third iteration loop of the LAPCAT-M8 preliminary design the concept cannot be considered as converging.

The vehicle-propulsion integration proved to be a difficult exercise and was underestimated at the set-up of the project. Based on the lessons learnt from the DLR design study, a redesign of the vehicle was suggested by ESTEC. The aim was to ensure a good aerodynamic performance for both subsonic and hypersonic speeds along with a large volume for hydrogen fuel, an alternative propulsion unit for the acceleration phase with enough thrust and finally, realistic dry and gross take-off weights. The dual mode ramjet propulsion unit was kept for the acceleration and cruising at Mach 8. The challenge was to ensure that each of the components, i.e. aerodynamics, propulsion performance, volume and weight would not degrade the other when combining them.
This optimization loop resulted in a dorsal placement of the propulsion unit, including the large intake ramp and nozzle **[D2.3.1]**. The aerodynamic performance was realized by using a blend of a waverider and a delta wing previously developed by DLR-AS for a Mach 12 speed. The poor performance of an ejector rocket was addressed by replacing it with a gas-generator fed air turbo-rocket which has a good and nearly constant specific fuel consumption over a wide Mach number range. Moreover, this choice also allows for efficient cruise over land in a subsonic mode, to loiter and to ensure the containment of jet noise. This turns the aircraft into a versatile and operationally flexible vehicle.

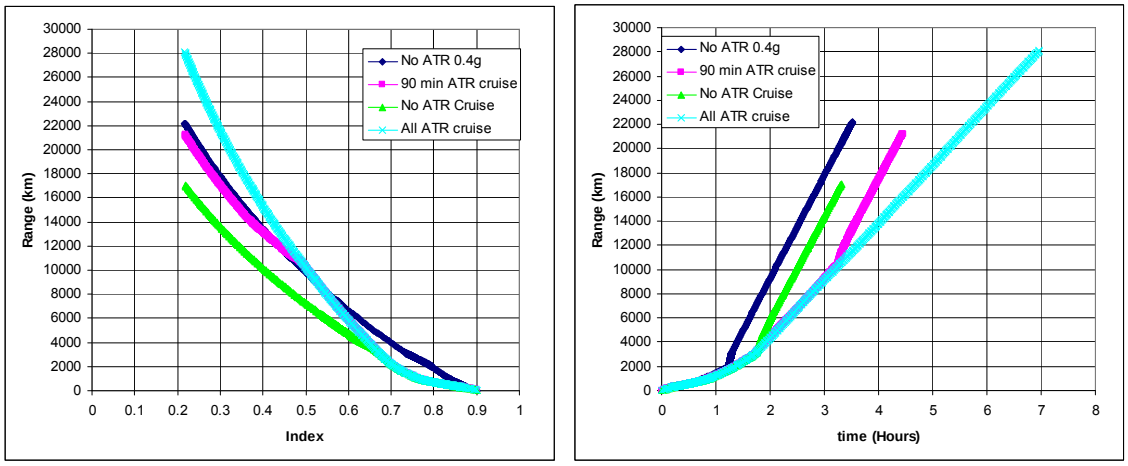

Achievable ranges and flight duration in function of structural index and different flying strategies for a Dorsal-Type Mach 8 vehicle: one curve is related to a higher acceleration load

The achievable range is strongly sensitive to the allowable acceleration loads. Higher loads lead to lower fuel consumption during the acceleration phase. The maximum g-loads on the passengers are limited to 0.2 and 0.4g in all directions. The GTOW was fixed at 600 ton which corresponds to the present achievement in classical aircraft, e.g. the Antonov-225 with a 600 to 640 ton GTOW and a 170 ton of empty mass. A 400km range with subsonic cruise was imposed prior to acceleration to supersonic speeds along with a controlled and powered deceleration phase. This first leg ensures that the aircraft is flying subsonically over land and then supersonically once over sea. Depending on the flying strategy, the vehicle turns out to have a range varying from 14000km to 22000km with a touch-down weight of 240 ton. The corresponding structural index (dry weight to GTOW) for these weights is fixed at 0.3, or 180 ton. A total of 60 ton for 300 passengers and accommodation, i.e. cabin, luggage, crew, galleys… is taken from the LAPCAT A2 vehicle estimates. The length, span and height are respectively 90m, 62.2m and 18.1m compared to 84m, 88.4m and 18.1m for the An-225. The internal volume of the concept can accommodate the 360 ton of fuel needed with a reserve volume of about 1100m^3 or 80 ton of fuel weight. The vehicle control is not examined in detail but consists presently of two all-moving fins with dihedral and ailerons for roll and pitch.

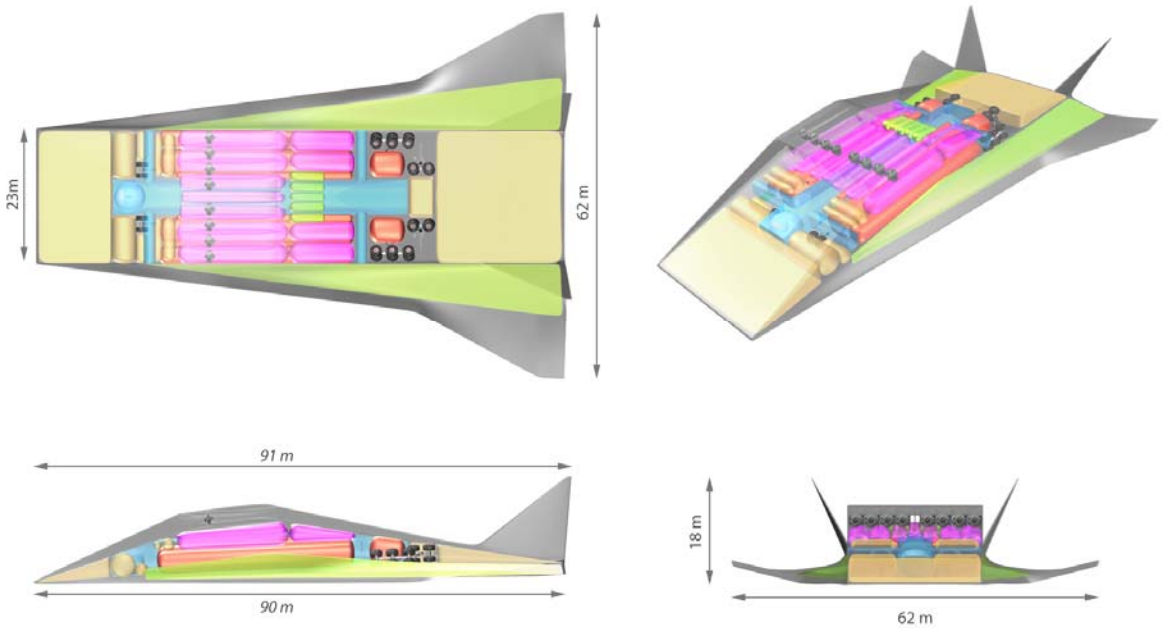

LAPCAT-MR1: Conceptual Design of a Dorsal-Type Mach 8 vehicle: blue indicates the passengers' area, other colours define different fuel tank shapes.

With this alternative design, the envisaged mission Brussels-Sydney is physically possible with part of the trajectory at a cruise flight Mach number 8.0 using a hydrogen-fuelled scramjet and a tuned trajectory strategy. Due to its versatility, the vehicle can optimize its operation for different long haul trajectories with flight times varying between 3 to 5 hours. The three hours trajectory profile corresponds to a total of 30' of acceleration and a cruising at Mach 0.8 with a range of 400km ensuring flying subsonically over land. Once over sea, a 10' acceleration allows to reach Mach 8 (axial load of 0.4g with a covered range of 2725km), followed by a 90' cruise at Mach 8 for 12,375km and a final descent and deceleration for 50' for 2200km. This total journey amounts to 17,700km which can be extended by cruising for some time at Mach 4-4.5.

The selected efficiencies or operational points for the different vehicle components were deliberately chosen as conservative allowing to account for margins and to avoid too optimistic conclusions. Further refinements with clear overall improvements are possible and within reach in the directions of:

- Aerodynamics: optimizing waverider design to cruise Mach number rather than the presently available M=12 shape due to decreased spillage and hence increase of L/D ratio,
- Propulsion: performance increase of air-turbo rockets by fuel pre-heating and switching towards expander cycles, of ramjet and scramjet by tuning the geometry wrt thermal choking…
- Improved intake efficiency,
- Optimizing the trajectory strategy in particular during the acceleration phase.

Detailed studies are still needed for the moveable intake geometry and its optimization towards a robust but lightweight configuration. The same applies for the nozzle.

A kerosene-fuelled high-speed propulsion system could not perform the mission due to the lower chemical energy content per kg of kerosene. Instead, a second design path to be followed was to pre-design a kerosene-fuelled ramjet RBCC for a flight Mach number of 4.0, where the range (thus the efficiency of the kerosene-fuelled RBCC) was to be maximized.

Basic RBCC architectures have been derived, intakes for the M4 and M8 RBCC propulsion system have been designed and cross-checked, guidelines for scramjet combustor and SERN dimensioning have been set up in order to achieve baseline system dimensions and cruise flight performance figures **[D4.2.1]**. These guidelines and new numerical results from CFD investigations could be used to systematically improve the RBCC model parameter input settings, like friction coefficients and combustion efficiency assumptions.

These in turn helped to obtain representative thrust, dimension and performance figures for the RBCC design point as well as for flight trajectory variations under discussion.

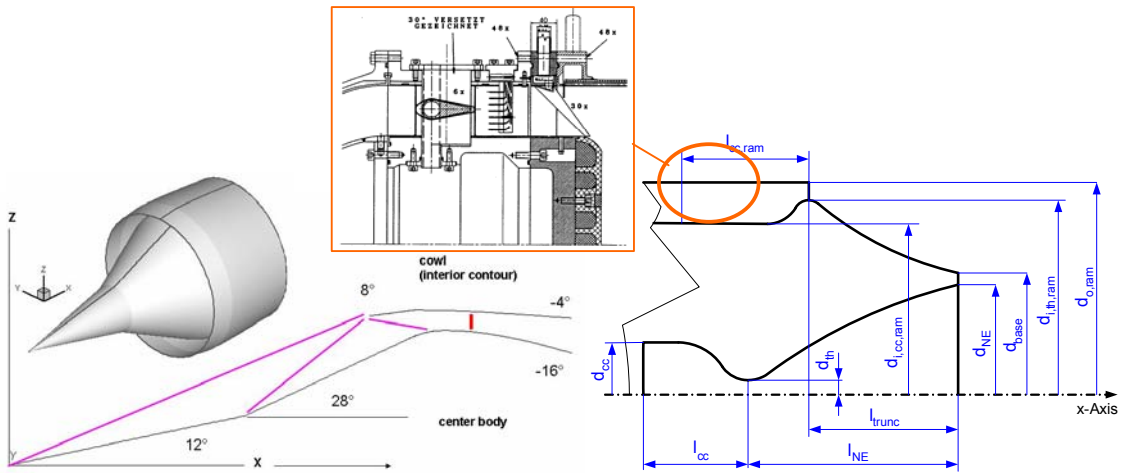

Rotationally symmetric RBCC concept (intake, annular ram combustor, truncated plug nozzle) for LAPCAT M4 vehicle

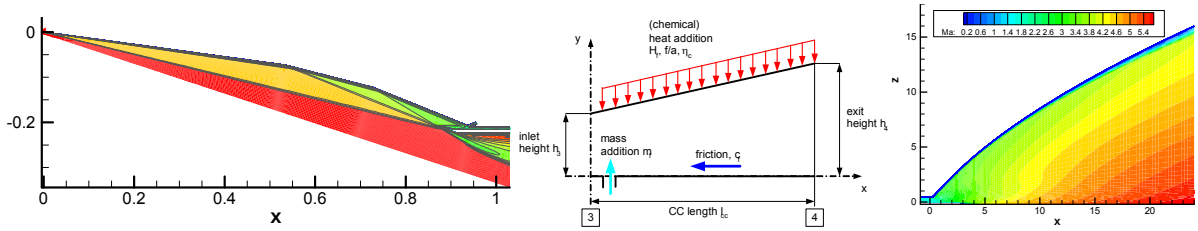

RBCC concept design and pre-dimensioning for LAPCAT M8 vehicle (intake, combustor, SERN)

This process was continued in the remaining period of LAPCAT by extending the design and performance estimation work to the other trajectory operational points and modes, like the ejector mode - as recommended during the mid-term review. Snecma came up with an improved analytical ejector model, integrated into their engine analysis tool COSAP and with a proposition for a mechanical ejector concept on which patent deposit has been realized by Snecma **[D4.1.2, D4.1.3].**

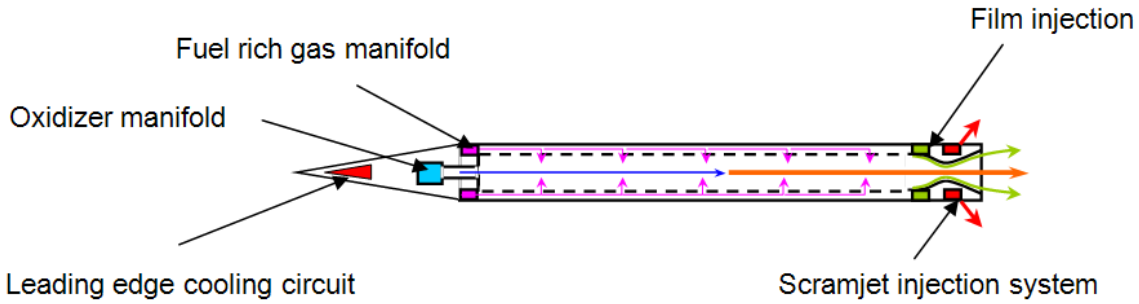

Ejector concept sketch

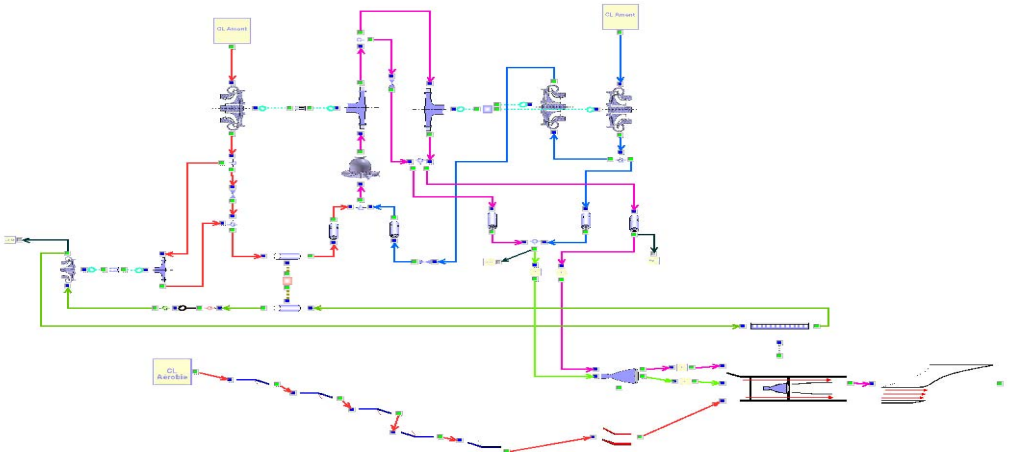

Propulsion system COSAP model graph – Take-off configuration

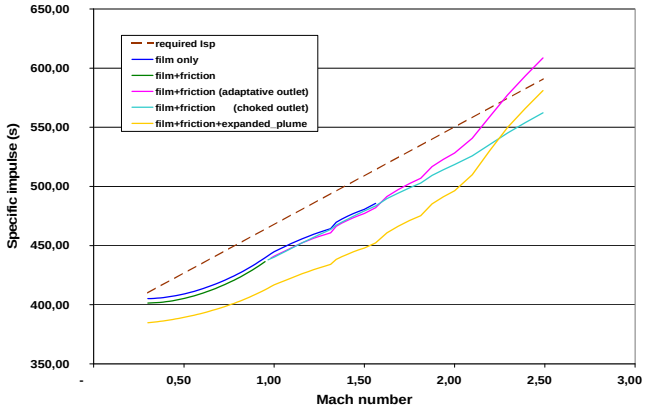

Ejector mode specific impulse evolution

From wall heat and pressure loads and cooling dimensioning data, first concepts on the structural configuration and thermal management of the M8 RBCC components were derived by EADS **[D4.2.3]** and DLR **[D4.2.2]**.

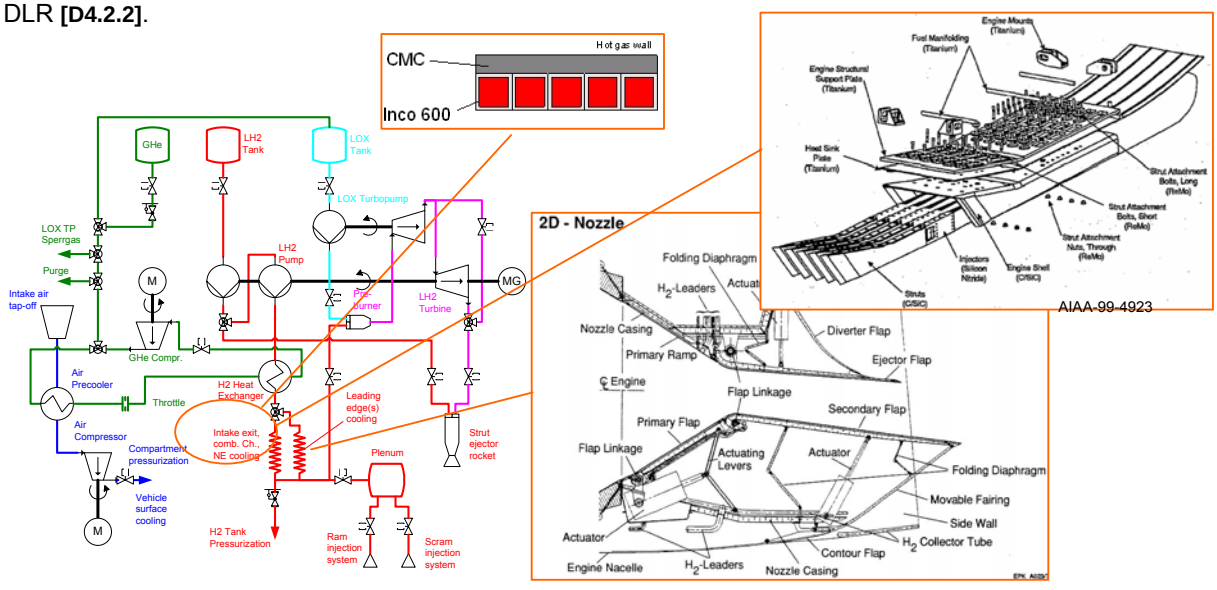

RBCC powerpack concept, thermal management and structural concept considerations

These concepts were used by DLR for first, parametric RBCC engine mass estimates. For the flight design point, the hydrogen propellant budget for the M8 RBCC appears to be conceptually sufficient for thermal cooling of the RBCC engine including forebody ramp and leading edges. The necessary auxiliary propulsion system however turns out to be unexpectedly complex even in the overall configuration in order to fulfil basic requirements derived from mission and functional analysis. DLR's M8 mass assessment highlighted the large, heavy, and partly moveable structures necessary for the RBCC due to the pressure and thermal loads encountered during Mach 8 flight.

Despite a recommendation in this respect from the mid-term review, this basic research programme could not meaningfully be tasked with the very heavy engineering work of deriving a consolidated RBCC system design concept, especially in the light of the conflict between the task, and the relatively small allotted resources within LAPCAT. Thus the system work package was confined to investigations of the main issues, and the general proposition of principle solutions.

2.2.4 WP5 Combustion Experiments

The main objective of the combustion experiments is to enhance the understanding of combustion physics which is a common key research topic to all advanced propulsion concepts. This Work Package covers experimental investigations of a wide range of relevant phenomena such as combustion under high-pressure or supersonic flow conditions, fuel preparation issues (atomisation, break-up…), turbulence and chemistry interaction, ignition delays and flame stabilization. The work package is divided into 4 tasks:

5.1. Supersonic Combustion Experiments in a Connected Tube Facility
5.2. Supersonic Combustion Experiments: Complete Airbreathing Engine
5.3. High Pressure Combustion Experiments: HC Disintegration Processes
5.4. High Pressure Combustion for LOX/HC

Task 5.1 Supersonic Combustion Experiments in a Connected Tube Facility

The main goal of the supersonic combustion experiments in the DLR connected tube facility M11 was to demonstrate the influence of the external shape of two different strut injectors on the mixing enhancement and pressure increase by the heat release due to combustion. In order to provide a reference data set for numerical code validation, measurements along the entire length of the model combustor were performed applying various optical diagnostic tools **[D5.1.1]**.

The scramjet combustor experiments were conducted at the DLR Lampoldshausen M11-4 test bench of the M11 test complex. The test bench was made up of an air heater at which various experimental setups can be mounted. The air heater is able to produce hot air under pressure with total temperatures of up to $T_{t,air}$=1500K by using H_2/O_2-burners. The oxygen mole fraction of the hot gas flow was kept constant at 21% by adding additional oxygen. The hot vitiated air was then expanded through a Mach 2 Laval nozzle into the actual model scramjet combustion chamber.

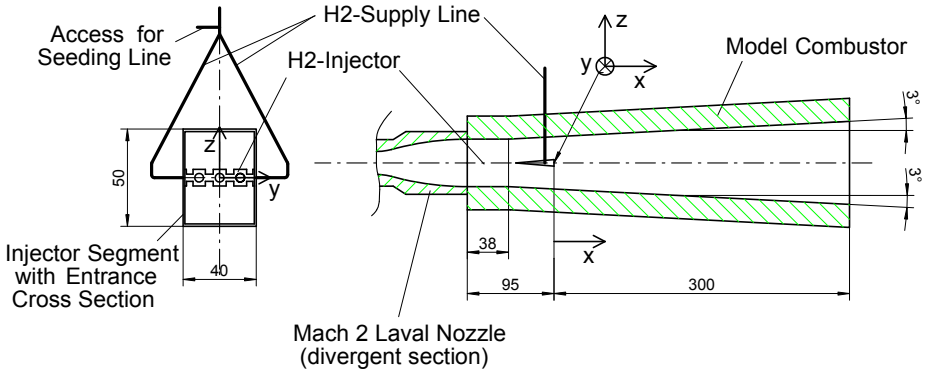

Scramjet model combustion chamber with installed injector.

One of the two hydrogen injectors, which are subject to this study, was installed horizontally at a time, spanning the combustion chamber from the left to the right side wall as can be seen in the sketches below. The injector nozzles were designed to introduce the gaseous hydrogen at a Mach number M_{H2}=2.3 into the Mach 2 air flow. The combustor entrance cross section had a width of 40mm and a height of 50mm. The combustion chamber width was kept constant. After 38mm of constant chamber height the top and bottom walls had a 3° opening angle to avoid thermal choking in reacting flow conditions. Windows were located on both side walls as well as on the top and bottom walls of the combustor for optical access. This allowed application of various optical diagnostic tools to the flow field and combustion process over the entire length of the model combustor. Various experimental techniques such as Particle Image Velocimetry (PIV), Laser-Induced Florescence (PLIF), spontaneous OH-emission, etc. were used.

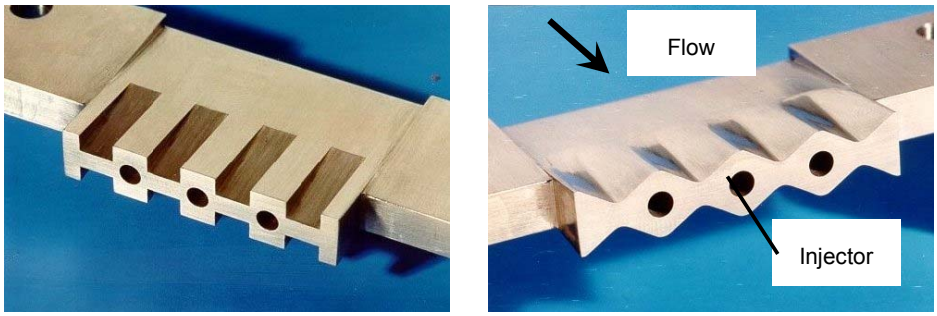

Studied injectors; left: USCER injector; right: WAVE injector.

Both studied injectors are wedge injectors and differ with respect of their outer shape. They were designed to produce gradients of static pressure, density and flow velocity over their surface, normal to the main flow direction. These gradients lead to downstream vortices, which are known to cause mixing enhancement. The USCER injector (left image of figure above) exhibits compression ramps and expansion ramps (or expansion troughs) both on the top and the bottom surface, creating areas of relatively compressed flow over the ramps and relatively expanded flow through the troughs. The thus created gradients in velocity, static pressure and density, which are oriented normal to the main flow direction, lead to downstream oriented vortices. The WAVE injector, in contrast to the USCER injector, has no such sharp geometrical discontinuities to produce the streamwise vortices. However, the wave shaped surface geometry causes gradients normal to the main flow direction of the above described kind.

The static wall pressure distributions at the top wall along the combustion chamber streamwise coordinate for both injectors at two different air flow conditions is shown below. In test case TC1 an air total temperature $T_{t,air}$=1300K and in TC2 a higher temperature $T_{t,air}$=1400K was used. The origin of the x-coordinate is located at the base of the injectors.

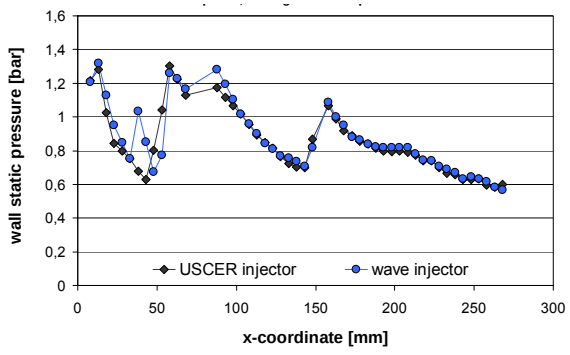

TC1 (non-reacting ("cold") test case, $T_{t,air}$=1300 K). Data points are averaged over experiment duration.

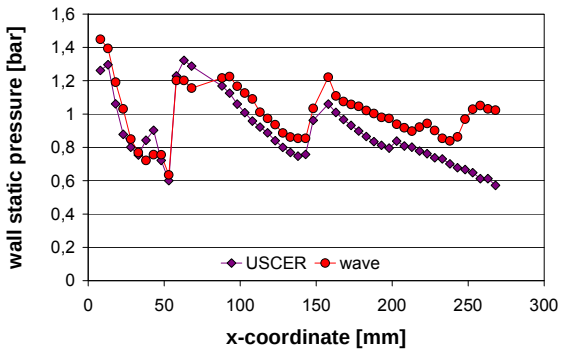

TC2 (reacting test case, $T_{t,air}$=1400 K). Data points are taken at experiment elapsed time t=3.224 s.

Wall static pressure distribution at the top wall for USCER and WAVE injectors; $T_{t,H2}$=300K, $\dot{m}_{H2}$ =12g/s.

The pressure traces can be correlated with the positions of the trains of shock and expansion waves, which are e.g. visible on Schlieren images. The left diagram shows the data from experiments with the lower air total temperature $T_{t,air}$=1300K, where no chemical reaction was observed. The pressure traces of both injectors are similar over the whole measured range, which indicate similar flow fields. The pressure traces at the higher air total temperature $T_{t,air}$=1400K (TC2) of both injectors, however, where combustion occurs, are quite similar only up to ca. x≈60mm as. Downstream the second pressure maximum, higher pressure values were measured for the WAVE injector in comparison to the USCER injector. This pressure difference becomes even larger downstream of the third maximum at x≈170mm. Also, the second pressure maximum at ca. x=70mm of the WAVE injector pressure trace is broader than for the USCER injector.

For the determination of the mixing characteristics of both injectors a Mie scattering setup with a KrF-Excimer laser emitting at a wavelength of λ=248nm together with an ICCD camera was applied. The emitted light was formed into a light sheet and guided to traverse the combustion chamber from top to bottom in the x-z-plane at y=0mm (center plane) and y=-5mm (halfway in between two injector nozzles). The hydrogen jet was seeded with Aerosil R812 particles to enhance the contrast between the H_2 jet and the surrounding air flow. From the obtained Mie scattering images, profiles of measured scattering intensity were evaluated at various x-coordinates in order to determine the H_2 jet thickness. This was determined to be the extension of the intensity profile at the point, where half the maximum intensity was measured, resulting in D_{FWHM} (full width at half maximum).

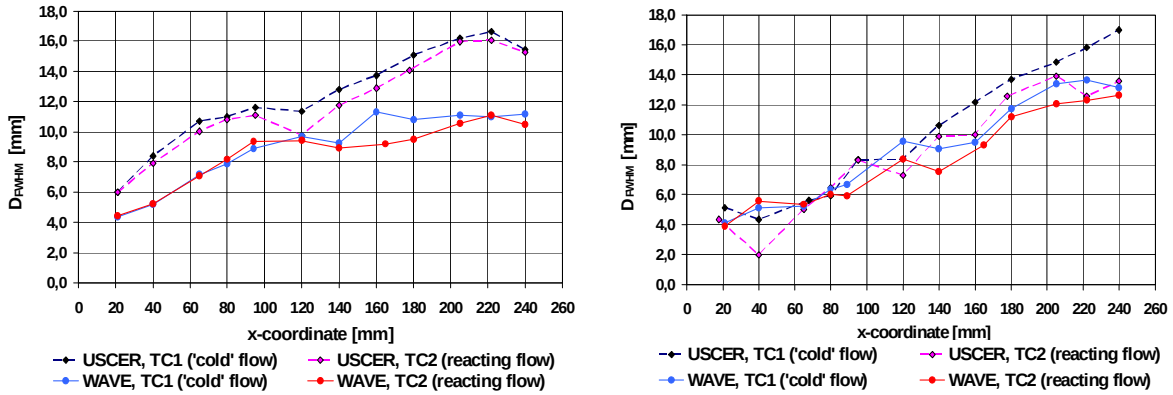

Growth of D_{FWHM}; left: center plane at y=0mm; right: measuring plane at y=-5mm.

The hydrogen jet thickness D_{FWHM} in the two measuring planes for both injectors and for both test conditions TC1 and TC2 are shown above. The diagrams reveal that injection from the USCER injector results in larger D_{FWHM} at both measurement planes. It is also obvious that D_{FWHM} is smaller for the reacting flow condition than for the pure mixing flow of TC1. Also can be seen on the right diagram (at y=-5 mm) that the D_{FWHM} growth rates of both injectors have strong similarities. Up to x≈120mm similar jet thickness D_{FWHM} values have been measured for both injectors, while downstream the USCER injector shows noticeably higher values. According to these measurements it is likely that the hydrogen-air-interface caused by the USCER injector is more convoluted in the near field of the injection while being rather flat in the far field and vice versa when installing the WAVE injector. Thus this convolution in the second half of the combustor seems to favour a rapid heat release as could be observed when using the WAVE injector.
In summary it can be stated that the obtained results show that the outer shape of the investigated hydrogen injectors has a distinct influence on the mixing and combustion process inside the model scramjet combustor. Laser diagnostic measurements of the extension of the hydrogen jet delivered indications that for the WAVE injector a more favourable 3-dimensional structure of the hydrogen-air-interface and mixing layer was created, resulting in a noticeably higher heat release in the reacting flow case.

The objectives of this task, the collection of a comprehensive set of experimental results suitable for validation purposes of CFD tools for a characteristic set of combustor entry conditions, have been achieved **[D5.1.2]**. Among the provided experimental data of supersonic hydrogen / air combustion obtained in the M11 test facility are wall pressure distributions taken with static pressure measurements, temperature profiles from CARS measurements, Mie scattering for the determination of the mixing characteristics and velocity data from PIV. Additionally, qualitative information about the position of shock waves as well as the mixing intensity at some position downstream of the injector which have been deduced from flow visualisation studies.

Task 5.2 Supersonic Combustion Experiments: Complete Airbreathing Engine

The supersonic combustion experiments of a complete generic scramjet configuration consisting of intake, combustor and nozzle were performed in the DLR High Enthalpy Shock Tunnel Göttingen (HEG). This is a unique European test capability of integrated scramjet configurations. The tests concentrated on the scramjet configurations used during the HyShot flight experiments. Due to the involvement of DLR in the HyShot I and II flight experiments, wind tunnel data of WP5 and the numerical data from WP6 could be compared to flight data. For the test campaign in HEG a new wind tunnel model of the HyShot II and IV configuration with improved spatial resolution of pressure and heat flux measurements and allowing high speed flow visualisation was designed and built **[D5.2.1]**.

The evaluation of the free stream conditions in the test section of the HEG free piston driven shock tunnel was based on numerical analysis using a suitable set of measured input parameters. First, the nozzle reservoir conditions were determined performing a 1-dimensional computation of the shock tube flow. Based on these nozzle reservoir conditions, the free stream was subsequently determined by numerical computation of the nozzle flow. Different RANS turbulence models were applied in combination with thermal equilibrium and non-equilibrium computations to determine the influence of different modelling assumptions on the obtained free stream conditions. The chemical non-equilibrium 5 species and 5 reaction rates set by Gupta was utilised for this investigation. Previous studies show good performance of this model for chemical relaxation in high enthalpy wind tunnel nozzles. The considered species are molecular and atomic nitrogen and oxygen (N_2, O_2, N, O) and nitric oxide (NO). Numerical results for the Pitot pressure profile (Pt2) at the nozzle exit plane in the HEG test section are shown below.

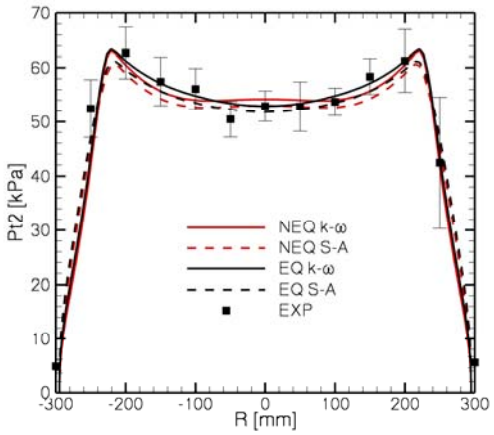

Pitot pressure profile at the nozzle exit for different models to describe the influence of turbulence and thermal relaxation in the nozzle flow (NEQ: thermal non-equilibrium, EQ: thermal equilibrium, S-A: Spalart-Allmaras turbulence model, k-ω: Wilcox k-ω turbulence model, EXP: experiment); 32km flight altitude.

Good agreement is observed between the CFD prediction and the Pitot rake measurements **[D6.5.3]**. The shape of the Pitot pressure profile changes with the assumption of thermal equilibrium or non-equilibrium. This is due to different ratios of specific heats in the region downstream of the nozzle throat caused by sudden vibrational freezing, which changes the local Mach number distribution and therefore the characteristics inside the nozzle. The shape of the boundary layer is predicted to be slightly different between the Spalart-Allmaras and the Wilcox k-ω turbulence models. The best agreement with the available experimental data (also the static pressure measurements, not shown here) was achieved with the application of the Wilcox k-ω turbulence model and the assumption of thermal equilibrium.

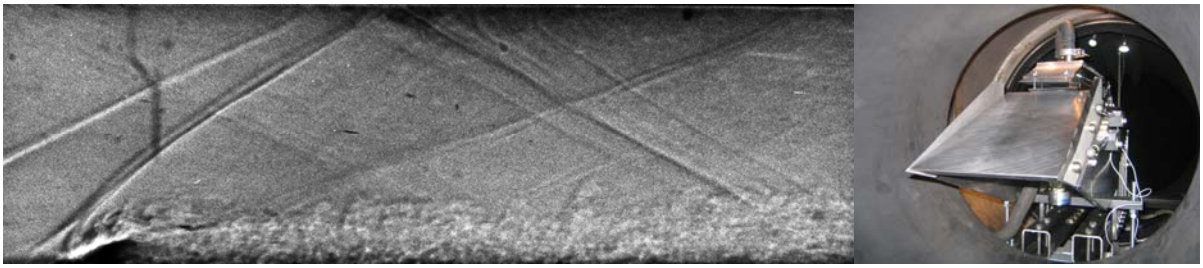

Schlieren visualisation of the wall normal gaseous hydrogen injection in the HyShot II combustor (left) and wind tunnel model installed in the HEG test section (right).

The flow path geometry of the wind tunnel model which is used in the LAPCAT ground based testing campaigns is identical to the fuelled flow path of the flight configuration of the HyShot II and HyShot IV supersonic flight experiments. This was done in contrast to the original plan to use the fuel-off and fuel-on sides of the flight geometry simultaneously in the HEG test section. The two reasons to use only one of the two flow paths, which can be run in either a fuel-off or fuel-on mode in the planned test campaigns are:

- To enable complete and detailed optical access to the combustion chamber, the model must be positioned such that the combustion chamber and test section windows are aligned. Therefore, the second flow path can not be positioned in the test diamond;
- By using only one model and performing only a fuel-off or fuel-on test, the model can be instrumented twice as much as each separate model in the dual model configuration.

During the process of defining the internal flow path geometry it was decided to modify the existing HyShot model in such a way that a second flow injection technique referred to as the HyperMixer configuration can be investigated. This geometry was used in the framework of a JAXA (Japan Aerospace Exploration Agency) scramjet flight experiment, which was launched as part of the HyShot program (HyShot IV) in March 2006. A successful flight of HyShot IV would have provided the opportunity to be able to compare two different types of fuel injection and the resulting mixing and ignition process obtained in wind tunnel tests and flight. Due to the failure of the flight experiment, no flight data will be available and the comparison will be restricted to wind tunnel and CFD data. However, compared to the original goal to use only one combustion chamber and ignition geometry, the chosen approach significantly increases the output of WP5. The injection, mixing and ignition process is the key technology for the development of an operational scramjet engine.

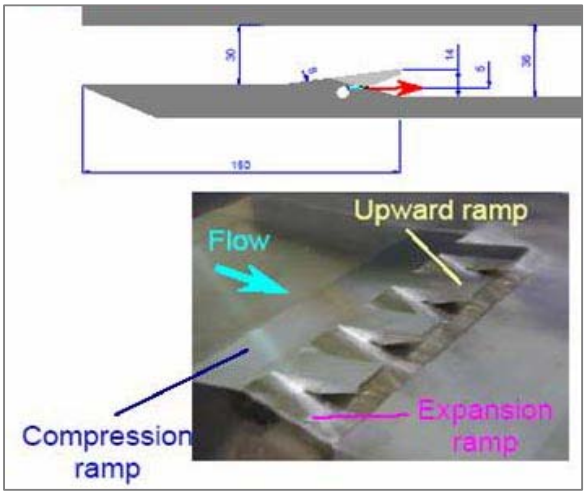

Hypermixer fuel injector configuration.

The initial plan was to modify the existing HyShot wind tunnel model. However, during the design process it became evident that for flow visualization of the combustion chamber and to enable both the HyShot and HyperMixer fuel injectors to be tested, a completely new model was required. In order to avoid a significant delay in the delivery of the new wind tunnel model, the planned workshop resources were redirected to personnel costs in the spacecraft section for the design of the new models. The LAPCAT scramjet wind tunnel models, including the instrumentation, has been designed and drawn in 3D using Auto-Cad 2004 **[D5.2.1]**. Compared to previous HyShot investigations in HEG, several improvements have been made regarding the model instrumentation usage and positioning. Further, recent research in HEG which was performed in the framework of the development of new operating conditions, showed that the pre-existing condition, which was planned to be used for the LAPCAT HEG campaigns, could be significantly improved. Therefore, the work plan was modified in order to successfully realize these improvements.

Two operating conditions related to HyShot II flight altitudes of 28km and 33km were applied. Surface pressure and heat transfer measurements on the intake, the combustor and the exhaust were performed. Further, high speed flow visualization of the injection process was obtained **[D5.2.2]**. The constant area combustor duct of the HyShot II configuration was designed to operate in a steady supersonic combustion mode up to a fuel equivalence ratio of $\Phi = 0.3$. With increasing equivalence ratio, a threshold value regarding the pressure rise in the combustor will be reached above which boundary layer separation und subsequent

unstart can occur. The knowledge of these phenomena is important in order to judge the performance characteristics of a scramjet engine. Therefore, experiments were performed in HEG with the HyShot II as well as the HyShot IV configuration using fuel equivalence ratios above the critical one in order to study the resulting unsteady combustor flow and to provide a database for CFD code validation.

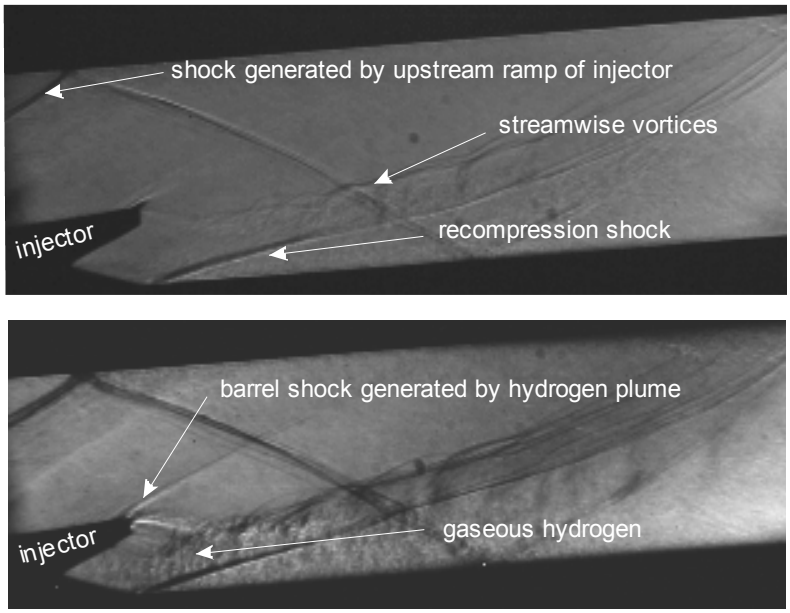

Flow visualisation of the HyShot IV combustion chamber flow in the vicinity of the hypermixer injector performed in HEG; 28 km altitude using air as test gas; angle of attack α = 0°. The images show the combustor without fuel injection (top) and with fuel injection using an equivalence ratio of $\phi = 0.327$ (bottom). Within the combustor section shown here, combustion was not yet initiated. The images were obtained using a Cordin drum camera and a HSPS NANOLITE KL-K sparcflash lamp.

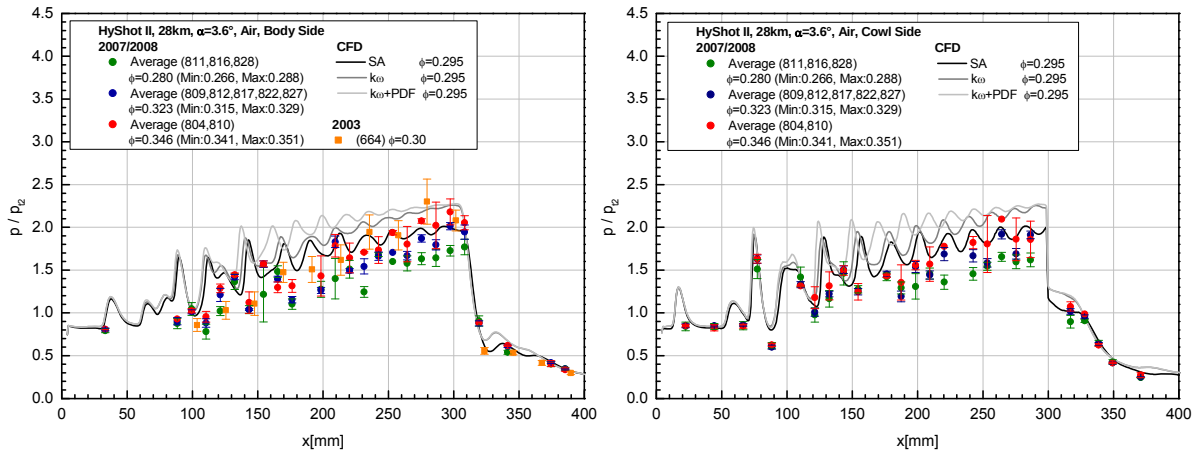

Summary of normalised surface pressure distributions on the body side obtained for the HyShot II combustor with fuel injection; 28 km altitude using air as test gas; angle of attack α = 3.6°. The CFD predictions result from the DLR TAU code using different turbulence models (SA: Spalart-Allmaras, kω: Wilcox kω, PDF: assumed probability density function approach for turbulence-chemistry interaction). The results obtained in the framework of an earlier investigation of the HyShot II configuration in HEG are also included here.

The normalised surface pressure and heat flux distributions on the body and cowl side of the HyShot II combustor with fuel injection are given in the figures above for HEG operating condition XIII (28 km) and an angle of attack of $\alpha = 3.6^{o}$. The experimental data obtained for this flow case was subdivided into three groups with different ranges of fuel equivalence ratio ($0.266 < \phi < 0.286$, $0.315 < \phi < 0.329$, $0.341 < \phi < 0.351$). Averaged values of the measured normalised pressure distributions are compared with

CFD predictions of WP6 and the normalised pressure distribution resulting from the HyShot II post flight analysis performed in HEG. The computed normalised pressure distributions were obtained with the DLR TAU code using different turbulence models and an equivalence ratio of $\phi = 0.295$. The Spalart-Allmaras model, the Wilcox kω model and the Wilcox kω model including an assumed probability density function (PDF) approach for describing the turbulence-chemistry interaction were applied. For all equivalence ratios the measured wall pressure distributions are characterised by a continuous increase along the combustor indicating supersonic combustion. The maximum normalised pressure value obtained in the combustor just upstream of the starting point of the thrust surface increases from $p/p_{t2} \approx 1.8$ to $p/p_{t2} \approx 2.2$ depending on the range of fuel equivalence ratio. The computed normalised pressure distributions depend on the applied turbulence model. In the upstream region of the combustor the obtained results are very close. However, in the middle and downstream region of the combustor, higher turbulent mixing is predicted by the Wilcox kω model resulting in a higher level of static pressure. At the downstream end of the constant area combustor, the kω model leads to a surface pressure which is about 12% higher than the one obtained with the Spalart-Allmaras model. The application of the assumed-PDF approach for the modelling of turbulence-chemistry interactions leads to a further increase of the achieved pressure level in the middle section of the combustor. Downstream of the fuel injection, the pressure increase due to combustion obtained with CFD is initially higher than the measured one. This over prediction is reduced when approaching the downstream end of the constant area combustor. The CFD result based on the Spalart-Allmaras turbulence model is in closest agreement with the experimental data. This comparison between measured and computed normalised combustor wall pressures indicate, that compared to the experiments, all the applied turbulence models predict a more effective air / hydrogen mixing process and thus a better combustion efficiency **[D5.2.2, D5.2.4]**.

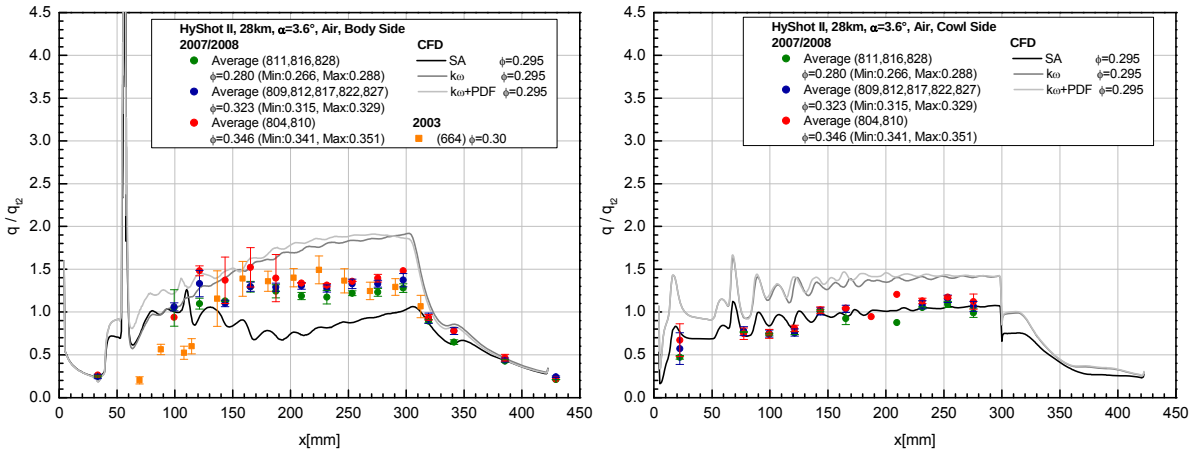

Summary of normalised surface heat flux distributions on the body side obtained for the HyShot II combustor with fuel injection; 28 km altitude using air as test gas; angle of attack α = 3.6°. The CFD prediction result from the DLR TAU code using different turbulence models (SA: Spalart-Allmaras, kω: Wilcox kω, PDF: Assumed probability density function approach for turbulence-chemistry interaction). The results obtained in the framework of an earlier investigation of the HyShot II configuration in HEG are also included here.

According to the normalised surface pressure distributions on the body side of the combustor, the continuous pressure rise due to combustion starts at $x \approx 115\ mm$. An increase of the normalised surface heat flux in this range of the combustor is more pronounced at higher fuel equivalence ratios. However, for all equivalence ratios, an increased heat flux level is observed downstream of $x \approx 115\ mm$. As can be seen in the figure above, the measured normalised heat flux is approximately constant within the combustor after the onset of combustion The heat flux level increases from $q/q_{t2} \approx 1.25$ to $q/q_{t2} \approx 1.4$ depending on the fuel equivalence ratio. On the cowl side of the combustor, the normalised heat flux level remains significantly lower than on the body side. An increase of the normalised heat flux level in the constant area combustor can be observed at $x \approx 140\ mm$.

The comparison between the measured and computed normalised surface heat flux distributions on the combustor body side reveals significant differences between the CFD predictions based on different turbulence models. Compared to the measurements, the Spalart-Allmaras model results in an under

prediction and the Wilcox kω model in an over prediction. On the combustor cowl side, good agreement between the normalised measured heat flux and the prediction resulting from the Spalart-Allmaras model was obtained.

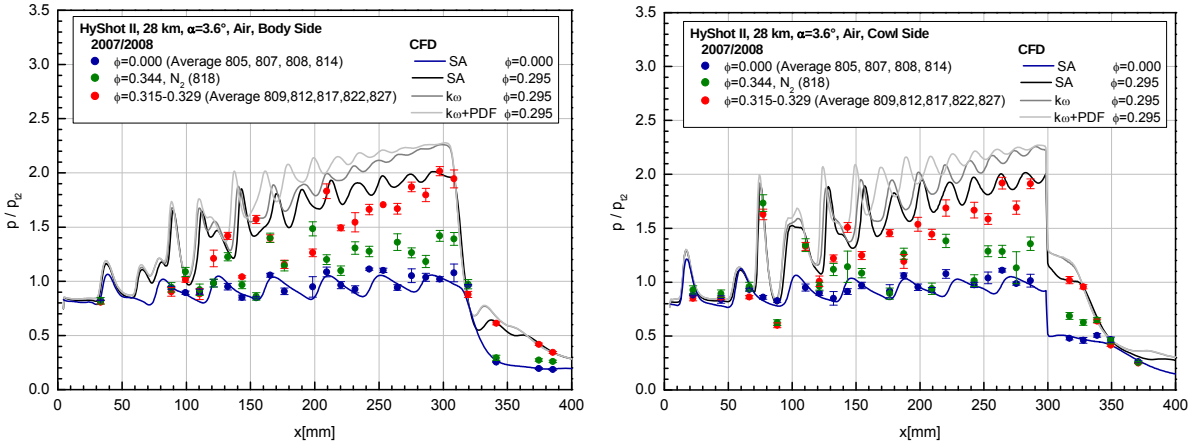

Normalised surface pressure distribution on the body (left) and cowl side (right) obtained for the HyShot II combustor with and without fuel injection; 28 km altitude using air and nitrogen as test gas; angle of attack α = 3.6°.

Normalised surface pressure and heat flux distributions on the body and cowl side of the combustor obtained from fuel off measurements as well as experiments using air and nitrogen as test gas including gaseous hydrogen fuel injection are compared in the figure above. Again HEG operating condition XIII and an angle of attack of $\alpha = 3.6^{o}$ were used. Compared to the normalised pressure distribution obtained in the fuel off experiments, the pressure level on the body and cowl side is first increased by using nitrogen as test gas including fuel injection and finally by using air including fuel injection. The pressure and heat flux distributions on the body side indicate that the combustion process starts downstream of $x \approx 115\ mm$. On the cowl side the effect of combustion can be observed downstream of $x \approx 140\ mm$.

The detailed analysis of the HyShot II flight data led to the conclusion that structural integrity of the flight model was compromised below 30 km. Therefore, comparison with the flight data was only performed for the data resulting from using HEG operating condition XIV which corresponds to a flight altitude of 33 km. During flight, the attitude of the HyShot II configuration varied with time as a result of a combination of roll and nutation. Roll is a rotation of the vehicle about its axis and nutation is a coning of the body axis about the velocity vector. Therefore, the angle of attack and the yaw angle of the vehicle changed in a cyclic manner with amplitudes that varied with time. From the flight data analysis it was extracted that in the flight altitude of 33 km, a positive angle of attack of $\alpha = 6.5^{o}$ at zero yaw angle was obtained. The measurements performed in HEG at this flight point suffer from the development of an unsteady upstream moving pressure wave possibly generated by flow separation in the downstream part of the constant area combustor. The upstream moving wave was observed after a quasi steady supersonic combustion mode with continuously increasing normalised surface pressure along the combustor duct developed. Two experiments with the fuel equivalence ratios of $\phi = 0.255$ and $\phi = 0.318$ were performed in HEG, while for the considered flight point, the equivalence ratio amounts to $\phi = 0.34$. For the comparison of the ground based testing data with the flight data, the normalised surface pressure distributions obtained in HEG were evaluated during two different test time windows in order to account for the development of the upstream moving pressure waves. The first test time window was placed during the establishment of the supersonic combustion mode while the second was selected at the end of the nominal test time window. Both resulting surface pressure distributions are compared with the normalised flight data in the figure below. During flight, a normalised surface pressure distribution with continuously increasing pressure along the combustor duct was obtained which is in good agreement with HEG data measured at the higher equivalence ratio during the early test time window. An indication of the development of an upstream moving wave is not present in the flight data. The difference between the flight and ground based test data related to the development of the upstream moving pressure wave might be related to differences in the test environment. The flight Mach number is approximately 7% higher than the free stream Mach number in the HEG tests. While the Pitot pressure of the flight experiment is well reproduced in the HEG tests, the static free stream pressure and temperature is about 13% and 18% higher in ground based testing. Consequently, the static pressure and temperature at

the combustor inflow is approximately 8% and 14% higher in the HEG experiments. The Mach number at the combustor inflow is 10% higher in flight. Therefore, the Korkegi separation pressure ratio in flight amounts to $p / p_{t2} \approx 2.7$. As can be seen from the figure below, this value is not exceeded in the measured flight surface pressure distribution.

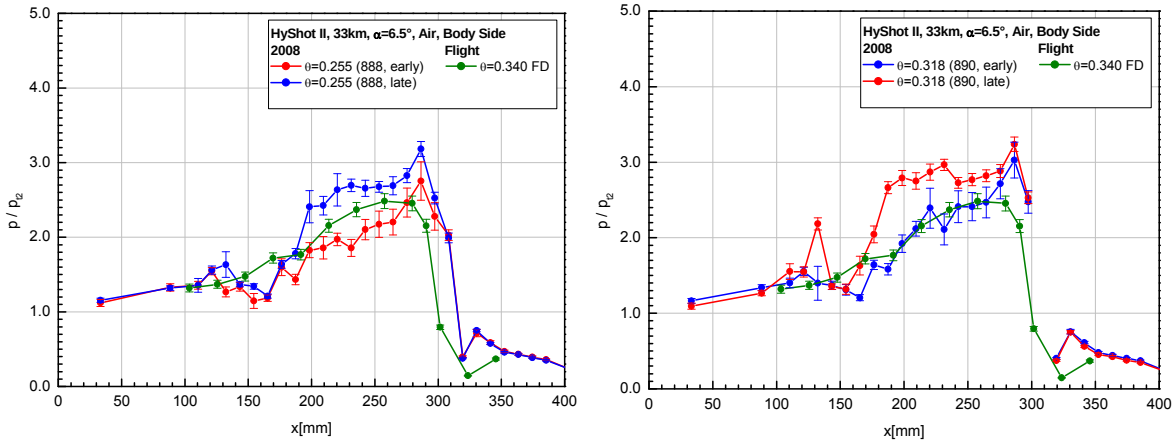

Comparison of the normalised surface pressure distributions obtained in HEG at two different equivalence ratios Φ = 0.255 (left) and Φ = 0.318 (right) with the flight data (Φ = 0.34); 33 km altitude; angle of attack α = 6.5°.

For the HyShot IV configuration steady and unsteady combustor flow cases were studied in HEG. In the figure below, a sequence of Schlieren images resulting from high speed flow visualisation of the HyShot IV combustor flow in the vicinity of the hypermixer injector using a SHIMADZU Hypervision HPV-1 digital camera and a HSPS NANOLITE KL-K sparcflash lamp as light source is shown. The images result from HEG run 870 ($\phi = 1.126$). The upper frame was taken at $t = 2.599\ ms$ during the development of the supersonic combustion mode, while the following frames show the arrival of the upstream moving wave for $t \geq 2.977\ ms$. After arrival of the wave at the injector position ($t \approx 3.5\ ms$), the shock waves upstream of the injector and in the upper part of the combustor downstream of the injector indicate regions of supersonic flow while in the lower part of the combustor downstream of the injector, the flow is subsonic.
During the first year of LAPCAT, it became obvious that a very crucial issue was the determination of the combustion chamber length of the LAPCAT M8 vehicle. Therefore, additional work was performed to further investigate the relevant phenomena and derive conclusions which supported the system design of the Mach 8 vehicle. Two directions were followed. One study was related to the aero-mechanical optimization of injector strategies whereas the other study focused on the aero-chemical scaling aspects. Both of these are detailed below.

Extensive CFD investigations for the full scale combustion chamber were performed by ESTEC to estimate the required dimensions and performance of the flight configuration combustion chamber **[D5.2.5]**. The flow conditions for this configuration are taken for a combustion chamber with a high compression intake, Mach number 3, 1bar static pressure and 1300K static temperature. The combustion chamber dimensions are related to the fullscale combustion chamber of the DLR M8 supersonic vehicle. The height of the combustion chamber is fixed at 0.3m. Following the strategy with wall injection on both upper and lower combustion chamber wall, the computational domain employing symmetry conditions is reduced to H=0.15m and a width depending on the injector spacing. The flow topology is shown below for a 5x10 cross size duct at a length of 12H=1.8m. The turbulence of the incoming air intake boundary layer needs to be considered. It enhances the mixing and combustion process which reduces the penetration and damps the vortex generated by the injection process. The combustion process changes the flow topology significantly depending on the equivalence ratio. With an equivalence ratio of Φ=1.0 thermal choking with a normal shock in front of the injector occurs. At Φ=0.7, a stable combustion process including a large subsonic reverse flow region behind the injector is observed. The combustion takes place in a subsonic region behind the injector, but also further downstream the duct where the flow is again accelerated to supersonic speed. Due to the supersonic combustion process at Φ=0.5, the averaged pressure increases almost linearly in the duct. The combustion efficiency reaches 78% at a total pressure loss of 43%. Further optimisation of the duct geometry and injector spacing will increase the maximum possible equivalence ratio. The results show that within a

combustion chamber length of 1.8m, the required combustion efficiency of 65% can be reached. Therefore, a combustion chamber length in the range of 2-4m seems to be possible.

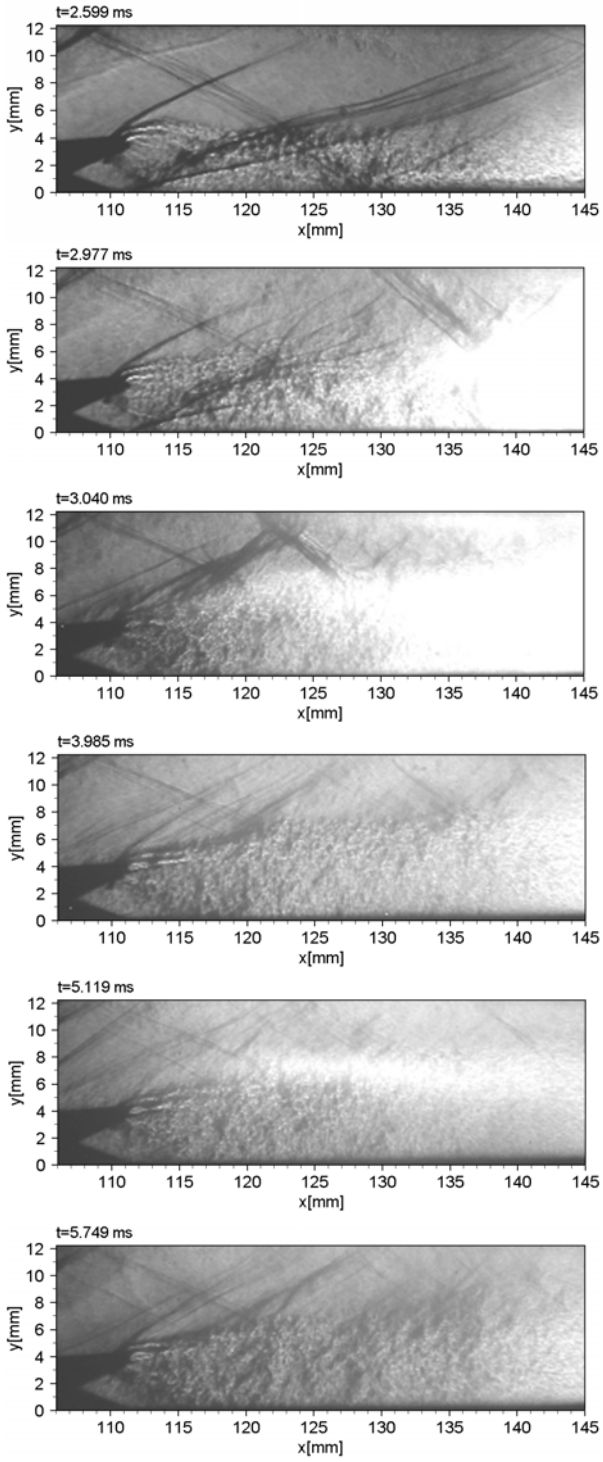

Schlieren images of the unsteady combustor flow in the vicinity of the hypermixer injector for supersonic combustion mode (t = 2.599 ms) and after arrival of the upstream moving pressure wave (t > 2.977 ms); Fuel equivalence ratio Φ = 1.126 (run 870); 28 km altitude using air as test gas; angle of attack α = 0°.

The application of the pL-scaling for a scramjet combustor with wall normal injection was investigated numerically by DLR **[D5.2.3]**. At present there is no ground based facility which is able to test a full size scramjet engine over the entire flight path of a hypersonic vehicle. On the high speed end, impulse facilities can be used to test scramjet performance but these investigations are limited by the sizes of the available test section. Due to the complexity of flight test especially at large scales and the uncertainties in the predictions of CFD tools which are still present, a strong interaction of ground based experiments flight tests and CFD is necessary to gain further insight into the flow physics of scramjet propulsion units. Further, the establishment of scaling laws to relate data gathered from subscale experiments to full scale configurations is highly desirable. Providing sufficiently short chemical time scales (large Damköhler numbers) this scaling reduces to the reproduction of the Mach number, Reynolds number and wall to recovery temperature ratio in the test facility. However, the assumption of large Damköhler numbers is not valid for many (subscale) scramjet flows. The chemical time scales are governed by the temperature, the density and mixture fractions. If the temperature and mixture fractions are kept constant, the chemical time scales with the density for two body reactions (ρL scaling) and with the square of the density for three body reactions (ρ^2L scaling). The consideration of ρL scaling, which, at constant temperature and composition, produces also an identical Reynolds number led to the simplified assumption that scramjet combustor flows are similar if the product of static pressure and combustor length scale (pL) is kept constant. This pL-scaling approach was subject of previous experimental and theoretical investigations with partially successful application to a strut injector configuration.

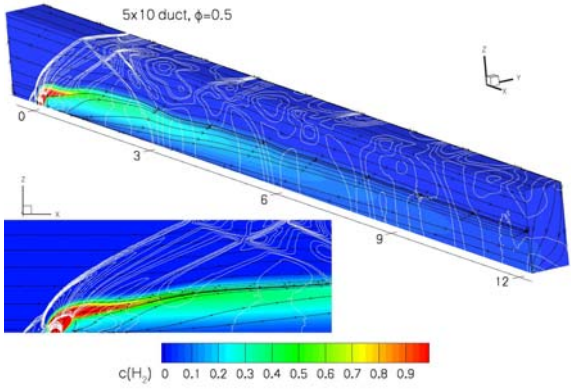

Flowfield topology for full scale duct (duct aspect ratio 5x10, Φ=0.5)

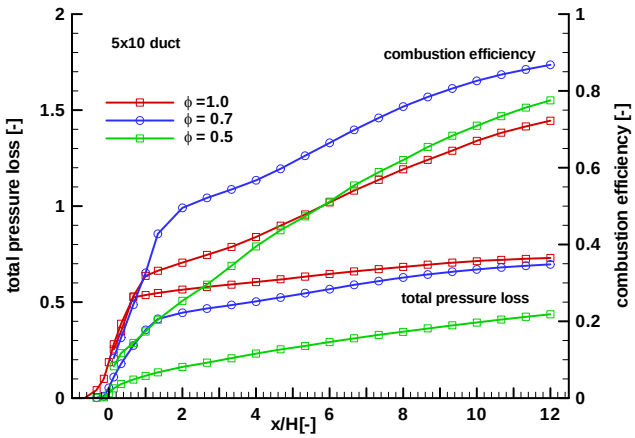

Combustion efficiency and total pressure loss for 5x10 duct with variation of equivalence ratio

Chemical time scales for the hydrogen combustion in a well stirred reactor were computed with the DLR Tau-code using a modified Jachimowski reaction mechanism. A typical result for temperature history compared to reference data from literature is shown in the left part of the figure below. The right part of this figure shows the dependency of the chemical time scale on the combustion pressure.

The results show that at the present conditions the chemical time does not scale directly with the pressure. This is due to three body reactions which dominate the hydrogen consumption after ignition. The complete reaction time scales in the low pressure limit with $p^{1.72}$ which is in good agreement with the empirical value of $p^{1.70}$ which was derived in previous studies. The deviation of this scaling towards the high pressure limit is due to the approach of the second explosion limit of hydrogen were the production of relatively stable HO_2 and H_2O_2 starts to slow down the ignition process. From $p^{1.7}$L=const which is concluded from the figure above follows that a change in pressure has a more important effect on the chemical time scale than a proportional change in length scale. At typical HyShot II conditions (T=1200K, p=1bar) the chemical time scale is about 170μs. An estimate for the convective time scale is the combustor length of 0.3m divided by the inflow velocity of the combustor of 1700m/s which is about 180μs. Thus, the applicability of pure pL-scaling for this flow regime is not justified. However, the porthole injection with the associated shock system generates local flow regions of high temperatures and pressures which serve as flame anchors and the convective time scales in the recirculation regions are much higher than the worst-case estimate mentioned above. These effects promote the applicability of pL-scaling and, therefore, it is not clear a priori if pL scaling is appropriate for this scramjet configuration or not.

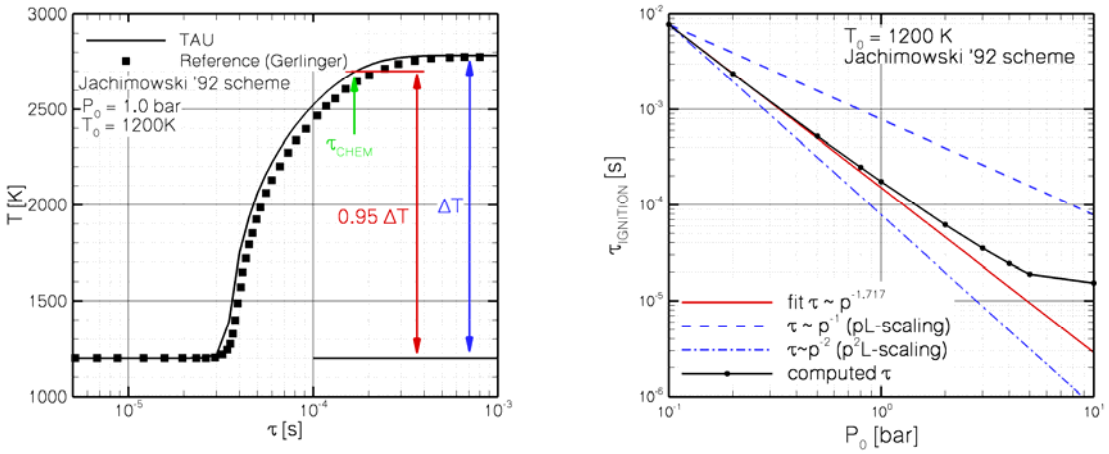

Left: temperature evolution in time for a stochiometric well stirred reactor at constant pressure. Definition of the chemical time scale τ_{chem} and validation of the results obtained by the DLR Tau-code. Right: Dependency of the chemical time scale τ_{chem} on the pressure for a well stirred reactor.

Numerical experiments to test the pL-scaling at the HyShot II configuration with porthole injectors were performed. A coarse grid with approximately 300,000 grid points was used. The inflow was assumed to be constant over the combustor entrance plane. The inflow conditions for the reference configuration were chosen to approximate the HyShot II combustor entrance at the flight altitude of 27km.
The obtained pressure distribution for the reference case is compared to the result on the fine grid for the HEG condition shown in the figure below. The pressure results on both grids are similar. Hence, the neglect of the leading edge shock of the boundary layer bleed and the use of the coarse grid for the scaling investigation does not affect the main flow characteristics.

Starting from this reference condition, the inflow pressure and the size of the combustor was varied by up to a factor of 10. For each case the product of pressure and length scale was kept constant. A summary of the considered conditions is in the figure above. It shows the resulting pressure distributions in the combustor.

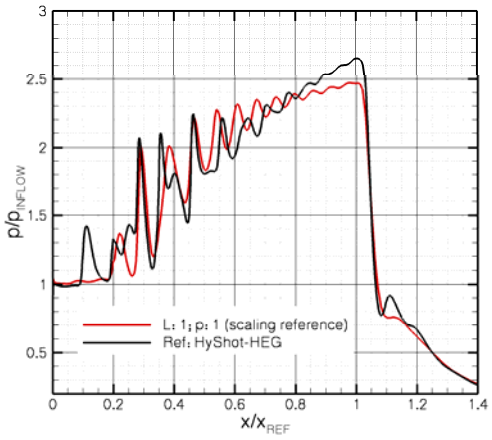

Configuration	Combustor length [m]	Pressure at combustor entrance [kPa]
L: 1; p:1	0.3	100
L: 2; p:0.5	0.6	50
L: 10; p:0.1	3.0	10
L: 0.5; p:2	0.15	200
L: 0.1; p:10	0.03	1000

Conditions at combustor entrance for all configurations:		
Velocity	1750	m/s
Mach number	2.5	
Temperature	1250	K
Equivalence Ratio	0.29	

Comparison of the combustor pressure distributions of the reference solution for the scaling investigation with the result for the HEG conditions and inflow conditions used for the scaling investigations.

When the inflow pressure is halved and the length scale doubled (L:2; p:0.5 case) the combustor behaves similar to the reference configuration. The peak pressure which is reached close to the combustor exit is only slightly less than the reference peak pressure. The pL-scaling fails when the inflow pressure is reduced by a factor of 10 with the length scale changed accordingly (L:0.1; p:10 case). Here, the increased length scale is not sufficient to compensate for the longer chemical time scale which is increased approximately by a factor of $10^{1.7}$. The resulting peak pressure is significantly less than for the reference configuration.

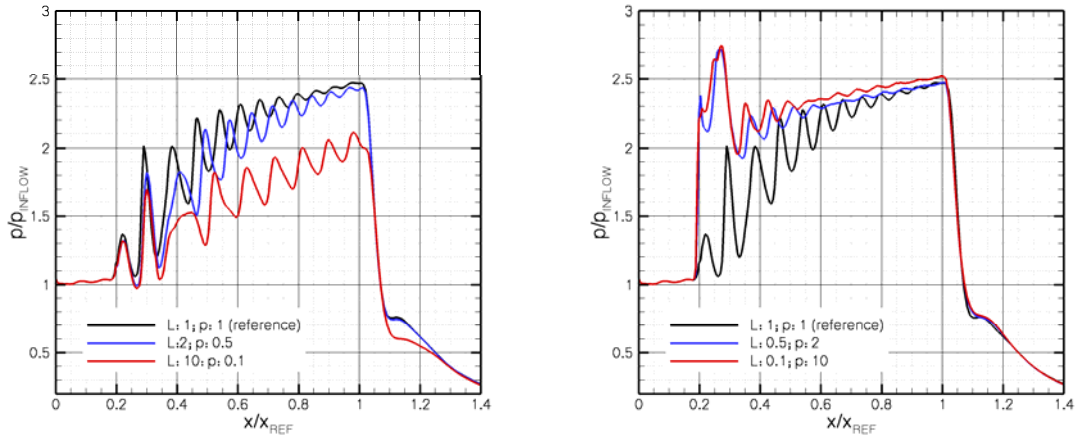

CFD results from the pL-scaling of the HyShot combustor. Left: decreasing pressure and increasing length, Right: increasing pressure and decreasing length. L: ratio of combustor and p: ratio of combustor entrance pressure to the reference configuration.

An increase of the inflow pressure (and according decrease in length scale) does not produce results which are similar to the reference configuration. The reason for this is a change in the flow topology. The increase in pressure causes an increase in hydrogen consumption and heat release already in the vicinity of the injector. This increased heat release is not entirely compensated by the decreased length scale and results in the development of a large recirculation zone downstream of the injector. Most of the combustion takes then place in this subsonic recirculation which generates the pronounced pressure peak in the upstream region of the combustor. Since for this case the convective time scale becomes very large compared to the chemical one the pL-scaling converts back to a Reynolds-number scaling and the results for the cases with a pressure increase by the factors of 2 and 10 behave very similar.

In summary it was found that the pL scaling which was successfully applied to many other combustion cases needs care when it is applied to Scramjet conditions. The typical chemical time scales are governed by two and three body reactions which obey to different scaling laws. The performed CFD analysis indicates that for the considered HyShot scramjet configuration at representative flight conditions the pL-scaling law works only for moderate decrease of pressures and increases in length scale.

Task 5.3 High Pressure Combustion Experiments: HC Disintegration Processes

The aim of the research activities in task 5.3 is to develop a new test rig for studying hydrocarbon fluid disintegration in the subcritical and supercritical regimes through simplified and systematic experiments. The experimental study focuses on binary systems, specifically hydrocarbon fuels (i.e. single component surrogates) in argon. Despite their technical relevance, the disintegration of hydrocarbon binary and multi-component systems has been scarcely studied due to the occurrence of mixture effects, which complicate the quantitative data analysis. The objective of these experiments is threefold: 1) to assess the effect of thermodynamic parameters (e.g. injection pressure, ambient gas density, fuel temperature, etc.) and fuel properties on spray characteristics; 2) to provide quantitative data on hydrocarbon binary fluid disintegration under subcritical and supercritical conditions; 3) to relate the experimental results (e.g. spray angle, spray penetration length, disintegration regime) to literature data on pure-component fluid disintegration and standard atomization, in order to extend the existing empirical correlations for the different break-up regimes to binary systems.

As the test facility, a recently developed double diaphragm shock tube was selected **[D5.3.1]**. The facility is equipped with a square test-section to allow flow visualization in the post shock region, a skimmer to dispose part of the boundary layer, a fast-response injector, a fully automated gas-filling system, and a new control system and electronics. The ITLR shock-tube is specifically intended for the investigation of fundamental processes related to fluid disintegration and mixing under realistic engine conditions. During the experimental program in WP 5.3, it became soon evident that, due to boundary layer effects, a gradual increase in temperature and pressure could be detected behind the reflected shock during test time. The non-constancy

of the test conditions had a severe impact on the spray characteristic as revealed by the high-speed visualization tests, thus hampering considerably the reliability and reproducibility of the experimental results. As a remedy, a variable-area driver section was developed in order to compensate for shock attenuation effects and realize quasi-steady chamber conditions. The basic idea is to utilize the rarefaction waves in the driver chamber in a controlled manner. These waves are reflected from the driver chamber walls and subsequently propagate downstream towards the test section. As soon as these waves reach the region behind the reflected shock, they counterbalance the local pressure/temperature increase, thus resulting in a facility virtually free of shock attenuation. The selected profile is such that, for a prescribed post-shock temperature T_5 (Mach number M_S), quasi-constant test conditions, over a wide range of post-shock pressures (typically $10 < p_5 < 50$ bar) are guaranteed. To produce the continuous driver area reduction, a conical insert is used, shown in the figure below on the left. The insert is made of several single elements, which are glued to each other employing a circular tongue and groove joint. The contour design and optimization of the conical inserts is made with a quasi-one-dimensional code for modelling transient-flow facilities. The figure on the right side shows the spatio-temporal evolution of the pressure within the test section. As can be clearly seen, the pressure distribution is basically constant, over the entire test-section, both in space and time and only very faint deviations in the pressure profiles (typically < 2%) are observed.

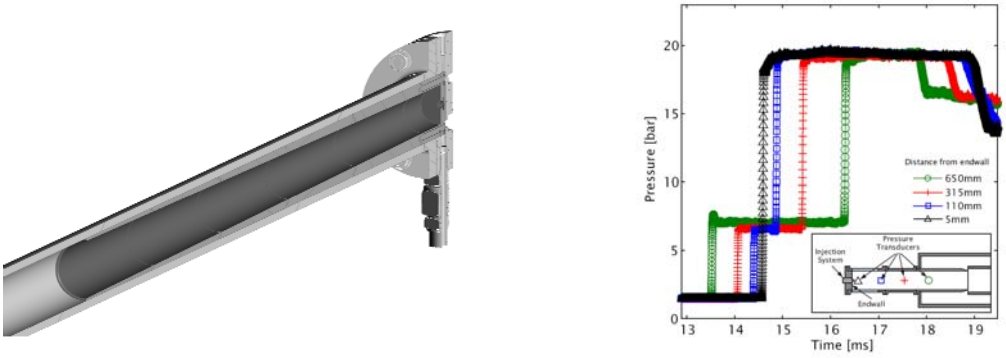

Conical insert; left: Detailed view of the variable area driver section; right: Spatio-temporal evolution of the pressure within the test section. Post shock conditions: T_5 = 950 K, p_5 = 18 bar.

During the first experimental program in WP 5.3, it became soon evident that no transcritical and supercritical jet behaviour could be observed. This could be due to the fact that the injection temperature of the fuel (roughly 300 K) is too low for transcritical effects to be observed on a macroscopic level. As a remedy, the following actions have been taken. First, for a better planning and analysis of the experiments, dedicated software has been developed for calculating the fluid-phase equilibrium composition of the binary system dodecane/argon as function of chamber pressure and temperature. The method employed is described in detail in the deliverable **[D5.3.2]**. Second, the fuel injector had to be redesigned and adjusted in order to enable injection temperatures at least as high as 630K **[D5.3.3]**.

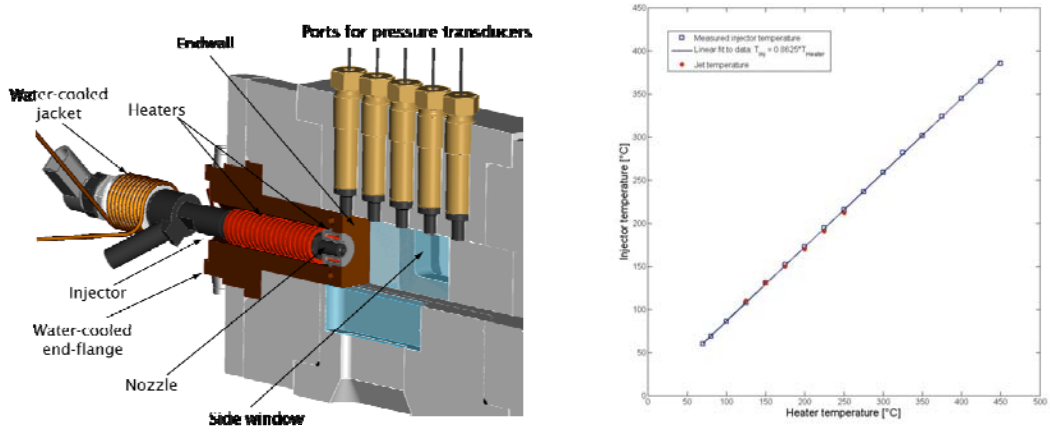

Modified injector; left: View of the injector assembly; right: Calibration curve for the injector/fuel temperature.

The figure above (on the left side) shows the modified injector assembly in detail. For the regulation of the fuel temperature, two compact high performance tubular cartridge heaters are employed: the first one (180 W) is used to heat-up the fuel in the nozzle to the target temperature; the second (240 W) is wrapped around the injector body, in order to preheat the fuel. Thanks to the two-heater solution, a higher heating power can be applied to the nozzle region to compensate for thermal losses. Furthermore thermal stresses within the injector are thereby reduced. Both heaters are electronically regulated by laboratory PID controllers. In order not to damage the injector electronics, an additional water-cooled jacket has been designed to maintain all electronic components at room temperature. Due to that the piston rod, which steers the opening mechanism of the injector, had to be extended to 10mm. Moreover, an in-house electronic device has been developed to monitor the temperature of the magnetic coil. Since all window ports are at direct contact with the end-flange, it is mandatory to keep all metal parts at a moderate temperature, in order not to induce thermal stresses in the glass windows and hence lead to thermal fractures. All four sidewalls of the end-flange are therefore equipped with a water-cooled circuit. The behaviour of the modified injector has been characterized over a range of injection pressures (80—1300 bar) and fuel temperatures comprised between 20 and 300°C. Independently from the specific choice of injection parameters, the injector's performance remained unaltered with respect to both response time (typically 400 μs) and uniformity of the fuel temperature distribution within the injector and the nozzle. The figure above (on the right side) presents a calibration curve, which relates the heater temperature (i.e. the temperature set by the PID controllers) to the injector temperature. The term injector temperature denotes both the temperature of the metal in the body of the injector and in the nozzle. As can be immediately seen in the figure, all points fit a linear curve, which can subsequently be used to relate the fuel temperature to the heater temperature. The fuel temperature has also been measured by positioning a fast response thermocouple directly at the nozzle exit. The steady state temperatures measured lie in close neighbourhood of the calibration line as well, thus corroborating the assumption of equality between fuel and metal temperature.

Having verified that both the chamber and injection conditions are well-defined and show good reproducibility, the actual measurement campaign has been started. For the experimental investigations, the following nozzle is employed: D = 236 μm, L/D = 4. The test conditions are varied as follows: 10-42.5 bar for the ambient pressure, while the chamber temperature is fixed at 950K. The fuel injection temperature can be varied between 20°C and 300°C. As test fluids, n-dodecane and n-hexane (as exemplary hydrocarbon fuels) in argon have been chosen. The disintegration process was visualised by means of macroscopic high-speed shadowgraphy (at a frame rate of 100000 fps) and the analysis of the images acquired has been fully automated by means of an in-house image processing software. A final analysis of the experimental data is available in **[D5.3.3]**. Note that the experimental campaign includes also the analysis of the fuel break-up and atomisation process in the near-nozzle region of the injector, using magnification optics and a short-pulse diode laser system, as the light source. The focus of the measurements is on the dynamical behaviour of the fuel jets, with specific emphasis on the analysis of the liquid jet morphology **[D5.3.5]**.

The figure below presents a detailed comparison among the different test conditions in order to highlight the dependence of the primary breakup on chamber pressure conditions. In the figure, the axial distribution of the jet spreading angle (θ) for a subcritical fuel temperature of T_f = 373.15K (i.e. a reduced temperature $T_r = T_f / T_{crit}$ = 0.73) and different chamber pressures, corresponding to reduced pressures in the range $0.33 \leq p_r \leq 1.40$. At low subcritical pressures (i.e. $p_r \ll 1$), a "standard" atomisation behavior is observed in the near-nozzle region meaning that the spreading angle increases with increasing chamber densities. At higher chamber pressures ($0.90 \leq p_r \leq 1.40$), only a faint increase of the lateral spreading is found with chamber density. Similar conclusions were drawn in the analysis of macroscopic spray experiments conducted at similar conditions [see Stotz *et al*. (2008), Hiroyasu and Arai (1990), Naber and Siebers (1996), Chehroudi *et al.* (1985)]. In this region, a linear increase of the lateral spreading with axial distance is found for all pressures, which is consistent with the macroscopic observations. This linear trend can be explained in terms of development of a shear layer and entrainment of surrounding ambient gas, which leads to an enhanced lateral spreading of the jet. At near critical temperatures (T_f = 448.15K, T_r = 0.9), all curves converge to equal values for all pressure conditions investigated. Moreover, the absolute values of the spreading angles tend to the limit $tan(\theta) \approx 0.2$. The observed behaviour corroborates one of the main conclusions from the macroscopic analysis: in the near-nozzle region, the experimental results support the hypothesis that the jets behave similarly to an incompressible gas jet, provided that one of the two parameters p_r or T_r is larger than1 and the other one is above a specific value ≈ 0.8 - 0.9.

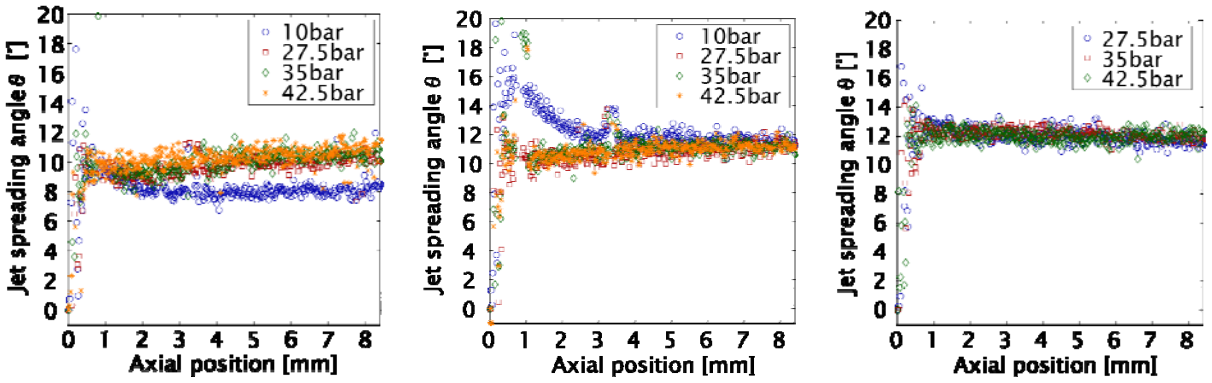

Influence of the chamber pressure on the jet dispersion. Time averaged spreading angle θ versus axial distance; left: T_f = 373.15K; centre: T_f = 448.15K; right: T_f = 523.15K.

A different behaviour is found for a chamber pressure of p_5 = 10 bar. At the nozzle exit, very large angles are observed. This discrepancy in jet behaviour is due to a completely different phenomenology. For fuel temperatures in the range of 373.15 ≤ T_f ≤ 523.15K and chamber pressures p_5 ≤ 20 bar, a jet with the appearance of an under-expanded jet forms at the nozzle outlet, thus generating much larger jet spreading angles. For lower back pressures, a normal shock (a Mach disk) is detected in the jet. At supercritical fuel injection temperatures of (T_f = 523.15K, T_r = 1.03), the jet lateral spreading in the near-nozzle region is independent of the chamber pressure and its average value is about $\theta \approx 12°$. In contrast to the experiments conducted at subcritical fuel temperatures, the angles do not show a rising trend and stay pretty constant over the full observable length.

Besides the analysis of the jet dispersion, the structures within the flow were analysed using a two-point correlation method to derive turbulent flow structures and visible length scales from the shadowgraph images. The results obtained for four different conditions are shown in the figure below. In the top row, the fuel temperature is varied from subcritical to supercritical values (T_f = 373.15K and T_f = 523.15K), whereas the chamber pressure is kept constant at a subcritical value p_5 = 27.5 bar. In the bottom row, the same two fuel temperatures are investigated, while the pressure is at a constant supercritical value of p_5 = 42.5 bar. As can be seen, the results for the lower fuel temperature (on the left hand side) are very similar, both in structure and absolute value. A minor difference between the two is that the shear layer is slightly thicker and more dispersed for the higher pressure case. The same remark holds for the lateral spreading of the dense region, which is slightly larger for the higher pressure conditions.

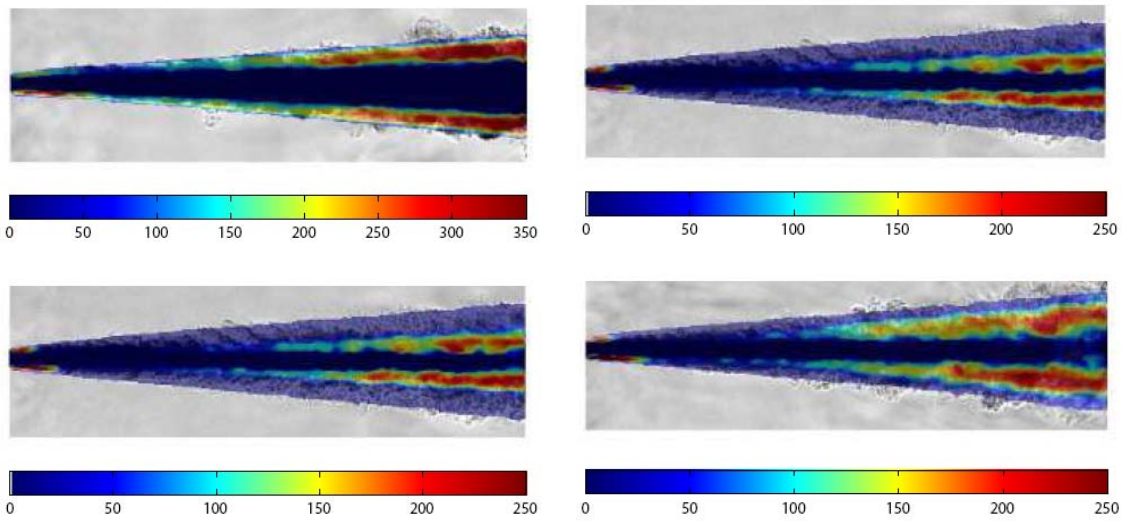

Average visible length scales L for different experimental conditions in µm; top left: T_f =373.15K, p_5 = 27.5 bar; top right: T_f =523.15K, p_5 = 27.5 bar; bottom left: T_f =373.15K, p_5 = 42.5 bar; bottom right: T_f =523.15K, p_5 = 42.5 bar;

With increasing fuel temperature, the dense region becomes narrower and reaches a value of the order of the nozzle diameter (for T_f = 523K). The difference between low and high fuel temperatures is clearly visible, when comparing the images on the left to those on the right. The average length scales are (locally) up to 60% smaller for higher fuel temperatures, whereas the structures are clustered towards the centreline. Especially for a chamber pressure of p_5 = 27.5 bar, the structures dissipate rather quickly in lateral direction and a large amount of the shear layer consists of structures smaller than the resolution of the optical system. For the nominally supercritical case of p_5 = 42.5 bar and T_f = 523K, the structures calculated are of the same order as those for p_5 = 27.5 bar and T_f = 523K. Their spatial extension, however, is notedly broader and the fluid in the shear layer seems to have a more ”bulky” appearance, whereas for p_5 = 27.5 bar finer structures dominate. In general, the calculated length scales and thus the visible structures are symmetrically distributed across the jet. Both the absolute values as well as their local broadness is similar for low fuel temperatures. For the highest fuel temperature T_f = 523K, an explicit widening of the ”structured” shear layer is apparent, it almost doubles when increasing the pressure from p_5 = 27.5 bar to p_5= 42.5 bar, while the diameter of the dense core stays quasi constant. The calculated absolute values of the length scales also seem to be larger for higher pressures, thus conferring the jet a ”bulkier” structure at higher chamber pressures.

Task 5.4 High Pressure Combustion for LOX/HC

Quantitative optical diagnostics is required for basic investigations of LOX/CH4-combustion chamber processes and to validate the prediction ability of models used to simulate these processes. In the frame of WP 5.4.1 the application of coherent anti-Stokes Raman Scattering (CARS) has been adapted to CH4/O2-combustion and the performance of the diagnostic method has been demonstrated in cryogenic LOX/CH4-spray combustion.
A literature review revealed that published literature on CARS diagnostics of methane flames mainly treats CH4/air combustion due to its obvious relevance to technical applications. Extremely fuel rich CH4/O2 flames (Φ=10-13) have been investigated by ONERA using CARS with methane as probe molecule. No application of CARS to a combustion chamber at conditions representative for LOX/CH4-fueled rocket thrust chambers is reported up to now.
It has been shown that use of methane as probe molecule for CARS thermometry delivers a limited diagnostic yield. Methane at fuel rich conditions typical of rocket combustors undergoes thermal dissociation at elevated temperatures and is not present in the reaction products for CARS diagnostics. Methane can only be expected in flow areas with temperatures below ~1100K. Diagnostics of methane will therefore deliver information restricted to flow regions near to the injector head. By analysing the equilibrium composition of CH4/O2-mixtures and by performing CARS diagnostics in a laboratory burner for various mixture ratios and pressure conditions, potential probe molecules other than CH4 have been investigated. Hydrogen appeared to be a major constituent of the dissociation products of the methane molecule. It has been shown that for all operational conditions H2 is available in sufficient amounts in the flame for diagnostics.

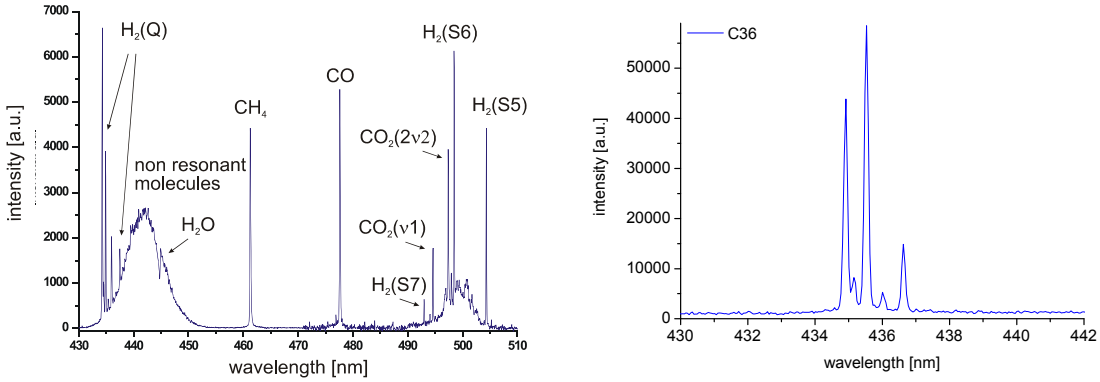

Left: CARS spectra obtained in a GOX/CH_4-flame; right: H_2-CARS spectrum from a LOX/CH_4 spray flame in the micro combustor

Within the LAPCAT program, the evaluation software, which is applied to process the CARS raw data, has been modified in order to simplify the interface and input data to become more user-friendly. At the same time it was updated to fulfil the requirements of the upgraded DLR system **[D5.4.3]**.

Based on these results, strategies for CARS-diagnostics of LOX/CH4-flames have been derived. The optimum approach for the diagnostics of O2/CH4 combustion is the simultaneous detection of H2- and CH4-signals as representatives for the reactants and reaction products respectively. H2 is the probe molecule of choice for thermometry. Methane density can be deduced from its CARS-signal, thus contributing important information on flow mixing and stratification upstream the flame front.
Furthermore, first test campaigns have been performed at the M3 test facility at distinct conditions with liquid oxygen and gaseous methane to verify the CARS system for the propellant combination to be studied.

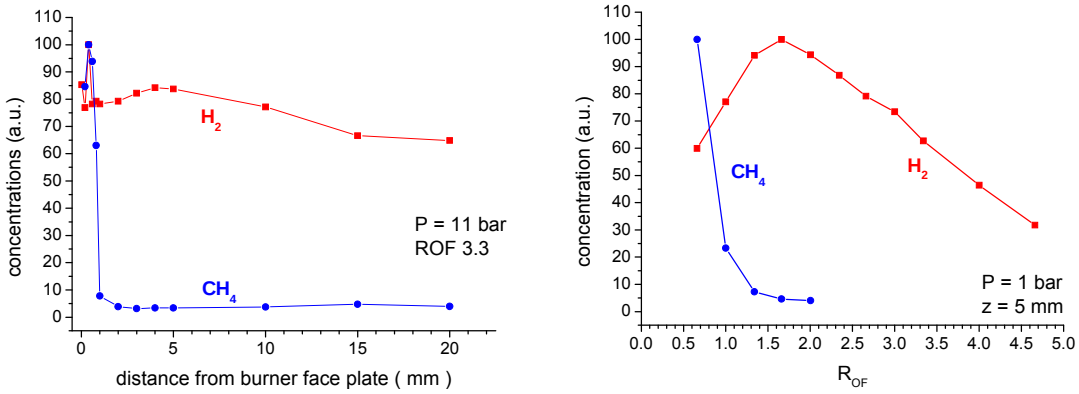

Methane concentrations measured with CARS in a laboratory burner as function of the distance downstream the burner face plate (left) and as function of the mixture ratio (right)

The objectives of the subtask modelling of high pressure fuel rich LOX/methane combustion were the determination of operating conditions, the establishment of an experimental data base, the identification of the best suited base mechanism and its necessary adaptation/modification to the operating conditions and the subsequent reductions to a skeletal model and in a further step to a global reduced model which is as short as possible to become implemented in CFD tools but maintaining its predictive capabilities **[D5.4.2]**.
Previous reports provided information on the operating conditions of pressure, temperate and mixture ratio: 1 bar < p < 60 bar, 900 K < T < 1800 K and 1.0 < Φ < 3.0. The literature study allowed establishing a sufficiently broad data base resulting in the determination of the Leeds mechanism as the base mechanism. The necessary modifications were made in order to allow for an application to the operating conditions mentioned above. Furthermore, potential methods for mechanism reduction were evaluated and a reduction strategy developed which guarantees based on a step by step approach with continuous validation a mechanism construction with minimum losses of predictive capabilities. One of the key elements of the development methodology was to rely only on thermo-chemical data derived from first principles which are validated with selected and extensively verified experimental data base and to reduce as much as possible the inclusion of fitted parameters.

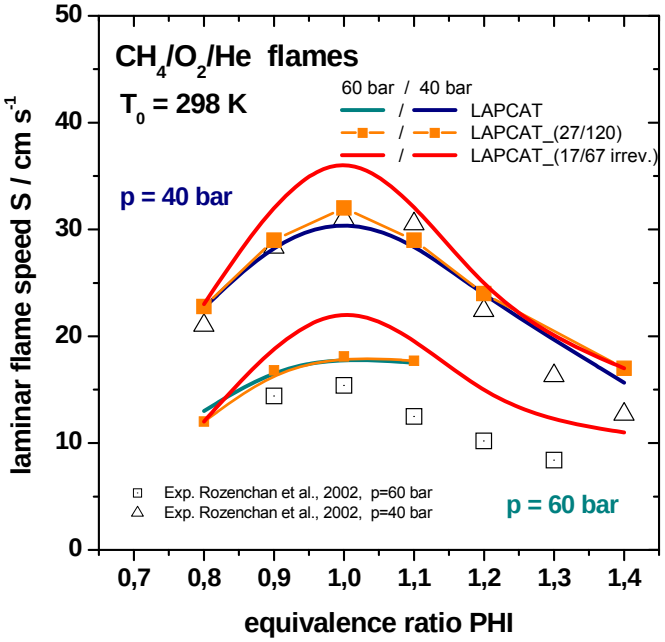

The detailed reaction mechanism for high pressure methane combustion which was developed as the input kinetic scheme for further reduction comprises 43 species and 352 reactions. In a first step, this detailed mechanism which allows for the prediction of heat release and the formation of poly-aromatic hydro-carbons as typical precursors of soot, a capability which is mandatory to model as well the fuel-rich combustion conditions of rocket mode operation, has been reduced to a skeletal one which comprises 27 species

and 120 reactions applying standard procedures and methods for kinetic mechanism reduction. Both, the large data base and the extremely broad parameter range made it absolutely necessary to perform the necessary analyses and data handling and processing applying specifically developed software tools. In a second step, the skeletal model mentioned above was reduced further to an again shorter mechanism with only 21 species and 67 reactions applying a combined chemical lumping and quasi-stead state assumption approach. Extensive validation applying the data base which has been established within the first phase of the project and which is still continuously extended and updated, reveal that all the models mentioned above satisfactory predict flame velocities and ignition delays data. It is worthwhile mentioning that all the models include are, N2, He as inert species since almost all experimental data was achieved with the presence of one of these species.

The M3.1 test facility at the DLR German Aerospace Center in Lampoldshausen, operated in former tests with hydrogen and oxygen (in cryogenic or ambient state), has been upgraded for the use of methane as propellant **[D5.4.1]**.

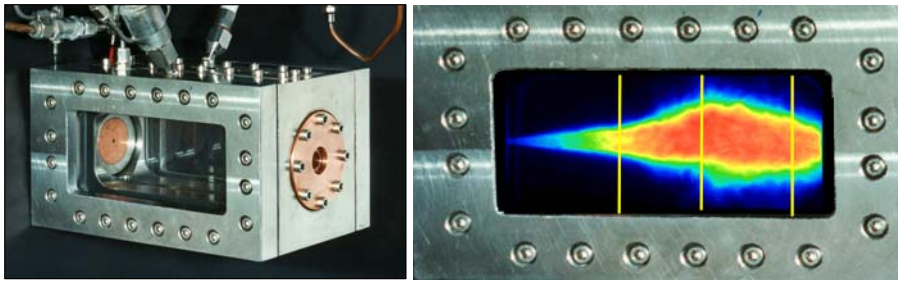

Left: Micro combustor for the investigation of cryogenic spray combustion using methane and LOX.
Right: LOX/methane flame visualization

A new fuel with different physical properties with respect to hydrogen needs special attention for the design of the feed lines and the injector head. Due to feed line pressures of up to 40 bars and a feed line temperature spread of about 100 K, the calculation of real gas properties is a must. Moreover knowledge of propellant properties is required for the prediction of injection and combustion properties for the correct operation of the test bench and for the design of new injector heads. New software for determining the thermo-physical properties and the flow characteristics of methane has been written and validated.
This tool has been applied for the design of supply lines and a single injector head for the M3.1 micro-combustor test facility. Five injectors with different injector diameters have been manufactured. The supply lines and required valves, as well as the sensors used to supervise the propellant properties and the new injector head have been integrated into the test bench and the micro combustor.
For each new test facility or for any major modification to existing hardware, acceptance tests must be performed to assure the correct functionality of the hardware and its accordance to the specifications. These procedures have been successfully accomplished.

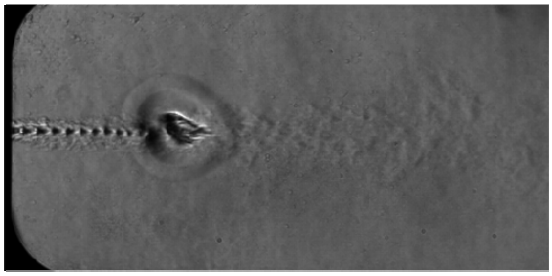

Blast wave following the gas break down induced by the ignition laser

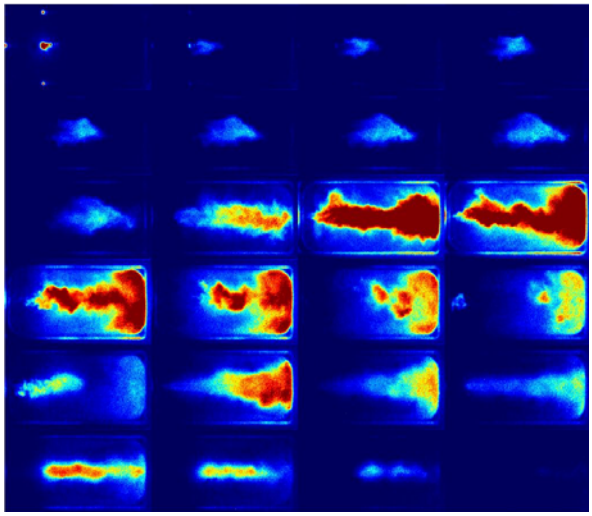

Flame evolution during the ignition transient of a O_2/methane-flame after laser ignition

Ignition and flame anchoring of a coaxial gaseous methane-oxygen jet have been studied using high speed visualization techniques **[D5.4.4]**. In order to pin-point the exact moment of ignition and thus precisely trigger the cameras implemented for these visualization techniques, laser ignition was opted for. Several ignition scenarios (”blown out”, smooth” and strong ignition”) have been found with specific phenomenology, depending mainly on the time delay between propellant valve opening and ignition, “ignition delay”. The time necessary for flame anchoring is shown to depend on the momentum flux ratio of the injected propellants. Attached and detached flames were observed and it was found, that high momentum flux ratios favour the establishment of a flame attached to the injector. For detached flames, higher chamber pressures result in smaller lift-off distances.

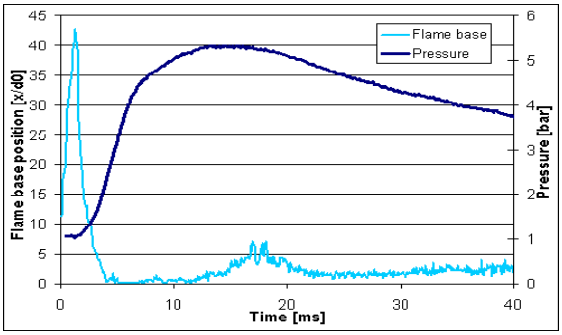

Flame stabilization and pressure evolution during the ignition transient

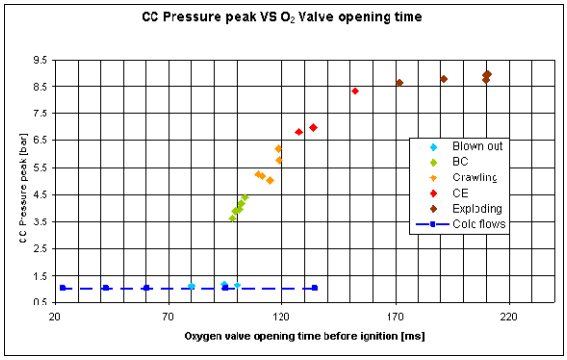

Ignition pressure peak as function of the LOX-valve opening time

Stationary LOX/CH4 spray combustion has been investigated in order to characterize qualitatively and quantitatively the reactive flow field. The spray phenomenology is visualized by back-light imaging thus delivering information on the process of atomization and the spatial distribution of LOX droplets. The extension of the reaction front is recorded by imaging the emission of the OH-radical in the wavelength region in the vicinity of 310nm. This allows analyzing of the flame anchoring at the injector and the evolution of the flame due to the progress of combustion downstream of the injector. Quantitative data on the temperature field are obtained by CARS thermometry. It had been foreseen to determine at two downstream positions radial temperature profiles in the flow field. Due to unforeseen hardware failures (CARS laser, feed system pressure reducers, MCC-components) the planned test matrix for the experiments on stationary combustion suffered some delay. Preliminary results confirmed the suitability of H2 as probe molecule in CH4/O2-combustion in rocket model combustors.

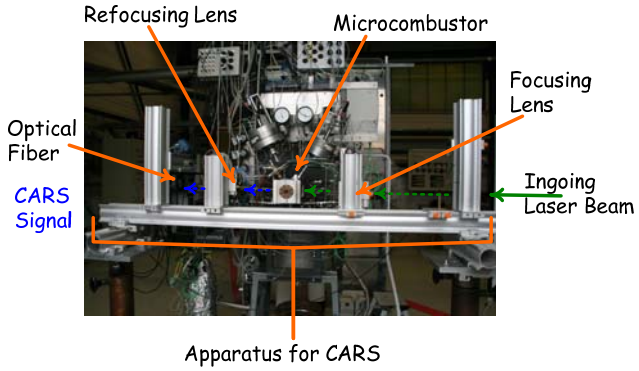

CARS Setup at the M3.1 Test Bench

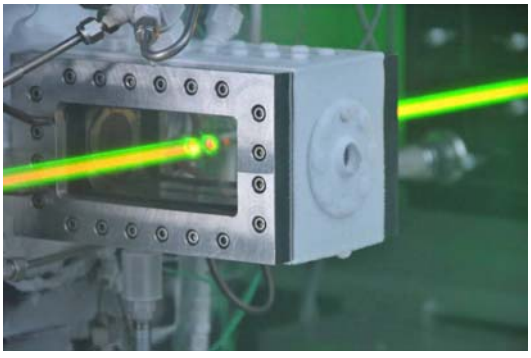

Incoming CARS Laser Beam

An extensive analysis of the results obtained shows a dependency on the overall mixture ratio, with however an impact of the local mixture ratio. The presence of a lower H2 threshold for detection using CARS was observed. Changes in the feeding temperature of gaseous methane appears to have an impact on flame characteristics, such as flame angle. Initial observations show that decreasing the methane temperature decreases the flame angle.

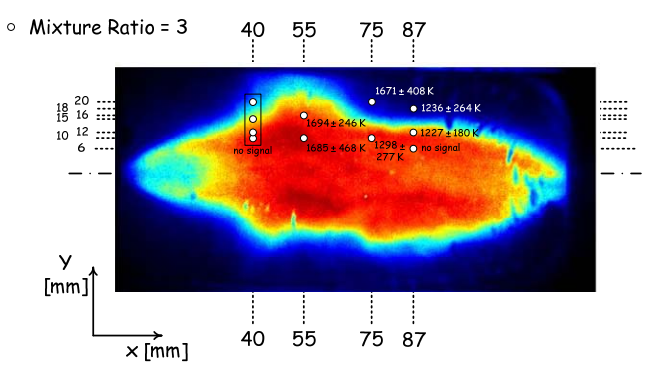

CARS Thermometry Results for ROF = 3

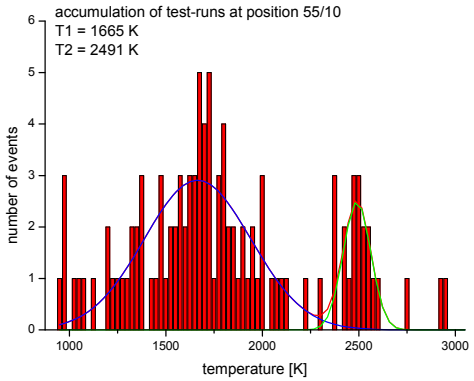

Temperature histogram at location (55/10): bimodal distribution, indicating a stratified flow at the measurement location

Sooting was assessed qualitatively and is not a problem for oxygen-methane combustion, in that sooting levels are extremely low.

In summary it can be stated that the main anticipated achievements of this work package could be obtained. Deviations from the time schedule were encountered due to originally not foreseen design and manufacturing issues of the integrated scramjet wind tunnel model, unforeseen physical phenomena resulting into a modification of the test set-up for HC disintegration, the non-applicability of a particular measurement technique for high pressure combustion for LOX/HC and hardware failures related to the M3 micro combustor.

2.2.5 WP6 Combustion Modelling and Validation

Task 6.1 RBCC High-Pressure Combustion Modelling for Lox/HC

The extension and validation of the existing axisymmetrical EADS code Rocflam-II towards LOX/HC (Hydrocarbons, i.e. Kerosene and Methane) chemistries was the main topic in WP6.1. The necessary fluid data and reaction schemes have been selected and implemented **[D6.1.1]**. The reaction model in Rocflam-II consists of a tabulated equilibrium chemistry with a PPDF (*presumed probability density function*) approach to model turbulent combustion. Code validation has been carried out on available sub- and generic fullscale engines to the satisfaction of the involved EADS combustion modelling specialists **[D6.1.2]**. In the meanwhile the first company-internal spin-off of these LAPCAT achievements could be generated by employing the enhanced code in other preliminary development phases of engines prior to entering a regular development program.

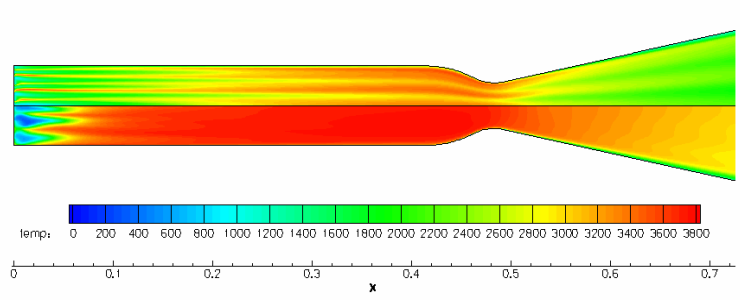

RBCC configuration with HC/LOX combustion in rocket combustion chamber (top showing the non-premixed and bottom the premixed injection).

Task 6.2 High-Pressure Turbulent Combustion Modelling for LOX/HC

The main objectives of Task 6.2 were:

- modelling finite-rate chemistry and non-ideal gas behaviour in the simulation of high-pressure LOX/HC combustion
- developing and using a 3D numerical solver for the calculation of transient chemically reactive fluid flows.

The pressure based module of the existing CIRA code C3NS (Combustion Three-dimensional Navier-Stokes) was selected as starting point for the present task. This module was initially able to solve RANS equations for unsteady, subsonic/transonic, turbulent flows of a generic multi-component mixture of reacting ideal gases around 2D, axis-symmetric or 3D geometries

During the first year of the project, a thermodynamic model able to properly describe propellants injection in high pressure LOx/HC combustors has been developed and implemented in the C3NS-PB flow solver **[D6.2.1]**. Two different approaches (compressibility factor formulation and analytical formulation) have been selected: the accuracy and robustness of both approaches have been preliminary assessed through comparison with experimental data available in literature. Furthermore, the compressibility factor formulation has been implemented in the flow solver and a suitable test case (RCM-1, "Nitrogen Cryogenic Injection", DLR Lampoldshausen, 2001) has been selected to test the capabilities of the model in typical rocket operating conditions (supercritical injection pressure, trans-critical injection temperature): the CFD simulations have shown a good agreement with experimental data, as shown in the figure below.

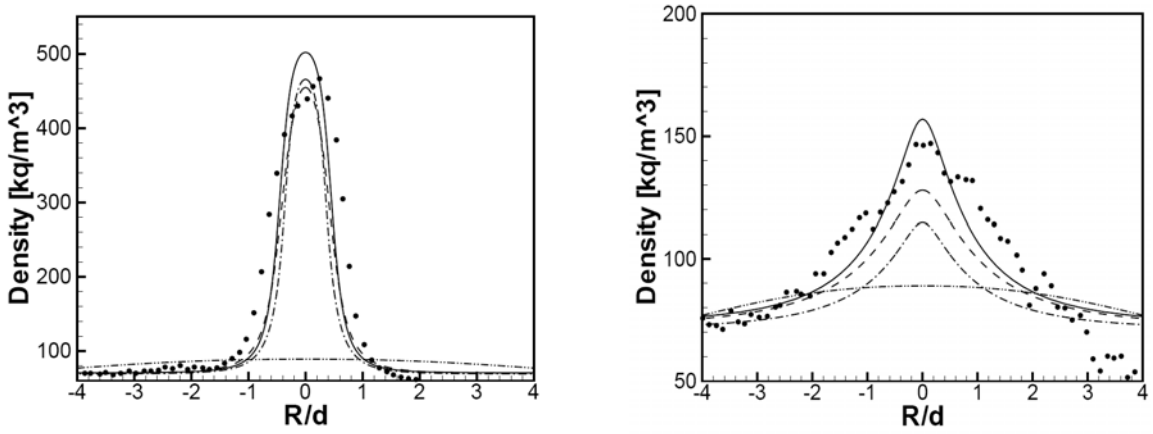

(a) *x/D*=5 *(b) x/D=25*

Density profiles: comparison between different levels of *real gas* corrections: ——: Full correction (EOS, thermodynamic and transport data); – – – – – – –: Partial correction (EOS and thermodynamic data); ·····: Only EOS Correction; ·····: Ideal gas; • Experimental data.

During the second year of activity, a trade off analysis of finite rate chemistry models for oxygen/methane and oxygen/kerosene has been carried out. Due to the complexity of the oxidation process for hydrocarbons, detailed schemes (usually involving tenths of species and hundreds of reactions) can not be directly embedded in a CFD solver, as a huge increase in the computational effort would result. For this reason, two reduced mechanisms, able to describe the combustion process with reasonable accuracy (in terms of ignition delay time and adiabatic flame temperature) in the operating conditions typical of a rocket based combined cycle engines (i.e., high pressure and fuel-rich mixture) have been selected **[D6.2.2]**. The selected mechanisms have been verified against the predictions of detailed mechanisms and experimental data available in literature **[D6.2.3]**.

A turbulent combustion model (based on the Partially Stirred Reactor assumption) has been also implemented in the code: such model is the extension to finite-rate chemistry (with an arbitrary number of species and reactions) of the Eddy Dissipation Concept model.

Moreover, a preliminary test campaign has been carried out in order to evaluate the impact of the modelling on the computed engine performances: a text matrix of seven 2D axis-symmetric simulations have been completed, considering both fuel lean and fuel rich combustion, with both the ideal and real thermodynamics models: the results of one of this tests are depicted in the next figure. The results show that in fuel rich conditions, typical or the LAPCAT Mach 8 vehicle, the real gas effects on the fluid-dynamics cannot be neglected leading to large errors in the evaluation of pressure and temperature (16% of under-estimation) and on the specific impulse (8% under-estimation)

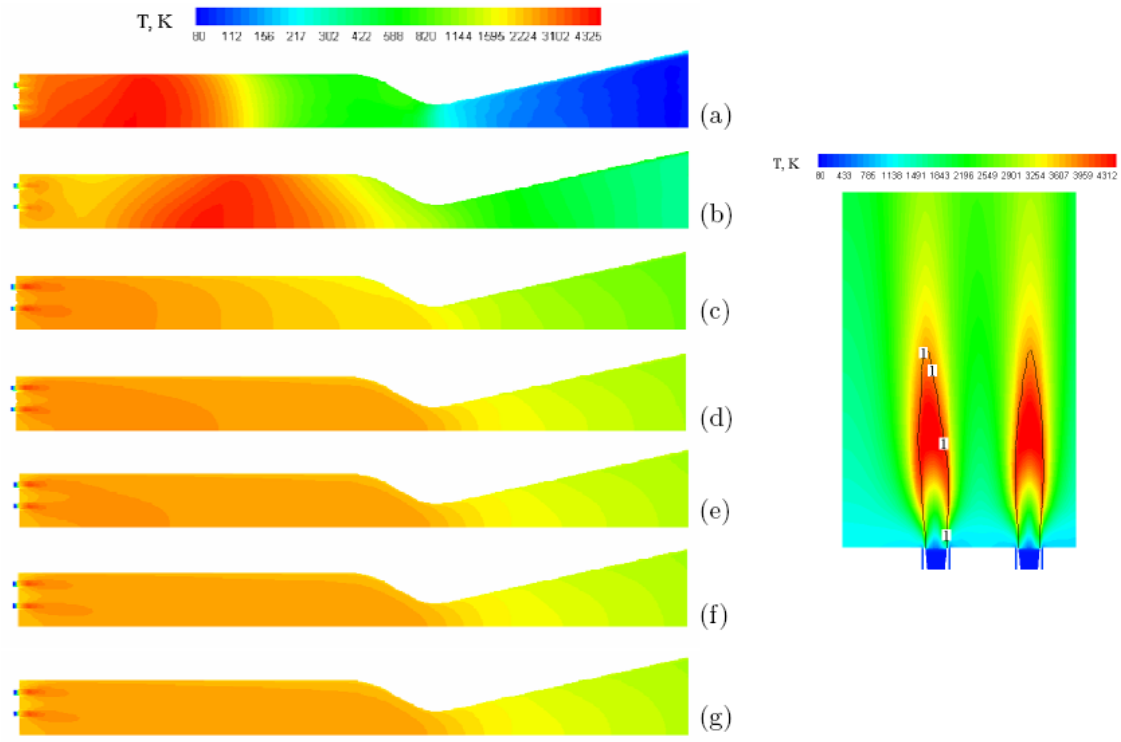

Left: Temperature time evolution (a) t=3.0 ms, (b) t=6.0 ms, (c) t=9.0 ms, (d) t=12.0 ms, (e) t=15.0 ms, (f) t=18.0 ms, (g) t=20.0ms. Right: Temperature contour and ER=1 iso-lines at steady state (20 ms)

During the third year of activity, the models which have been previously developed and embedded in the CIRA solver C3NS, have been used to perform some three dimensional simulations of a rocket engine with a realistic injection plate configuration **[D6.2.4]**. Some simulations of the equivalent two dimensional geometry have been performed in order to find the proper 2D injection configuration for reproducing 3D flow fields, in terms of both global performance parameters (such as the specific impulse) and local properties (such as the composition at the exit section).

Moreover, during the last year, the CIRA solver C3NS has been improved with new wall-function formulations in order to better describe the turbulent boundary layer and capture wall related quantities, such as shear stresses and more importantly, wall heat fluxes. This models have been validated through performing some test cases available in literature, and then applied to the rocket engine simulations, both 2D and 3D.

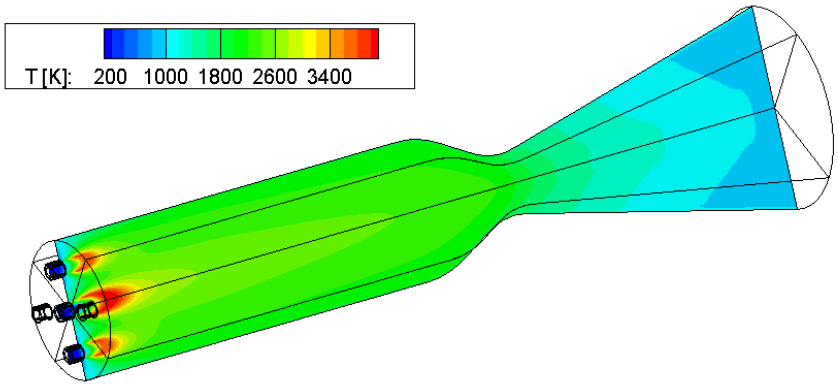

Temperature contour for 3D simulation with realistic injection plate

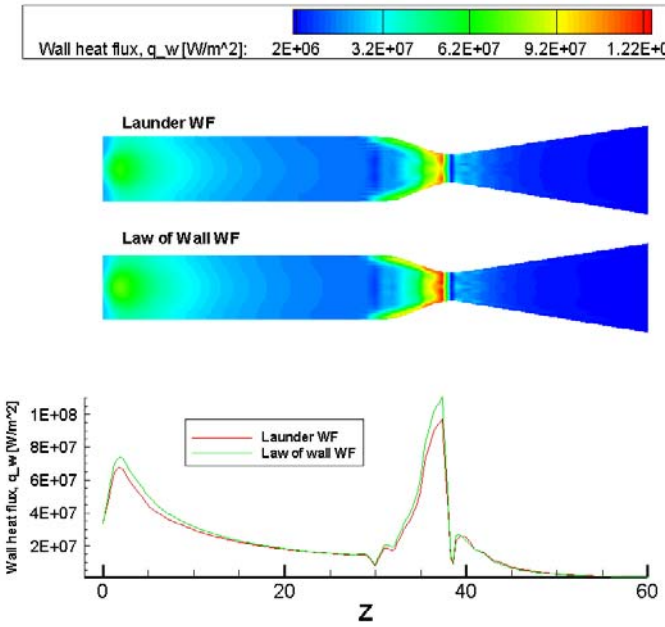

Comparison of 3D wall heat flux using two different near-wall formulations. On the top: distribution of wall heat flux on the combustion chamber wall. On the bottom: wall heat flux extracted on the line y=0.

Task 6.3 Ramjet Combustion Modelling

In the frame of WP6.3, the EADS code Rocflam-II, which has been validated in WP6.1 for LOX/Kerosene and LOX/Methane combustion, has been adapted and applied to an Air/Kerosene Ramjet engine **[D6.3.1]**. Here, liquid kerosene droplets are injected into a gaseous air surrounding, simulating atmospheric conditions at a sea level altitude of ca. 25 km. The air is already compressed and heated up in an inlet previously, so the combustion process will take place under subsonic conditions. The Ramjet design is preliminarily taken from WP 4. Using this configuration and varying the injection conditions, combustion efficiencies and characteristic velocities could be predicted and their plausibility be checked for the first time in a manner analogous to “classical” rocket combustion chamber engineering analysis.

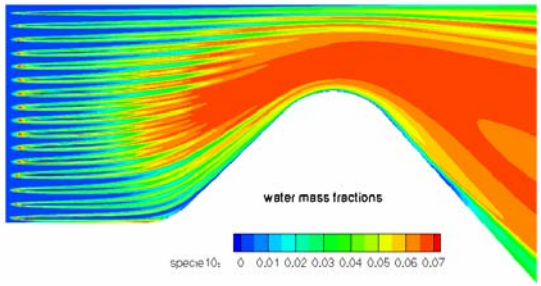

Air/Kerosene combustion in Ramjet mode showing water mass fraction.

The HC combustion modelling work progress described in the WP6.1 and WP6.3 formulation was achieved with fewer resources than originally expected. Due to this, and due to the interest in the combustion of Air and hydrogen in LAPCAT, EADS Astrium focused on WP6 to engineering-level Air/H2 combustion modelling in order to extend the available rocket experience with LOX/H2 combustion towards an Air/H2 chemistry and to supersonic combustion **[D6.3.2]**.
The two codes applied were the EADS in-house Rocflam-II 2D-RANS multiphase code, and the commercial Ansys/CFX code package with emphasis on 3D flows. Two test cases, a lifted supersonic (Cheng experiment) and a lifted subsonic flame (Cabra experiment) were recomputed. The results were examined in the light of the industrial engineering approach to the numerical tools, namely equilibrium chemistry with ppdf approach and one-step global reaction scheme.
Both industrial codes available to EADS Astrium predict flame shapes and lengths reasonably well. However, using one-step global chemistry overestimates the flame temperature and OH concentrations, while the equilibrium chemistry does not predict the flame lifting well. During the effort, shortcomings in the commercial CFX code regarding the use of detailed chemistry modelling with turbulent combustion were discovered so that CFX was rated to require further development for computing reactive, turbulent flows.

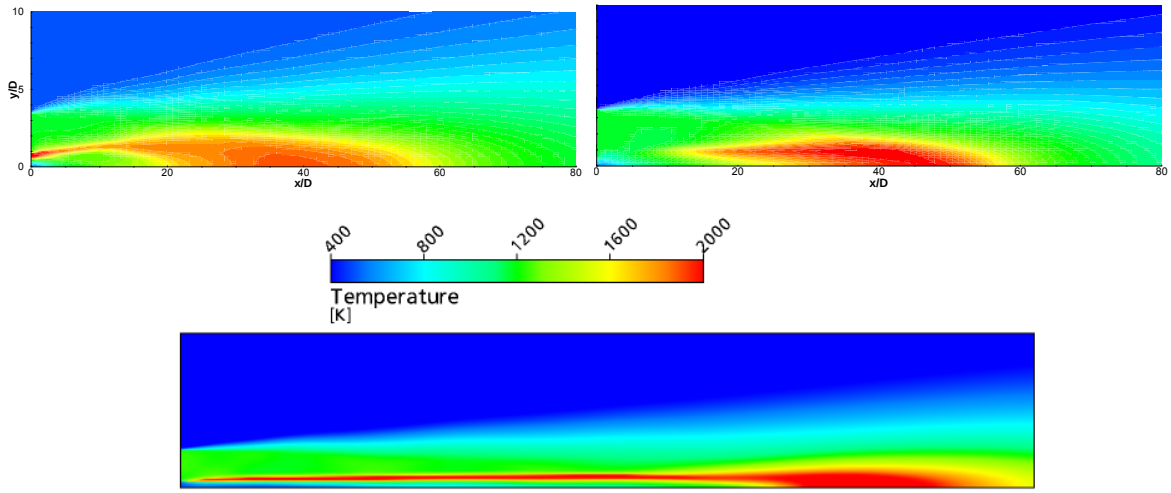

Rocflam-II simulations of H2/Air supersonic combustion Cheng experiment: top left: equilibrium chem./PPDF, supercritical droplets; top right global chem./EDC, supercritical droplets; bottom: CFX global chem./EDC (solver predicts a flame length, which is much too long)

Task 6.4 Supersonic Kinetic Combustion Modelling

The main topics of task 6.4 were the development, verification and validation of the density-based module of the CIRA code C3NS for supersonic combustion phenomena simulation **[D6.4.1]**.

During the first period of LAPCAT, the capabilities of an initial version of $C3NS_{DB}$ (version 1.0), able to consider only air as an ideal gas, have been extended to generic multi-component mixture of reacting gases. In particular, species mass-fractions balances have been added to the system of governing equations, together with a point implicit method to compute the species source terms. Furthermore, the thermodynamic models have been modified in order to consider general mixtures of thermally perfect gases.

The description of combustion processes in a scramjet engine requires finite-rate chemistry models, because residence times are the same order of magnitude as the chemical characteristic times. Therefore, during the second period of LAPCAT, a trade-off analysis of kinetic schemes has been performed to select a reduced chemical kinetics mechanisms suited to properly describe the oxidation of hydrogen, methane and kerosene in the conditions of interest for the LAPCAT M8 engine **[D6.4.2]**. In particular, different behaviours between hydrogen and hydrocarbons have been pointed out, which are here summarized. In the analyzed thermodynamic conditions the H_2-air mixtures burn within a small portion of the combustor length. On the other hand the heat release process for both kerosene and methane is much slower, therefore, a minimum length needed to achieve full combustion could be of the same order of magnitude as the assumed combustion chamber length; so to analyze combustion process, in WP6.4, the H_2-Air combustion has been considered.

Moreover, detailed chemical kinetic mechanisms, although accurate, involve a number of reactions and species too large to be included in a multi-dimensional flow solver, so has been made an analysis in order to select chemical reduced kinetic mechanisms that reproduce, in a satisfactory way, the detailed mechanism, selected as reference, in terms of adiabatic flame temperature and ignition delay time.

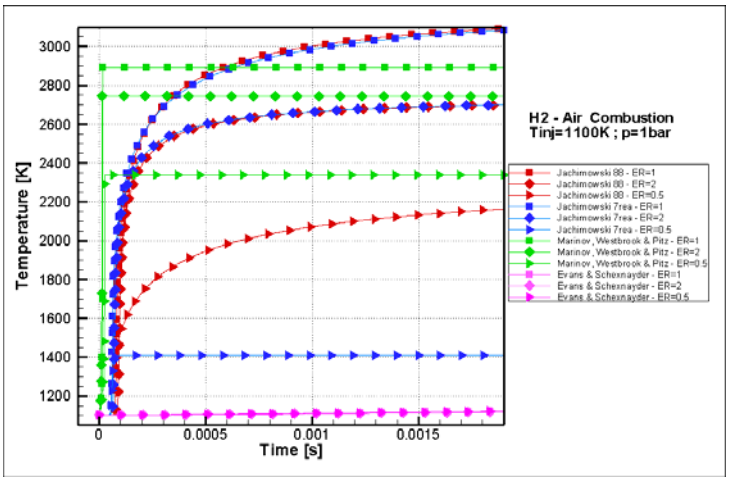

Example of chemical kinetic scheme trade-off analysis for Air – H_2 combustion: T=1100 K, p=1 bar

In the third and final period of LAPCAT the validation and testing phase of the supersonic combustion simulation code $C3NS_{DB}$ has been carried out **[D6.4.3]**.

Therefore, some flow problems have been selected from relevant literature in order to obtain a verification of the implemented models and a validation by comparing numerical and available experimental data.

In particular, 2D flow problems, reproducing supersonic mixing and combustion processes have been investigated, moreover, some 3D tests have been proposed including a scramjet tip to tail simulation. The following four tests, representative of typical supersonic combustion configuration, have been analyzed.

- TC-1: normal Injection (mixing)
- TC-2: parallel Injection (mixing and combustion)
- TC-3: supersonic combustion in rectangular channel (mixing and combustion)
- TC-4: scramjet tip to tail simulations.

The first case has been selected to verify and validate the code capabilities to predict the complex wave pattern and separation caused by the transverse injection of gaseous hydrogen in a supersonic air-stream, typical in scramjet combustors.

In the second one, the code has been tested for the simulation of mixing and combustion processes in presence of strong supersonic shear/mixing layer.

The third is a demonstrative flow case reproducing mixing and combustion in typical conditions scramjet combustor chamber conditions.

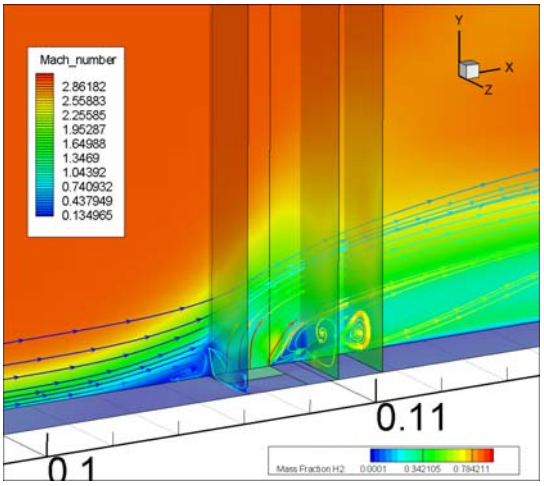

TC-3: Zoom of the injector region, Mach contour and streamlines coloured with H_2 mass fraction

The last test case is a tip to tail simulation of a scramjet wind tunnel model flow case representative of a scramjet tip to tail laboratory model developed and tested at the University of Queensland. It has been selected to assess code capability in the simulation of all the structures typical of a scramjet engine flow, such as: compression, shock induced ignition, supersonic combustion and expansion. Some results are shown in the following figures.

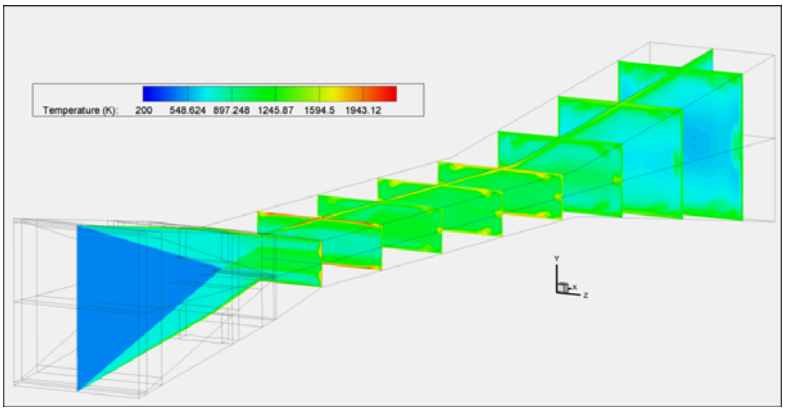

TC-4: Fuel-off case, temperature contour slices

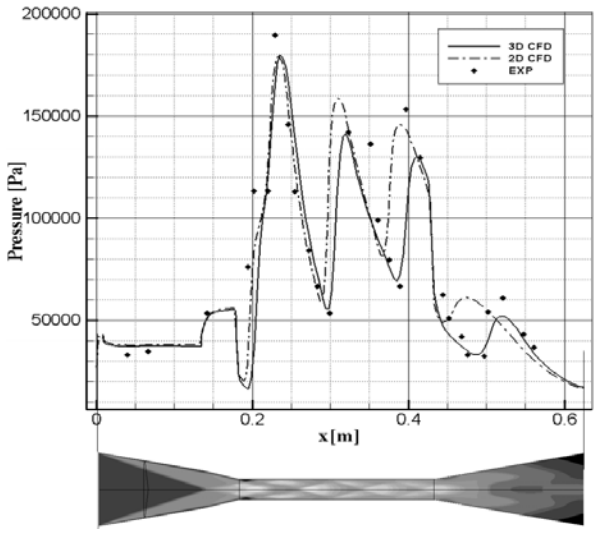

TC-4: Fuel-off case, scramjet model centreline wall pressure comparison with experimental data

The agreement obtained between numerical results and experimental data shows that the code is able to predict the mixing and combustion processes in typical scramjet engines configurations, this as confirmation that the main objective of the task is achieved **[D6.4.4]**.

A 1:1 duplication of the wind tunnel model was tested 2003 in HEG. The data resulting from the HyShot II flight and the HEG experiments have been compared with a detailed analysis of the flowfield topology based on the variation of the equivalence ratio. Detailed numerical analysis was performed for the flow conditions in HEG corresponding to 27.1 km altitude during the flight test. In 2007, a new ground test campaign with additional pressure ports, heat transfer gauges and glass side windows of the combustion chamber was launched in HEG within the framework of LAPCAT on which the present numerical study is based on. The targeted equivalence ratio during the tests was 0.3 which is below the limit for thermal choking and should ensure a pure supersonic combustion.

Beside the fuel-on and -off condition numerical simulations have been done with the Spalart-Allmaras turbulence model and the 2-equation k-ω model **[D6.4.5]**. As explained before, the k-ω model leads to a higher heat release and pressure rise due to the enhanced mixing and combustion process. This is also a result of higher turbulent viscosity level in the boundary layers entering the combustion chambers being enhanced by the shock reflections in the duct. The shock patterns are well resolved, the maximum dimensionless pressure reaches 1.8 (SA) and 2.02 (k-ω) as shown in the figure below. The results are sensitive to the turbulence modelling. The pressure peaks are shifted due to a slightly different flowfield. Since the shocks undergo multiple reflections in lateral direction and at upper/lower walls the shifts increase with increasing *x*. Analyzing the flowfield unveils that the flow is close to sonic speed with local subsonic pockets (close to the injector symmetry plane). Every strong shock impingement leads to a subsonic pocket. The Korkegi correlation predicts separation at a dimensionless pressure of 2.3. Due to the almost sonic flow over a large part of the combustor close to the injector plane the shocks being reflected inside the duct are closer to normal. Therefore, more but weaker pressure peaks in the combustor for the results based on the k-ω turbulence modelling occur.

Also on the upper wall, the numerical results show a good agreement with the experimental data for both fuel-on and -off condition. The shock positions are well predicted, the shifting of the shock impingement points due to different turbulence modelling can be seen. The pressure increase is well predicted employing the k-ω turbulence model; the experiments show slightly different values only at x=0.24 and 0.25.

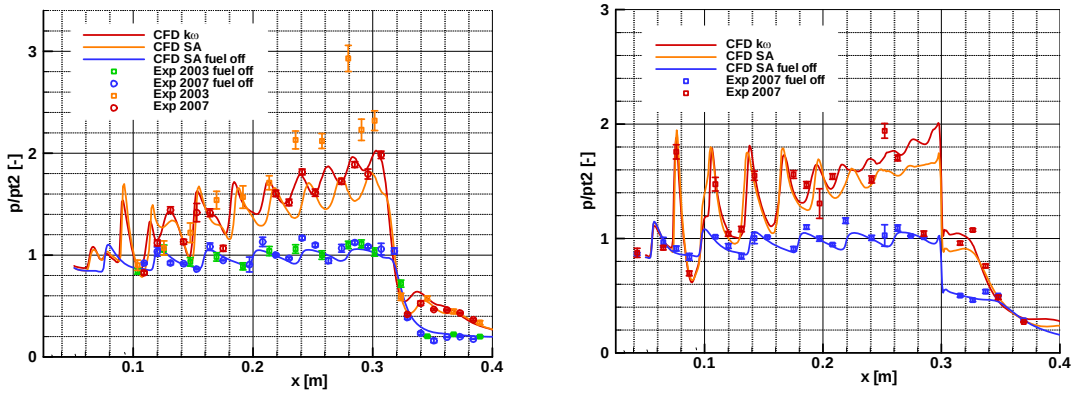

Air-tests, pressure at lower wall (left) and upper wall right) at spanwise symmetry plane

Additional data extraction was done to investigate the possible reason of the discrepancies concerning the heat flux between experimental and numerical results. These discrepancies occur mainly at the lower wall, where the fuel injection in located. The heat flux at the injector symmetry plane on the lower wall is compared with data originating from 1, 2 and 3mm spanwise offset I shown below. It shows clearly the presence of a large gradient in spanwise direction. Since the computational domain is about 10mm wide but more than 300mm long, a slight asymmetric behaviour originating from e.g. the positioning accuracy (yaw angle), manufacturing accuracy (injector position, diameter) is the most possible explanation.

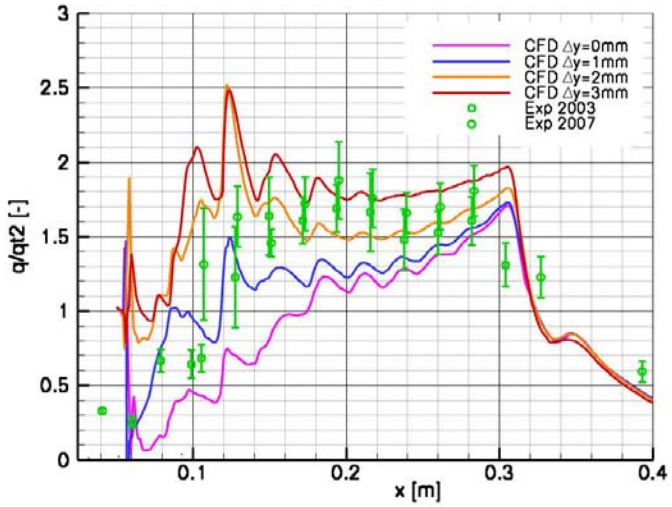

Air-tests, heat flux at lower wall (injector plane, 1mm, 2mm and 3mm spanwise offset)

WP 6.5: Turbulent Supersonic Combustion Simulation: Assumed PDF

The main objectives of Task 6.5 were:

- Extension of the DLR TAU Code for supersonic hydrogen combustion (RANS + assumed PDF) resulting in the provision of an efficient and flexible CFD platform for the design of complex advanced hypersonic transport vehicles
- CFD support for WP5

During the first project-year a laminar combustion model for a gaseous hydrogen / air mixture was implemented in the DLR Tau code by DLR-AS-RF in Gottingen. This model is largely based on the existing code infrastructure for the aerothermodynamics of the re-entry flight of space vehicles (chemical non-equilibrium and equilibrium flows). Partition functions for individual species and appropriate mixture rules are used to compute the thermodynamic and transport properties of the reacting gas mixture. This offers the possibility of future model extensions (e.g. multi temperature models to account for thermal nonequilibrium). Basic test were used to verify correct implementation (detailed description in the Lapcat-Deliverable **[D6.5.1]**). Several reaction rate schemes with different level of complexity have been implemented in the code.

During the second period, the TAU code was further extended with an assumed PDF method to account for the influence of the turbulent flow in Scramjet combustors on the chemical production rates. These extensions and the corresponding validation are described in detail in the deliverable **[D6.5.2]**. The assumed PDF approach was chosen from many available turbulent combustion models for the following reasons:

- Wide range of applicability for premixed, non-premixed and partially premixed combustion and different Damköhler numbers,
- Limited computational cost, high robustness and straightforward implementation,
- Convergence acceleration techniques can be used because the PDEs for the needed temperature and concentration variances have the same form as the Navier Stokes equations (contrary to e.g. multi-dimensional PDEs used for transport PDF methods that need to be solved with particle methods).

The complete supersonic combustion model in TAU therefore consists of models for reacting multi-species flows in chemical non-equilibrium and models for the turbulence-chemistry interaction. It was validated and tested using experimental benchmark results for a supersonic coaxial burner which produces a lifted flame at typical Scramjet flow conditions (Cheng et al., Vanderbilt University). The flame lift-off distance and flame structure could be reproduced by the numerical investigation of the test case using the DLR Tau-Code. It should be noted that differences in the numerical solutions occur mainly due to the application of different turbulence models.

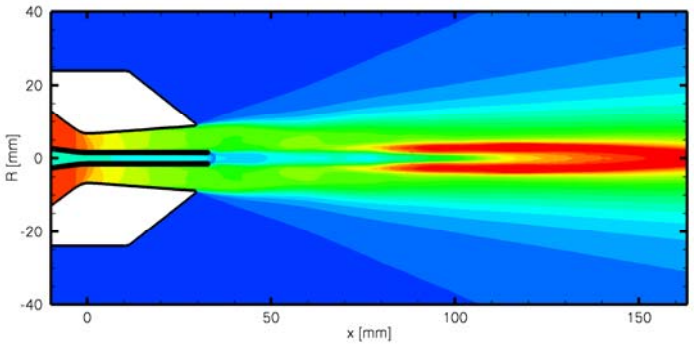

CFD result of the temperature field for the lifted supersonic flame of the Cheng-Burner ***[D6.5.2]***

The work in task 6.5 during period 3 concentrated on the application of the numerical simulation tools to the HyShot scramjet configuration in close interaction with the experimental investigation in task 5.2. The experiments were further supported with additional CFD analysis of

- the transient starting process of the porthole injector system
- the flow in the wind tunnel nozzle to calibrate the free stream conditions in the HEG facility
- the flow past static and Pitot pressure probes to assess their characteristics at the corresponding flow conditions

The numerical simulations of the complete flow-path including the wind tunnel nozzle and the HyShot Scramjet configuration show good agreement with the experiments. Wind tunnel results of performance characteristics (combustor) pressure rise and surface heat loads of the HyShot II scramjet configuration were reproduced by CFD. Uncertainties of numerical tools linked to different turbulence models were identified. A detailed description of this activity is given in the deliverable **[D6.5.3]**.

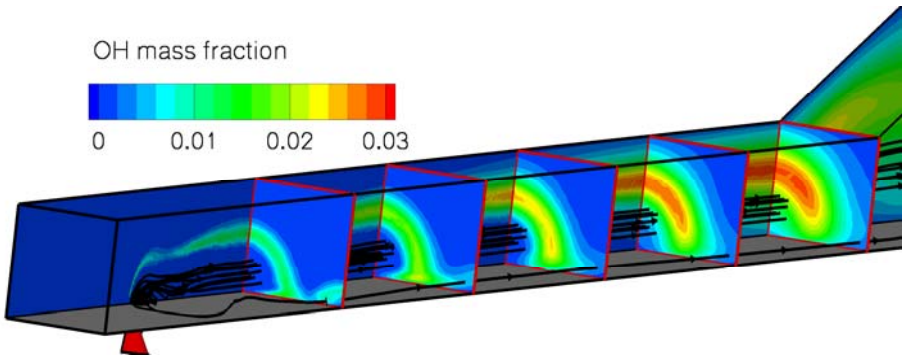

CFD result of the flame structure (OH concentration) in the HyShot-II combustor with porthole injection

The main objectives of this task were achieved. The CFD results for supersonic combustion configurations that were obtained with DLR-TAU code show good agreement with experimental and numerical benchmark data. The additional capabilities of the code to handle complex geometries with unstructured and hybrid grids including mesh deformation and chimera and the option of time accurate simulations using a dual time stepping technique qualify it as a CFD platform for the design of complex airbreathing propulsion configurations.

WP 6.6: Turbulent Supersonic Combustion Simulation: Multi-Variate Assumed PDF Approach

In WP6.6.1 the study concerning the applicability of several hydrogen/air reaction mechanisms for scramjet applications has been performed. Seven detailed (9-species, 19- to 27-step), one reduced (7-step, 7-species) and one global kinetic scheme have been investigated by DLR-VT at Stuttgart **[D6.6.1]**. The basic result is that at critical conditions close to the ignition limit of hydrogen (this corresponds to low flight Mach numbers of a scramjet) only detailed mechanisms are able to accurately predict the ignition delay correctly. However, there are also significant differences between the detailed kinetic schemes and the best suited

mechanisms for scramjet simulations are identified. The next figure shows the investigations of a lifted turbulent jet flame with supersonic inflow (Cheng et. al.) employing different reaction mechanisms.

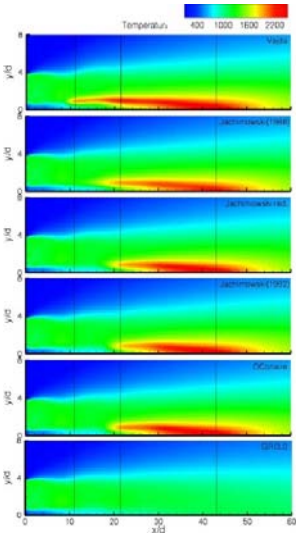

2D temperature fields of Cheng-experiment employing different reaction mechanisms

In WP6.6.2 three different lobed strut injectors in a M 2.8 model scramjet were investigated numerically **[D6.6.2]**. The struts differ in length and thus create different amounts of circulation. The comparison of the different struts has shown that the shortest strut has the best mixing and burning efficiencies (with and without combustion) in the middle and far field, while the longest strut performs best in the near field, respectively. The differences in the losses in total pressure are relatively small (the shortest strut has the greatest loss in total pressure compared to the other two struts). In the standard configuration lifted flames are obtained that are stabilized by shock waves. Additionally a modification of the standard configuration (increased air inlet temperature) has been investigated where an attached flame stabilized by a subsonic bubble has been observed. Furthermore the effect of an assumed PDF approach on the combustion process has been investigated. Thereby the use of the PDF approach yields to a shorter ignition delay and higher temperature. Hence turbulence chemistry interactions have a strong effect on the combustion process and should be taken into account. The figure below shows the calculated temperature distribution of the combustion chamber with different lobed strut injectors.

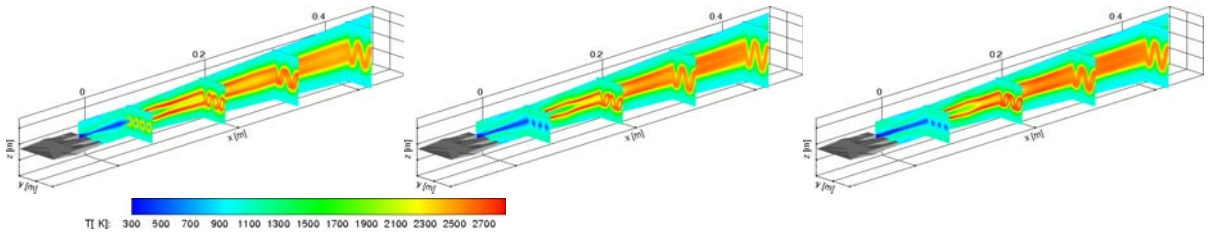

Calculated temperature distribution of the combustion chamber with different lobed strut injectors

In WP6.6.3 the ground experiments of the HyShot configuration performed at the High Enthalpy Shock Tunnel Göttingen are investigated numerically, in particular shot 663 of the test campaign in 2003, using the scientific in-house code TASCOM3D of DLR-VT. Different inflow conditions (without fuel, fuel into nitrogen, fuel into air) have been investigated and compared with the experimental data. The agreement of the numerical simulation with the experimental data is reasonable in all cases. The numerical results are discussed in detail **[D6.6.3]**. A lifted flame has been observed for the inflow conditions of shot 663. Additionally it has been shown that the combustion occurs in a mainly subsonic area. The right figure shows the calculated water distribution of the HyShot combustion chamber.

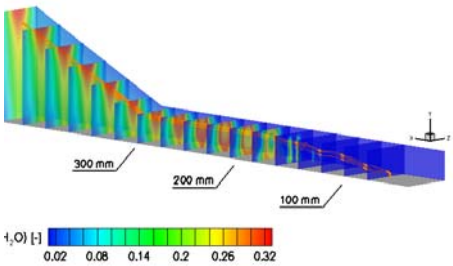

Calculated water distribution of the HyShot combustion chamber

In WP6.6.4 an assumed PDF (probability density function) approach has been investigated concerning its use for scramjet applications. Because only one supersonic combustion experiment is available where detailed PDF data is provided, a subsonic hydrogen jet flame has been chosen as a second test case. It has been shown that the kinetic scheme, the turbulent fluctuations and the chosen grid are of great importance for an accurate prediction of ignition delay and of the lift-off height of the supersonic flame **[D6.6.4]**. Moreover, PDF structures have been investigated at different positions in the flames and a study concerning the accuracy of the chosen approach is performed for both flames. The figure below shows the calculated mean temperature distribution of a subsonic hydrogen jet flame. Indicated are positions for comparison with experimental data. The squares (pos. 1 to pos. 5) indicate locations, where PDF structures, rate constants and reaction rates are investigated. The other figure shows 1D marginal PDFs of temperature and hydrogen mass fraction at different positions in the flow field obtained by experimental (dots) and numerical (line) data.

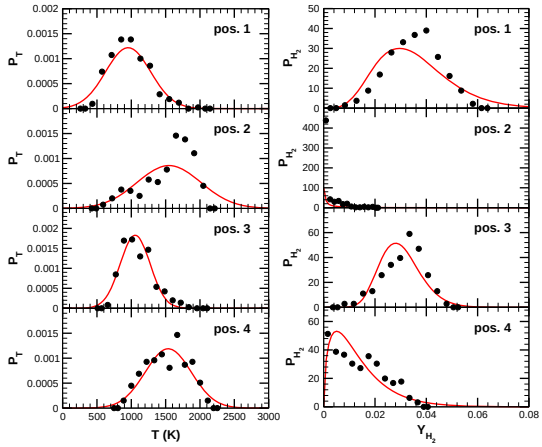

1D marginal PDFs of temperature (left side) and hydrogen mass fraction (right side) at different positions in the flow field.

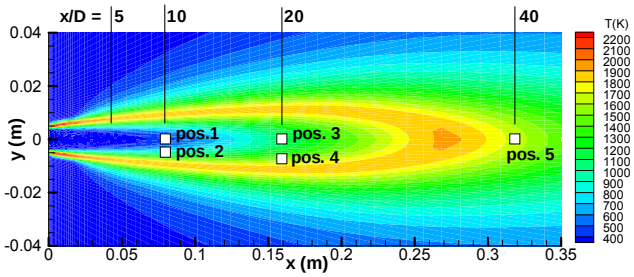

Calculated mean temperature distribution of a subsonic hydrogen jet flame

WP 6.7: Turbulent Supersonic Combustion Simulation: LES-SGS modelling

In WP 6.7 a novel subgrid scale model for LES of supersonic reactive flows has been developed [D6.7.1]. In order to develop this model, the analysis of the physics of supersonic combustion has pointed out that in supersonic flows the compressibility plays a key role on mixing and combustion. In fact, despite Papamoschou and Roshko stated that compressibility suppresses mixing in 2-D at the convective Ma_c>0.6, dimensionless analysis at DMA shows that by increasing streamwise vorticity, mixing is fast and efficient. In particular, by analyzing the dimensionless Navier-Stokes equations, it can be shown that baroclinic and compressibility terms become as important as vortex stretching in the supersonic regime. Furthermore, at Ma>1 also chemical kinetics and combustion are influenced by the dilatational term ("$\nabla \cdot u$"). The SGS model for Large Eddy Simulation (called ISCM) has been derived taking into account the effect of the Mach number on mixing and combustion. The ISCM LES SGS model of WP 6.7 has been tested using the NASA-Langley test case, where hydrogen is injected obliquely (30°) at Mach 2.5 into a Mach 2 airstream.

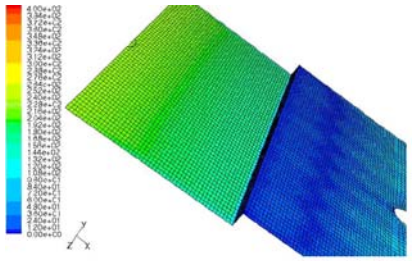

Instantaneous Contour of Wall Y^+ in the first part of the combustor

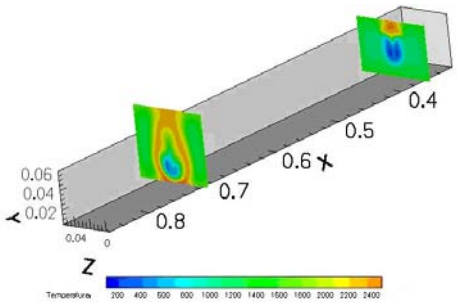

3D view of the numerical averaged temperature field at X=0.35 cm and X = 0.7 cm

Three-dimensional LES were performed with the FLUENT 6.3 ™ code commercial code to simulate the flowfield in the NASA Langley combustor model [D6.7.2]. The FLUENT code was also validated. Double precision has been used. The LES solver is a coupled, upwind, explicit, third-order MUSCL, accurate both in space and time.

The SCRJ combustor geometry of the left figure has been mapped by a 3-D grid. This domain was discretized with a grid of 700 points in the streamwise direction, 46 points in the cross-stream direction, and 60 points in the spanwise direction. The grid was made finer near the step and the fuel injector. The number of hexahedral cells of the computational domain is 1,563,994, for a total of 1,626,578 nodes. Only the first

800 mm of the whole length of the combustor (1234.2 mm) have been simulated. With this grid, a very small wall Y^+, of order 4-8 has been obtained near the step and the H2 injector, where the NASA experiment predicts bow shock formation. At the inlet the grid should probably be further refined to allow a better prediction of the boundary layer. That is, however, not as important as the region where fuel and air are mixing.

Both the shock departing from the step and that just upstream of fuel injection are predicted by simulations, this leading the two counter-rotating vortices generation along the stream direction. Also shocks reflection between the upper and the bottom walls is correctly predicted.
These simulations have shown that the ISCM subgrid model is in better agreement with experimental data than the Smagorinsky-Lilly model: in fact, while the Smagorinsky-Lilly model predicts neither combustion nor vortex structures, the ISCM model predicts flame anchoring, streamwise vorticity and temperatures close to those observed in the experiments.

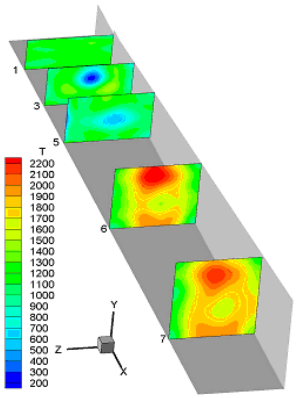

3D view of the experimental average temperature field

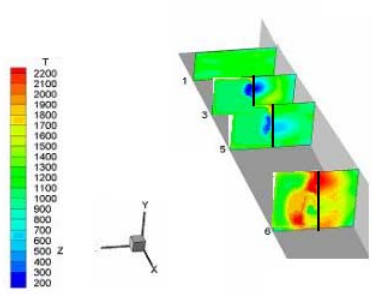

Numerical averaged temperature field at X=0.3 cm, X = 0.7 cm and X=0.8 cm

The major result of this work is that combustion may be made to take place in a short distance (about 1 m or less) by supersonic injection of hydrogen inside the supersonic airstream. Further, the results indicate that a hot spot due to reflecting shocks positions itself just downstream of the fuel injector exit into the airstream. This hot spot is the primary responsible for anchoring the flame, that at a conventional (e.g., constant and uniform) turbulent Sc number = 0.7 number moves back and forth with a frequency of about 2500 Hz. This unsteady behaviour is not predictable using RANS approaches, and shows the actual physical structure of the supersonic flame. Simulations with a locally variable Sc number (as predicted by the new model developed in LAPCAT for species transport, see later) have shown that the flame is still unsteady, but the amplitude of the oscillations is lower than in the case of constant Sc. Numerical result are in a reasonably good agreement with experimental results (right figure above)

Experiments indicate a rather distributed combustion; simulations with a conventional Sc have shown that combustion is mostly confined near the air/H_2 mixing region. By looking at the physics of the small scales and at their influence on the scalars turbulent transport, a novel SGS model for the turbulent diffusivity (species transport) has been also developed. In this new SGS model, the scalars transport is no longer supposed to be proportional only to the eddy viscosity, i.e. to the small scales turbulent velocity, but also to scalars fluctuations that must be accounted for. This advance in the ISCM model may therefore be the key to better reproduce experimental results. Numerical simulations with the new model now running have begun to show that combustion is spread over a larger region, in better agreement with the NASA measurements. The pressure and temperature distribution are also very well matched.

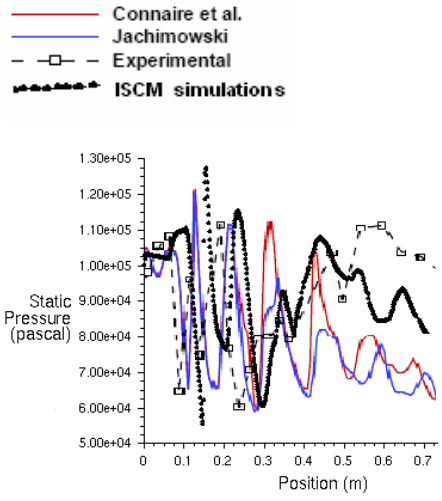

Comparison of the Pressure distribution along centerline of bottom wall obtained with the ISCM model (black line), Connaire kinetic sheme Results by Keistler (red), Jachimowski kinetic scheme results by Keistler (blue) and the experimental results (broken line)

Attention has been also put in WP 6.7 on scaling laws for the mixing and chemistry of supersonic combustion. Although not originally contemplated in this WP, scaling laws were examined in order to produce a rough but workable first cut for the combustor length. In fact, combustor length shapes vehicle length, especially

where cross section is maximum, thereby affecting strongly overall weight at take-off. The conclusions reached so far from theory and simulations indicate that at low air inlet temperature (about 1000 K) combustion length, L, is controlled by the interplay between kinetics and turbulent mixing. At lower temperatures kinetics times are longer than those associated to mixing, and the flame anchoring process is definitely controlled by kinetics. At higher air T of order 1100 K and higher, kinetics is fast, as shown also by results of WP 6.6 (see below), so that combustion length is dominated by mixing time. Scaling in this regime becomes more complex but still suggestive of short combustor length (of order 1 m) *provided* fuel jet(s) are also fast. A relationship has been derived that has successfully predicted flame attachment length in very good agreement with the experiments at NASA-Langley.

The second item explored during these three years has been the possibility of replacing low density LH_2 with combustible gases obtained by pyrolysis of LHC such as, for instance, kerosene or LCH_4 (natural gas). The analysis shows that pyrolysis of liquid HC is feasible by utilizing the HC as coolant of hot external (e.g., leading edges) or internal (e.g., combustor walls) surfaces. Said otherwise, the endothermic heat of decomposition of liquid HC is capable of cooling hot vehicle parts while at the same time yielding combustible species such as hydrogen, methane, ethylene and other gaseous HC at high pressure, to be injected inside the engine and thereby contributing to thrust. These positive findings are limited by the limited cooling capability with respect to that of LH_2.

Deviations from the project workprogram:

LES with hydrocarbons has not been performed because Hydrocarbons have been considered of low interest to the stated goal of LAPCAT (a long range passenger plane capable of Mach 8 flight from Brussels to Sydney). While LH2 looks probably capable of achieving this performance, LHC have been eventually ruled out on the basis not only of range capability, but also of cooling effectiveness.

2.2.6 WP7 Design and Aerodynamics of Propulsion Units

To design a hypersonic vehicle using an air-breathing propulsion system with positive net thrust is a major technological challenge. The major difficulty lies in the determination of the pressure and skin friction drag. The accuracy to predict pressure drag depends upon the ability to characterize the complex system of shocks (i) acting at the inlet and (ii) due to the interaction of the nozzle flow with the external flow; the accuracy to predict skin friction drag, on the other side, depends upon the ability to determine the boundary layer state, i.e. laminar or turbulent and its behaviour with temperature. Such difficulties derive from the fact that in ground based facilities it is not possible to simulate complete real flight environments. Consequently, the successful design of a vehicle powered by an air-breathing engine would be based tomorrow purely on computational fluid dynamics (CFD), but today the numerical tools present strong limitations, in particular concerning turbulence modelling and shock-wave boundary layer interaction. Thus, the objective of the work-package has been the validation of design tools to determine the propulsive efficiency of air breathing hypersonic vehicles, i.e. not the intent to design an efficient inlet or nozzle but to improve the knowledge of the hypersonic flow physics, in particular intakes and nozzles with respect to transitional and turbulent flows and unsteady flows

Task 7.1 Design and Aerodynamics of Intakes (DLR)

An air inlet representative of the LAPCAT Mach 8 vehicle has been designed by DLR-AS-WK (Cologne) in accordance to geometric constraints driven by the vehicle (WP2) and in accordance to requirements of the flow at the inlet exit stemming from the combustion chamber (WP4) **[D7.1.1]**. The design tools included DLR in-house tools featuring one dimensional gas dynamic analysis, method of characteristics (MOC) and computational fluid dynamics (CFD). A planar inlet, named LC01k, consisting of two external compression ramps and a cowl that causes two internal compression shocks has been designed. At the design point of Mach 8.034 and a flight altitude of 34.134 km the inlet performance fulfils (or exceeds) all flow requirements, i.e. mass flow, static temperature and static pressure. Based on the LC01k, two wind tunnel models have been designed and manufactured, one used for the H2K blow-down test campaign and the other one for the HEG shock-tunnel. The H2K model is equipped with 23 static pressure probes along the centreline of the inlet and the diffuser and with two Pitot pressure probes in the diffuser to measure the total pressure recovery. The mass flow through the inlet can be determined by a connected throttle, which is also used to vary the back-pressure. Thus, the inlet performance can be evaluated in form of so called “throttle curves”, which show the pressure recovery over the captured mass flow ratio. Further, it offers the capability to test different boundary layer bleed configurations and also to test a “backward facing step”-approach to control

the separation of the boundary layer at the inlets expansion corner **[D7.1.4]**. Two windows in the models side walls allow to visualize the flow in the critical area near the throat and the boundary layer bleed by means of Schlieren optics.

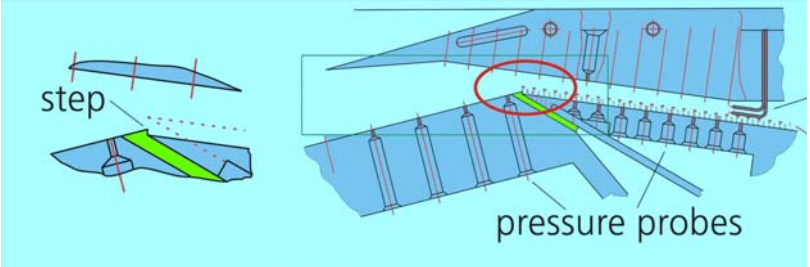

Schematic view of the Intake model for the investigation in H2K. In the right view the light blue box indicates the location of the model window; the red circle area is zoomed on the left hand side of the figure showing the boundary-layer bleed channel. The channel can be flush closed or building a backward facing step

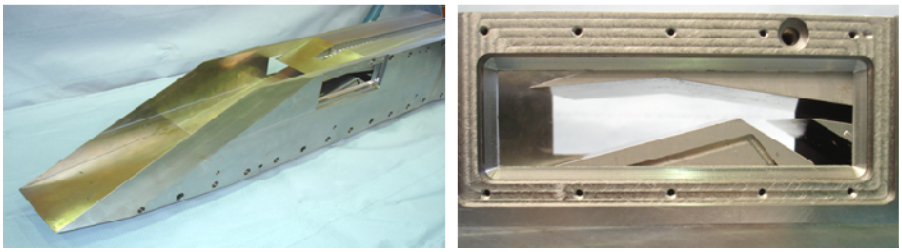

Intake model for the investigation in H2K. Left: top-down view showing the 2 compression ramps, the cowl and the model window. Right: view through the model window showing the cowl tip (top left) and the open bleed-channel (right).

First reporting of the experimental investigation in H2K shows inlet performances as expected **[D7.1.2]**. While the design of the inlet satisfy the flight requirements, under wind tunnel conditions the strongly reduced Reynolds number has as consequence that the cowl shock impinge the boundary layer earlier and the flow separates at the expansion corner before the boundary layer bleed. To prevent such separation, already observed during preliminary CFD analysis, a modified design for the wind tunnel model has been provided by ESA-ESTEC **[D7.1.4]**. It is a case of a so-called multi-shock compression inlet with extended bent cowl. The model used for the investigation in the HEG facility is simpler than that for the H2K but features also the above mentioned modification **[D7.1.3]**. It consists of a base plate and side walls with the cowl attached to the sidewalls. In between the sidewalls a slider plate is installed on to which the inlet and the combustor are fixed. The measurements in HEG are done to demonstrate that measurements for such a configuration in a transient working facility like HEG are comparable to the measurements performed in continuous running facilities like H2K.

Currently CFD rebuilding of the H2K-tests show that the carrier code used for the present numerical investigation, DLR-TAU, is able to capture almost all the dominant features, like the changes in flow features when the boundary-layer bleed-channel is open or close or due to varying Reynolds number **[D7.1.3]**. As depicted in the figures. Below, the numerical results obtained are very encouraging. Complete 3D Navier-Stokes computations using high order turbulence models like DES and LES have been used to assess the flow in inlets and nozzles and to account for the interference with the external flow under severe shock-wave boundary-layer interaction and unsteady shock-shock conditions **[D7.4.2]**. The present limitation of the TAU code corresponds for transitional flows respectively flow with embedded turbulent spots; in such cases, methods based on LES are very promising (see also Task 7.4). In particular, for the first time a complete mixed-compression hypersonic inlet is studied here using LES.

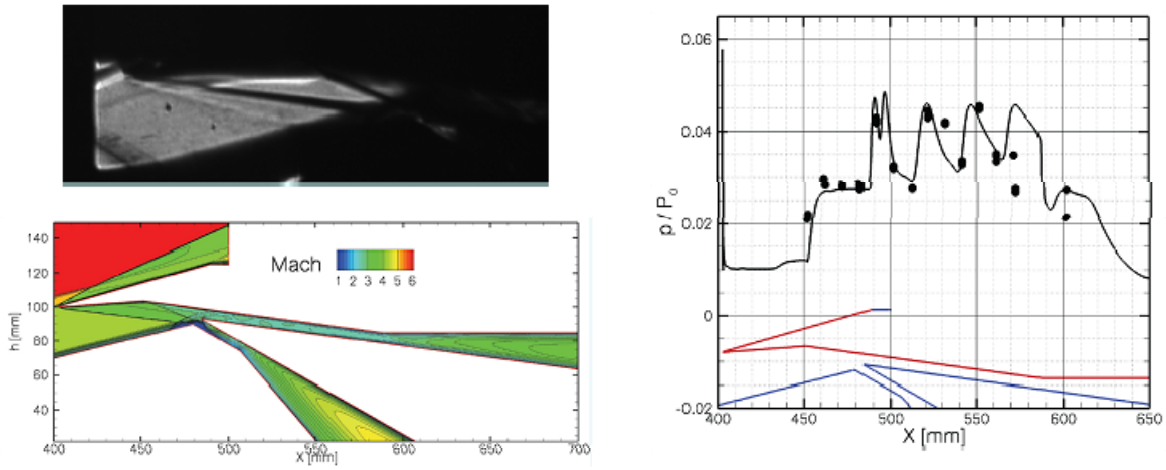

LAPCAT Mach 8 Intake-LC01k assessment (top-down model position). Top left: Schlieren through the model window during the test in the H2K facility. Bottom left: CFD simulation with the TAU code. Right: comparison of normalized computed and measured pressure along the wall of the cowl

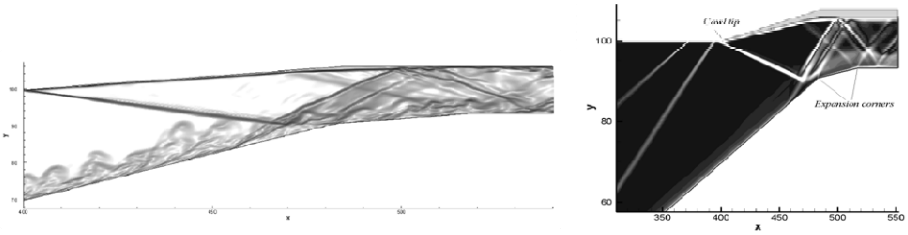

LES Simulations to assess the changes on the LAPCAT Mach 8 Intake-LC01k with closed bleed-channel (top-down model position). Left: pseudo Schlieren on the original Intake. Right: pseudo Schlieren of the modified Intake

Task 7.2 Nozzle Flow-Base Flow-External Flow Interaction (DLR-AS-WK: Cologne)

For the experimental study of the nozzle–base–external flow in the H2K facility a wind tunnel model of the SERN nozzle of the LAPCAT Mach 8 vehicle has been manufactured. The contour of the SERN nozzle has been designed by EADS-ST (WP4) in agreement with the requirements provided by DLR **[D4.2.1, D7.3.1]**. The model has a modular structure and thus enables it to be used for nozzle experiments with various nozzle geometries **[D7.2.1]**. In contrast to common nozzle-base flow studies in the past, which were done with compressed cold air, here the isolated air supply chamber of the model allows supplying the model nozzle with a supersonic air flow with total temperatures up to 1000 K. The model is equipped with 15 static pressure probes along the expansion ramp and the flap. Additionally, two transient pressure probes ("Kulites") are located at the flap to detect unsteady flows. Temperature and total pressure inside the settling chamber of the model are measured to determine the nozzle flow conditions. A Pitot rake that can be translated along two axes is located behind the model nozzle to survey the nozzle flow field. The "open" design of the nozzle without side walls allows for additional Schlieren visualizations during the tests.

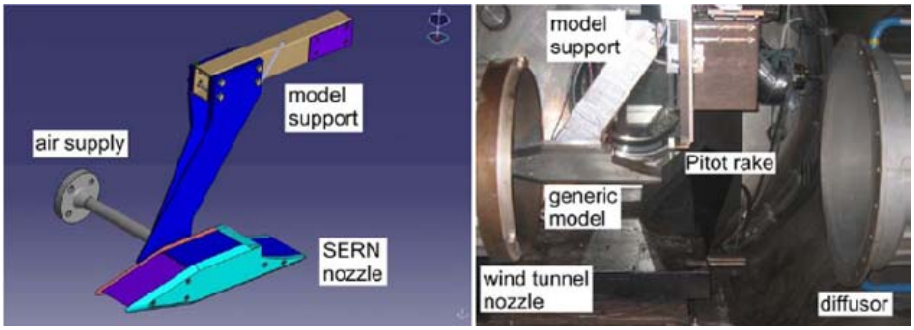

SERN nozzle model for the investigation in H2K. Left: schematic description of the model. Right: model installed in the test chamber of the H2K facility

The experimental results reveal the shear layer separating the nozzle. The wall pressure measurements help to show the influence of the flow on the vehicle and therefore as a consequence on the nozzle thrust. The experiments showed that from all the variables the nozzle pressure ratio has the largest influence on the nozzle flow field **[D7.2.2]**. The extent of the exhaust plume and the displacement of the ambient flow clearly grow with increasing nozzle pressure ratio. CFD results for the complete SERN nozzle including Laval nozzle and base (also called nozzle-flap) are performed according to the finding in Task 7.3. The computations are in good agreement with the experimental results but indicate a higher under expanded flow leaving the SERN nozzle (see picture below).

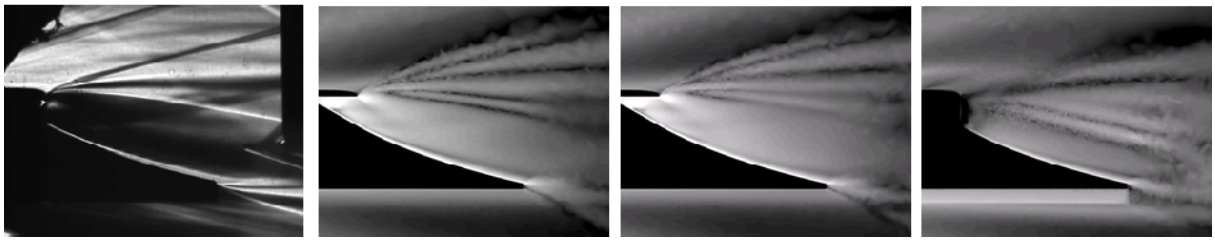

Left: Schlieren visualizations of the experiment (top-down model position) at nominal conditions. Following pictures: CFD simulations in 3 planes of different deep (outboard left to outboard right)

However, as shown in the figure below, quantitative good agreement is found with respect to the surface pressure values inside the nozzle and with respect to the nozzle-flow external-flow interaction indicated by the pressure field just behind the nozzle. Although a planar nozzle has been investigated, both numerical and experimental pressure fields show a strong three-dimensional nature of the exhaust gas flow **[D7.2.3]**.

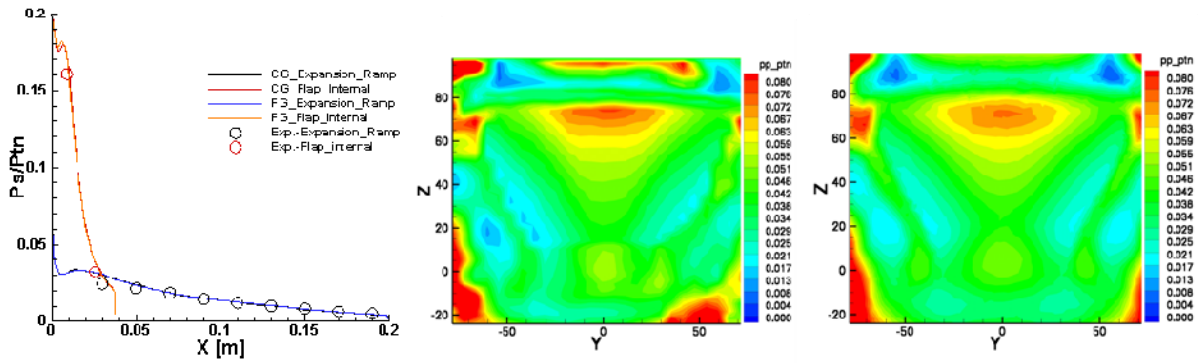

LAPCAT Mach 8 nozzle assessment (top-down model position). Left: comparison of normalized computed and measured pressure along the walls of the nozzle. Middle: field measurement of normalized total pressure. Right: computed normalized of total pressure

Task 7.3 Unsteady Aerodynamics of Nozzle Flows (DLR-AS-RF: Braunschweig)

To reduce uncertainties of turbulence modelling in the numerical simulation of base flow, nozzle flow and wake flows a detailed analysis of the capabilities of existent turbulence models of different type is necessary. To obtain realistic predictions of base flow-plume interactions as well as interactions with the external flow field an evaluation of these capabilities is of special interest. This is also important for a detailed understanding of the unsteady turbulent flow fields in the supersonic regime of such configurations.

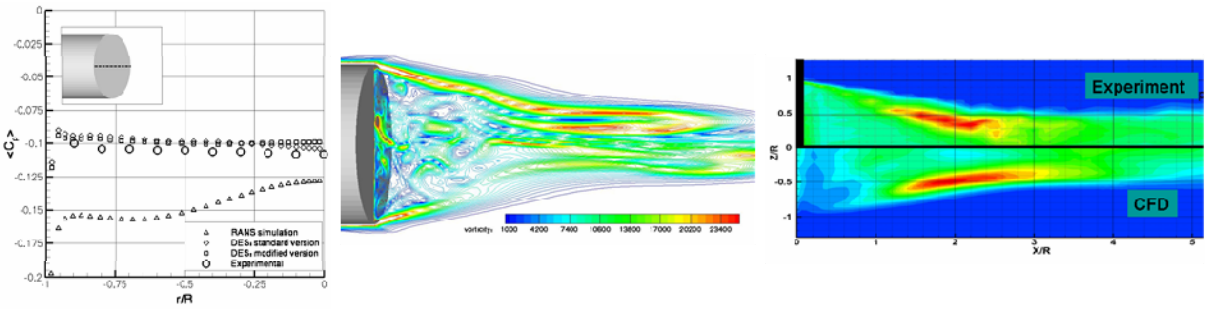

Numerical simulation of cylinder embedded in a Ma=2.46 supersonic flow using a detached eddy simulation (DES) turbulence model. From left to right: averaged pressure at the cylinder base; computed turbulent vorticity behind the cylinder; contours of experimental and numerical time averaged turbulent kinetic energy

For the base flow a supersonic axisymmetric flow field of a cylindrical base is investigated with several turbulence models since it is a well validated test case for unsteady supersonic separation including shocks and expansion waves (see above picture). Detailed RANS and DES investigations in on broad range of structured and unstructured grids of different resolution are carried out. In particular very promising results have been obtained with the DES model. Further, a cylindrical re-entry capsule under hypersonic conditions has been simulated with DES to show the extended capabilities of the model for higher Mach numbers.

The objectives of WP 7.3 are the unsteady aerodynamic effects of nozzle flow during start-up, shut-down or acceleration phase in order to be able to control the stability of a vehicle powered by an air-breathing engine, hence the validation of numerical tools concerning prediction of this flow regime is inevitable. Consequently are here also objectives the evaluation of RANS turbulence models to cope with unsteady separation. In a primary phase simplified configurations are chosen to earn experience with such regimes. Different RANS turbulence models (one and two equation) have been assessed for their ability to predict transient turbulent phenomena in separated nozzle flows as shown in the following picture **[D7.3.2]**.

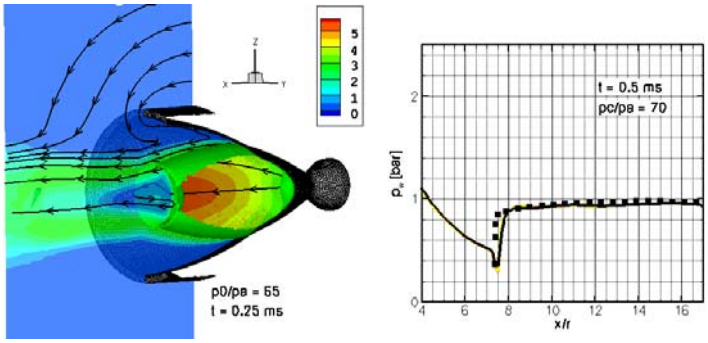

Numerical simulation of the unsteady flow inside a dual-bell nozzle. Left: 3D view of the nozzle flow topology. Right: comparison between computed (solid line) and measured (symbols) instantaneous pressure

But also evaluation of hybrid turbulence models like DES (Detached Eddy simulation) has been assessed. The main focus has been to quantify the improvement of accuracy of capturing transient flow phenomena correctly and the computational cost needed for this improvement. Computations of different stage of complexity are carried out using the DLR-TAU code and validated for the simulation of transient nozzle flow phenomena using appropriate experimental data (see picture below). This is mainly due to the need to accurately predict the side forces acting on the nozzle structure and the need to identify possible resonance phenomena with the unsteady wake flow which impose important constraints on the design of future high speed air breathing propulsion vehicles.

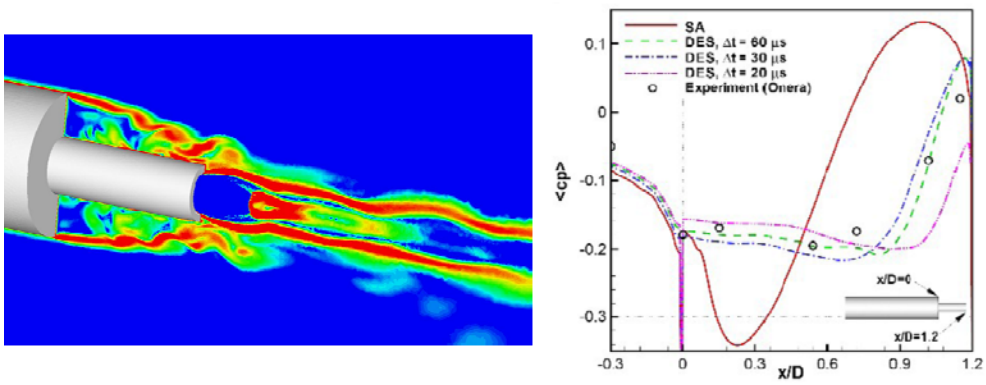

DES simulation of a nozzle-flow base-flow external-flow interaction at transonic conditions Ma=0.7, Re=14 10^6 with an over expanded nozzle, cold gas flow. Left: shear layer of vorticity contours. Right: time-averaged computed static pressure (SA: Spalart-Allmaras; DES: Detached Eddy Simulation)

Finally, a complete vehicle has been investigated at different stages of geometric complexity including nozzle and booster plume. The configuration has been simulated mainly by DES, but for comparison also URANS simulations have been carried out putting in evidence once more the strong advantage of DES over the classical one and two equations turbulence models **[D7.3.3]**.

Taking advantage of the experience accumulated with the DES for nozzle-flow base-flow external-flow interaction, the technique has been applied for the first time to simulate the flow inside the LAPCAT Mach 8 combustion chamber when the fuel injection is provided by means a hypermixer (picture below)

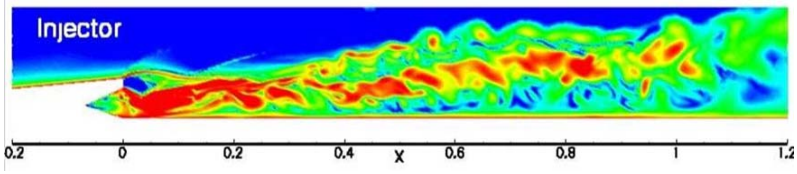

DES simulation of a Hypermixer as spin-off of simulation of a nozzle-flow base-flow external-flow interaction

Task 7.4 Compressible Transitional Effects on Intakes (SOTON)

Large eddy simulation (LES) of compressible flow with a mixed time-scale (MTS) subgrid model has been tested for three cases of turbulent and transitional flow: supersonic turbulent channel flow; propagation of localised transitional/turbulent spot in a supersonic boundary-layers and shock-induced separation bubble transition. The MTS model is found to perform well in the near-wall region without any ad-hoc near-wall damping functions. The subgrid-scale kinetic energy vanishes in the laminar regions, and it has been confirmed that this model perform well in predicting transitioning flows. A good agreement of the present LES predictions with the DNS results is observed for all test cases **[D7.4.1]**.

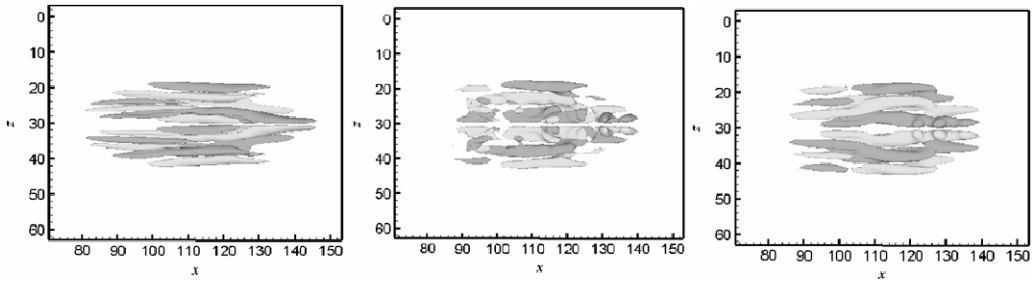

Iso-contours of wall-normal vorticity (+0.06,-0.06) at time t = 141 showing the spot envelope (Top view). From left to right DNS, no model and LES

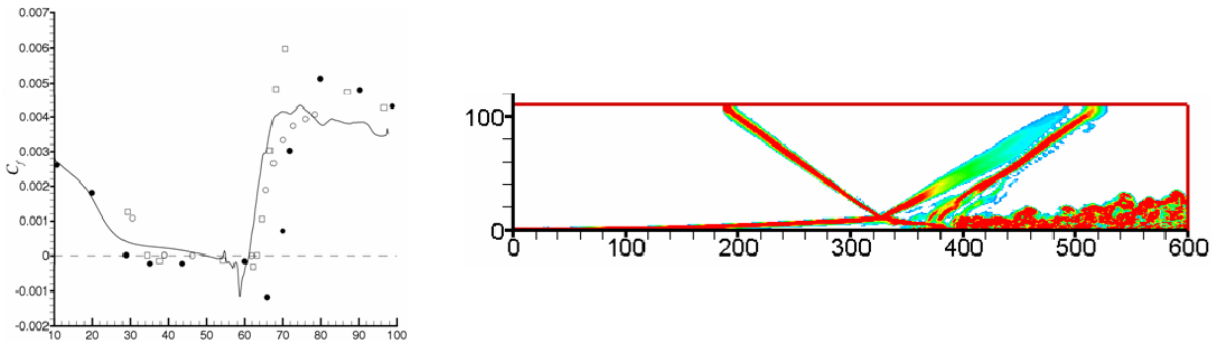

LES simulation of a M=2 oblique shock-wave boundary-layer interaction (pressure ratio p3/p1=1.9) inducing a laminar separation bubble and transitional flow at re-attachment. Left: mean skin friction distribution along the flat plate: solid line present LES; filled circle and open square LES of Teramoto (2005); open circle Experiments of Hakkinen et al. (1959). Right: numerical Schlieren showing the instantaneous flowfield at time t = 1811 at a spanwise location z = 30.

In a second step, large eddy simulation of compressible transitional/turbulent flow has been applied to simulate propagation of localised turbulent spots along the LAPCAT intake front ramp surface; transitional/turbulent boundary layer interaction with a shock wave near an intake compression corner, and turbulent flow over a convex corner with shock impingement upstream and downstream of the corner **[D7.4.2]**. Laminar-to-turbulent transition has been successfully triggered using localised blowing trips. Large amplitude disturbances have been used to create localised turbulent spots in a Mach 5 laminar flow along the intake ramp surface. The lateral half-spreading angle of the turbulent spot has been found to be around 3.4 degrees which is about a third of the value for low speed flows. A large separation bubble has been observed in the case of a shock wave interacting with a laminar boundary-layer along the intake compression corner. However, no separation has been observed when the boundary layer was in the late stages of transition. The extent of the separated region due to SBLI has been found to be highly influenced by the presence of a convex corner, as may be present at the combustor inlet.

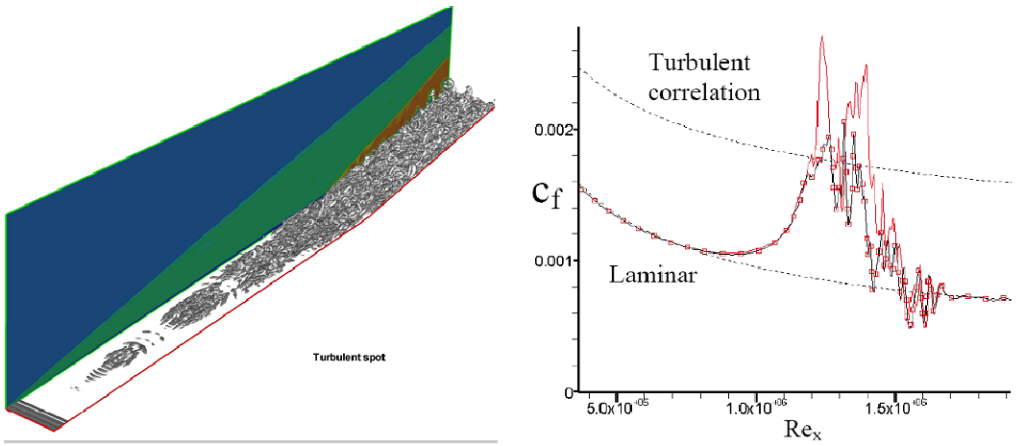

LES simulation of compressible transitional/turbulent flow along the LAPCAT intake front ramp surface. Left: evolution of transition/turbulent spots along the intake ramp superimposed with the density contours. Right: computed skin friction with LES, demonstrating that it is possible to have self-sustained transition to turbulence in a shock-induced separation bubble provided the pressure rise over the bubble is high enough.

Finally, the LAPCAT Mach 8 vehicle intake has been studied using the large-eddy simulation technique **[D7.4.3]**. The flow includes several examples of shock-wave/boundary-layer interaction for which LES has advantages over conventional Reynolds-averaged Navier-Stokes (RANS) and hence the results allow improving our understanding of laminar-to-turbulent transition processes, shock-wave/boundary-layer interactions (SBLI), separation bubble dynamics and shock/expansion interactions which are critical for the intake performance. Laminar-to-turbulent transition has been triggered using the technique previously validated by localised blowing trips in the first external ramp surface close to the intake leading edge. As in the validated case, the spots propagate within a Mach 5 laminar flow along the intake ramp surface. The transitional/turbulent shock interaction near the external compression corner has been found to enhance the transition to turbulence. Further downstream, the extent of the separated region due to cowl tip shock wave

impinging on the vehicle-side boundary layer is found to be strongly influenced by the presence of a convex corner. Perturbations from the vehicle side turbulent boundary layer are found to play a role in triggering laminar-to-turbulent transition along the cowl corner separation bubble. The complete details of the mean turbulent flow field along with the turbulence fluctuations are obtained for the flow entering the combustor inlet. This type of data should be useful in the future for simulating realistic combustor fuel-air mixing processes.

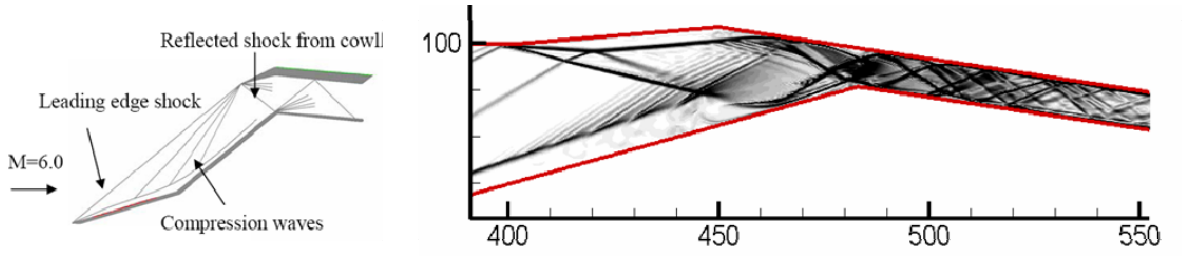

LES simulation of the LAPCAT intake. Left: schematic representation of the intake flow with closed boundary-layer bleed-channel. Right: numerical Schlieren (absolute value of density gradient) cut through the computational domain showing the flow field after the cowl shock (enlarged view)

Task 7.5 Intake Boundary-Layer Control (OXFORD)

The objective of Task 7.5 is to provide with decisive experimental data on the set-up and propagation of turbulent spots embedded in a hypersonic boundary layer by means of thin film gauge signals. The transition-trip device model to be used in the gun tunnel of the University of Oxford is a flat plate with detachable leading edge that can be pivoted allowing testing in a Ma number range 2 to 7, with sidewalls fitted with Schlieren windows. An array of 96 thin film gauges has been manufactured and bonded to the steel plate. The Oxford gun tunnel has been converted to LICH mode (Ludwieg Tube with Light Piston Isentropic Compression Heating) for steadier run times at the low stagnation temperatures required. Preliminary test results show that the flow is laminar along most of the instrumented test plate. Schlieren results show the presence of an oblique shock wave which develops from the test plate leading edge, whose angle confirms Mach 5.1 flow along the instrumented plate (matching the LAPCAT design condition). Further, two sets of boundary layer "trips" have been fabricated on two additional leading edge pieces. The results of the experimental campaign are reported in **[D7.5.1]**.

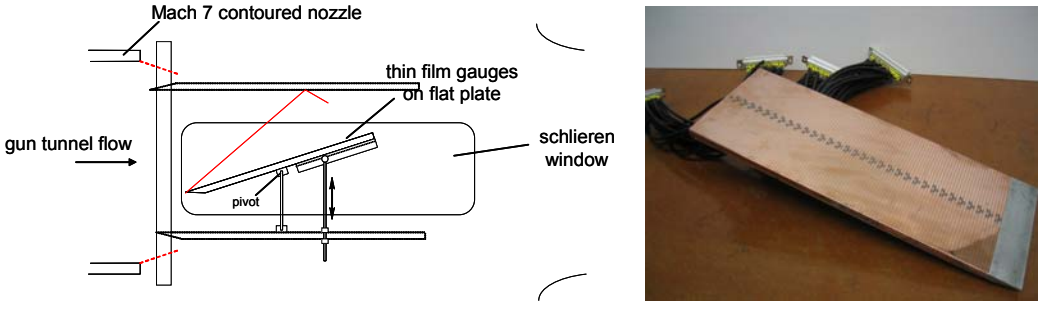

Schematic description of the tests in the gun tunnel (left). In the figure the plate mounted on the top, is instrumented with thin film gauges (right picture) to detect laminar/turbulent heat transfer levels and the propagation and/or merging of turbulent-spots

3. Technical resources

The High Enthalpy Shock Tunnel Göttingen

The High Enthalpy Shock Tunnel Göttingen (HEG) of the German Aerospace Center (DLR) is one of the major European hypersonic test facilities. HEG can operate over a wide range of test conditions: from low altitude high density Mach 6 flows, through the simulation of Mach 8 flow in approximately 30 km altitude, up to high enthalpy re-entry type conditions.

The HEG is a free piston driven shock tunnel. This concept was proposed first by the Australian shock tunnel pioneer Prof. R.J. Stalker in the early sixties. The HEG is one of the largest facilities of this type worldwide. It was built over the period 1989 - 1991 and was commissioned for use in 1991. Since then it has been extensively used in a large number of national and international projects.

The free piston-driven shock tunnel HEG consists of an air buffer also called secondary reservoir, a compression tube, separated from an adjoining shock tube via the primary diaphragm and a subsequent nozzle and test section.

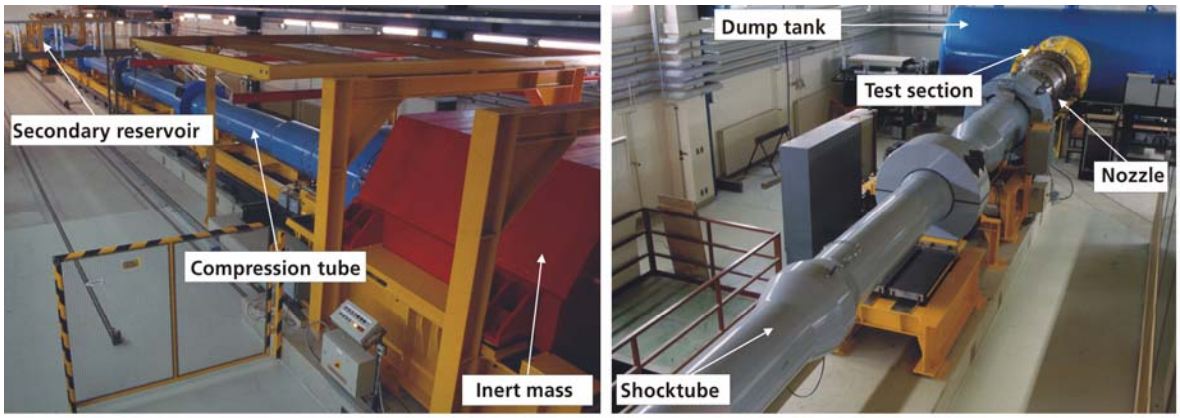

Photographic views of the High Enthalpy Shock Tunnel Göttingen (HEG).

The overall length of the facility is 60 m and it weighs 280 t. Due to the resulting forces of the piston motion the whole facility moves on a rail and bearing system. Approximately a third of its weight is contributed by an inert mass (see figure on the left side) which is used to reduce the recoil (tunnel motion).

Hypersonic blow down wind tunnel H2K

In the hypersonic blow-down wind tunnel H2K of DLR in Cologne, different contoured Laval nozzles can be used with Mach numbers in the range from $M\infty = 4.8$ to $M\infty = 11.2$, with unit Reynolds numbers (i.e. Reynolds number based on a reference length of 1m) in a range from $Re = 2.5 \cdot 10^6$ and $Re = 20 \cdot 10^6$. The nozzle diameter is 600 mm for hypersonic Mach numbers ($M\infty > 5$), for $M\infty = 4.8$ it is 360 mm. Depending on the flow conditions run times up to 40s are achievable. The figure shows the main components of the H2K facility. First, dried air with a maximum pressure of 45 bar is supplied to the electric heaters. There, the air is heated with an electrical power of 5 MW in order to study high temperature effects and to avoid condensation during the expansion of the flow in the Laval nozzle. The wind tunnel model is mounted in the free stream of the nozzle flow inside the test section. The static pressure inside the test section is decreased to a few mbar to allow for the build-up of the hypersonic flow. Behind the test section the flow passes a diffuser, is cooled down and finally caught in a sphere with low pressure level (“vacuum sphere”).

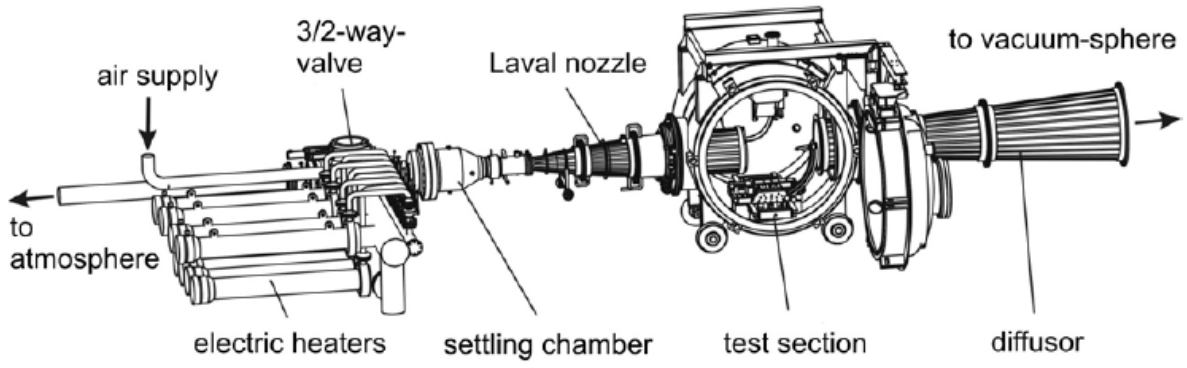

Sketch of the hypersonic blow-down wind tunnel H2K.

ITLR double-diaphragm shock tube

The double-diaphragm shock tube (DDST) at ITLR has a square test section (50mmx 50mm), although the driver and the driven section have a cylindrical cross section (72mm). A semi-direct connection between the cylindrical and the square part is realised by introducing a skimmer at the beginning of the test section which punches out a quadratic portion from the incident shock wave. The skimmer also disposes some part of the boundary layer which is subsequently fed into the dump tank. The driver has a length of 3000mm followed by the buffer which is 59mm long. The cylindrical part of the driven section is 8359mm long, the squared cross-section portion consisting of skimmer and test section is 1000mm long leading to an overall facility length of about 12.5m. A schematic sketch of the shock tube is given below.

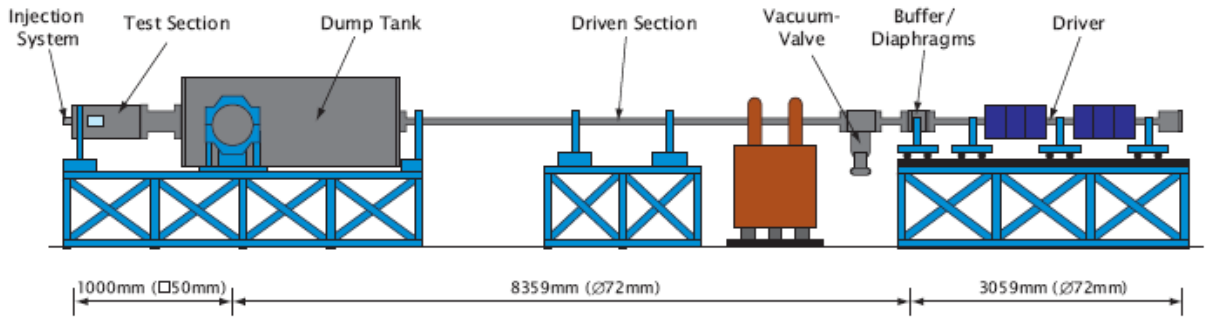

Double-diaphragm shock tube (DDST) at ITLR

Micro-Combustor M3

The micro-combustor test bench delivers propellants at representative temperatures which are fed by a single coaxial injection element into the combustor. The micro-combustor is equipped with two quartz windows giving full optical access to the complete combustor volume. The combustion chamber is operated without regenerative cooling, thus the runtime is limited to maximum 5s. Maximum pressure for combustion experiments is 1 MPa.

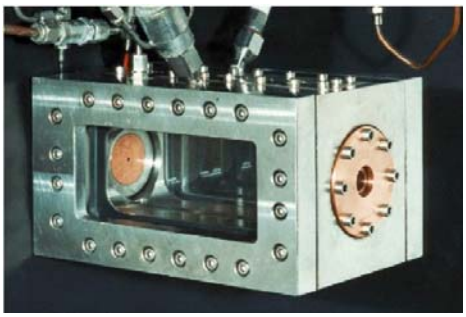

Micro combustion chamber M3

Connected tube M11-4

The scramjet combustor experiments were conducted at the DLR Lampoldshausen M11-4 test bench of the M11 test complex. The test bench was made up of an air heater at which various experimental setups can be mounted. The air heater is able to produce hot air under pressure with total temperatures of up to $T_{t,air}$=1500K by using H_2/O_2-burners. The oxygen mole fraction of the hot gas flow was kept constant at 21% by adding additional oxygen. The hot vitiated air was then expanded through a Mach 2 Laval nozzle into the actual model scramjet combustion chamber.

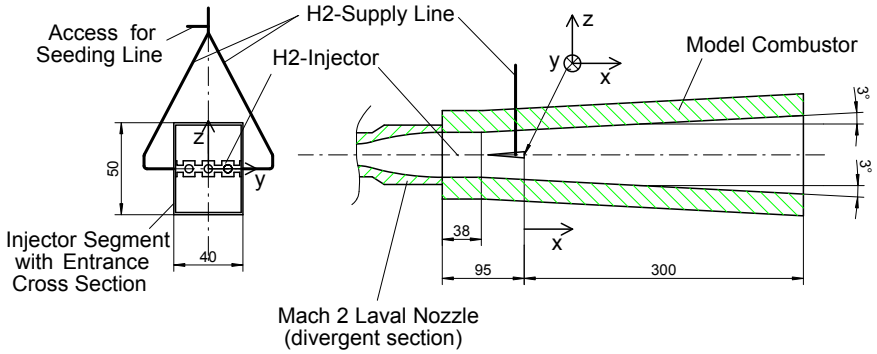

Scramjet model combustion chamber with installed injector.

Oxford University Gun Tunnel.

The Oxford University Gun Tunnel is a low enthalpy, intermittent hypersonic test facility. The facility can be operated two ways: (i) as a gun tunnel, and (ii) as a Ludwieg tube with isentropic compression heating (referred to as the LICH mode). The facility is capable of producing a hypersonic free-stream flow at Mach 6, 7, or 8, depending upon nozzle choice. With the use of additional post-nozzle expansion ducts within the test section, the facility is capable of producing even higher Mach numbers. Surface static pressure distributions, surface heat transfer distributions, drag coefficients, and lift coefficients can be measured using the facility. Flow visualization images can also be obtained using a digital Schlieren system. After the shock reflections from the barrel end plate and the piston, steady-state test times are nominally 20 ms for high Reynolds number and longer for low Reynolds number experiments. The test section is 914 mm long, and the cross section orthogonal to the flow is 610 mm square. The entire tunnel vents to a 28.3 m^3 dump tank through an isolation valve. In the present investigation, the LICH mode is employed, wherein the facility is operated as a Ludwieg tube with isentropic compression heating, as mentioned. With this arrangement, the driver and barrel are separated by a fast-acting valve rather than a breech section with bursting diaphragms. The valve is followed by a sonic orifice of 18 mm (which is considerably narrower than the 74.5 mm throat used for gun tunnel mode). Operation in LICH mode is similar to gun tunnel mode, but provides a considerably steadier flow, with less variation in stagnation conditions than when the tube is operated as a gun tunnel. Since the flow is nominally isentropic, it also heats up less. The LICH mode is employed for the present study, because relatively low values of inlet stagnation temperature are required to match the ratio of inlet stagnation temperature to wall temperature which is required to match the flow conditions of LAPCAT I hypersonic inlet flows. A schematic diagram showing the LICH mode arrangement for the Gun Tunnel is presented below.

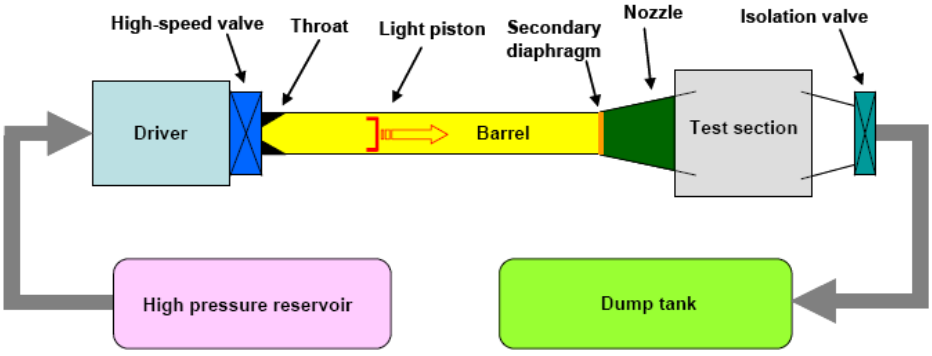

Oxford gun tunnel in LICH mode configuration

4. Conclusions and perspectives

The 3 years lasting LAPCAT activity allowed different partners investigating several high-speed passenger airplanes concepts in terms of propulsion units (TBCC vs RBCC), speed (Mach 4-5 and Mach 8) and propellants, i.e. hydrogen and hydrocarbons. The ambitious mission was to transport 250 to 300 passengers to an antipodal destiny. This condition forced the different teams to think 'out-of-the-box', opening the possibility to come-up with unconventional lay-outs in order to improve the overall vehicle performance.

The lower specific energy content of hydrocarbons compared to hydrogen indicated rather early in the program the limitation in potential range, in particular for the highest speeds. The Mach 4.5 vehicle, conceived by DLR-Sart, represents somehow an upper limit for kerosene as fuel. The vehicle has a GTOW of 720 ton and a span and length of respectively 54 m and 103m. The maximum possible range mounted nevertheless to 16,000 km. The engine is based upon a turbo based Variable Cycle Engine (VCE). The hydrogen powered Mach 5 vehicle of REL has however the potential to achieve an antipodal flight propelled with 300 passengers by means of 4 pre-cooled turbo engines, labelled as Scimitar, where the air compressor is directly driven by a closed helium cycle fed turbine. The use of hydrogen makes the aircraft also lighter (GTOW of 400 ton) but rather long (138m) due to its low fuel density. The span is limited to 41 m. A range of 20,000 km can be achieved allowing the construction of a realistic trajectory including subsonic manoeuvres and other procedures for sonic boom mitigation. Bringing the speed up to Mach 8, the vehicle needs for the upper end of the speed range a dual mode ramjet as propulsion unit. The use of an ejector rocket could not provide the necessary performance and related specific fuel consumption for the acceleration phase. It finally resulted into a diverging design. Only the use of an air turbo rocket (ATR) could provide the requested performance with an acceptable sfc. ESTEC integrated the ATR and DMR engines on top of a waverider based fuselage. This dorsal integration allowed improving the overall vehicle performance ending up with a GTOW of 600 ton despite the use of hydrogen. The length and span are respectively 90 m and 62.2 m. In particular the development of the Mach 8 vehicle concepts was rather tedious due to the larger impact the propulsion-fuselage integration had on the overall performance. Far more iteration loops were needed with an intrinsic strong coupling of propulsion and aerodynamics than for a conventional aircraft.

As most partners have a good know-how in high-speed aerodynamics, the largest focus went rather into air-breathing propulsion units and the related combustion process. This aspect is the least known and the least addressed in Europe compared with what is available in the US, Russia and Japan for similar applications.

Two important components of the Scimitar engine were designed for breadboard testing: the contra-rotating turbine and the heat exchangers for the air-cooling and the helium heater. Not only the components were tested conceptually but also the manufacturing process was put into place an a laboratory scale with the intended materials and tested under realistic pressure and temperature conditions. The demonstrated performances were close to the predicted ones.

Combustion experiments were driven by the need to acquire a profound know-how in both high pressure and high-speed conditions. As thermodynamic efficiency goes up with at higher combustion pressure and temperatures, the investigation on sub-, trans- and supercritical injection allowed quantifying the mixing processes for hydro-carbons (dodecane and hexane). Also the complicated ignition process of hydrocarbons has been quantified with various techniques such as OH-emission, Raman scattering, schlieren etc. for various equivalence ratios and pressure conditions. Methane was primarily investigated as a potential fuel for high-speed applications due to its cooling capacity when stored cryogenically and its reduced soot emission. So far the fuel was mainly investigated as an alternative fuel to kerosene for the RBCC and ramjet engines and to a lesser extent to assess its impact on the overall vehicle. Apart from improved cooling characteristics it has also a positive impact on the combustor life-time.

The definition and design of a dual mode ramjet requires novel insight and approaches which are generally not straightforward and are generally not publicly available. Therefore dedicated experiments in ground facilities allowed reproducing an in-flight experiment at several operational conditions for supersonic hydrogen combustion. This created a vast database for validation purposes of different turbulence combustion models. The unique test set-up with optical access allowed a better understanding of the transient as well as the anchoring and unstart process of the supersonic combustion. Connected tube tests investigated the lowest operational conditions for which mixing and ignition chemistry are dominating the combustion process. The measurement techniques allowed identifying the unsteady ignition pockets by means of OH-chemiluminescence, OH-LIF and Mie-scattering.

Depending on these operational conditions, different levels of complexity for turbulence combustion models are needed. The use of reduced chemistry models without the inclusion of turbulence-combustion models compared generally well for mixing controlled combustion. When ignition delays the heat release, more

elaborated chemistry reactions sets are needed including turbulence combustion coupling by means of e.g. transport PDF-models with or without multi-species approaches. Though LES has the potential to better reproduce the required mixing process up to the lower scales, the required mesh definition and chemical reaction set required for ignition delayed processes are presently out of scope for regular use.

The efficiency of the propulsion unit is also driven by the intake and nozzle performance. Their designs were derived by the first iteration of the Mach 8 vehicle concept but were kept generic enough for general application. Also the interaction with the external aerodynamics is evaluated experimentally and numerically. The high compression intake demonstrated its potential to operate without or with a minimal bleed which is essential for the overall vehicle performance. Also for the first time, LES demonstrated its potential to simulate highly compressible transitional processes on realistic long intakes representative for high-speed air-breathing vehicles. The single expansion ramp nozzle could be numerically simulated and reproduced the experimental campaigns. The interaction was observed but due its complex nature, the CFD simulations, based on RANS and DES allowed to better visualize and quantify the nature of the interaction.

Perspectives

The LAPCAT project allowed addressing some of the critical points crucially needed to enable high-speed transportation. Compared to classical aircraft designs, the difficulty for high-speed designs boils down in missing established rules and know-how to start off an iteration process for the different vehicle systems such as propulsion, structure, cooling, etc. Moreover, the high-speed aircraft require also a thorough integration of the propulsion unit with the airframe which is nearly non-existent for classical aircraft. For the latter, the aerodynamic and engine layouts have little interference and they can be optimized nearly independently from each other. Though the importance of this interaction was anticipated by the team and reflected in the project layout, it demonstrated to be the main design driver. Hence, the clear definition of the interfaces and the interactions of aerodynamics and propulsion need to be well addressed and assessed from the start. It also implicates that simplified but still representative models and tools need to be at hand for estimating the performance of the airframe and propulsion (intake, combustor and nozzle) during the first system design process. Each of these modelling blocks needs to be well verified upfront by experimental and numerical means. LAPCAT has formed the basis for this methodology with the main emphasis on propulsion and combustion. Though each of these models have their strengths, they have also limitations and restrictions due to inherent assumptions. Hence it is also of importance to verify the overall vehicle performance including an operational propulsion unit on a more detailed scale. These Nose-to-Tail (NtT) verifications should be performed both numerically and experimentally. Experimental set-ups of this kind are not evident and are hardly done. Having an engine at work during windtunnel tests poses a lot of safety constraints and operational difficulties for the windtunnel, not mentioning the complexity of the measurement techniques in hot environments and performance analysis such as net thrust and lift. Numerical NtT verifications require 3D CFD techniques for the external aerodynamics with different levels of complexity for the propulsion part going from 0D to 3D. In particular the latter approach is challenging in computer resources and robustness of the codes. These very same tools will then also allow to extrapolate to flight as there are no existing large high-speed ground facilities in Europe. These same NtT tools could then be used as the driver for a MDO-process to adapt the geometry or other parameters to improve the overall vehicle performance. A MDO approach has not yet been applied and adapted for high-speed cruise vehicles.

As part of the system toolbox described above, prediction and simulation of the different combustion processes and hence the thrust prediction are the key drivers for vehicle performance estimation. From this perspective, the combustion limitations need to be explored as they are decisive for the engine design point. However, little information is available for these conditions. Most research focuses too much on easy-to-ignite conditions which is too far off the desirable conditions. This requires further exploration of the combustion domain both for dual mode ramjets, i.e. lower than 1 bar and To=1000K, and for high pressure combustion, i.e. operation in fuel-rich conditions for turbine based engines. This entails both experimental and modelling investigations. In particular the latter will depend on good mastering of chemistry reactions sets able to predict accurately ignition delays as well as the mixing and turbulence combustion modelling in compressible flows.

More importantly, the technology and hardware development needs to be addressed ensuring the technology readiness level of all components is jacked up. This requires developing and testing hardware components at realistic conditions specifically for high speeds: intake, combustors, nozzle, compressor, turbines, materials, etc. not only for cruise conditions but also for acceleration. As a RBCC is not ideal as acceleration engine, there is a specific need to develop high thrust to weight turbo-based engines. Classical turbojets might not be optimal and other cycles need to be looked at such as Air Turbo Rocket engines.

Also early on in the process, the general lay-out of the vehicle needs to be tested by means of flight experiments to ensure and prove at least the integration issues of aerodynamic and propulsion and possibly manoeuvrability and long-duration flight to achieve thermal equilibrium. Only then the community will be ensured about its feasibility.

As new fuels, new flight altitudes and new speeds are considered, their impact on the environment needs to be explored as know-how is scarce for these applications. The use of hydrogen results in larger water vapour contents and Nox generation released at altitudes above 20 km. Similarly, the sonic boom impact needs to be assessed in terms of atmospheric propagation, sound level, carpet width and possible mitigation measures. Hydrogen as fuel has indicated its prominent role to achieve long-haul flight. Its cryogenic storage and large heat capacity are certainly sufficient to reject the integrated heat load. From this perspective, kerosene would already be disregarded as fuel. Only liquid methane could provide as hydrocarbon fule this capability. Due to its natural abundance, methane would be worthwhile to explore its potential on vehicle system level.

The LAPCAT project was a very unique opportunity to group for the first time such a wide supersonic/hypersonic community at European level and work on a common EC project related to civil air transportation. Where each of the partner had a particular background and expertise needed for this program, everybody has also clearly realized that their research is only a part of a complete system and therefore their output depends a lot on the conditions dictated by the vehicle system. The outcome of LAPCAT will certainly form a guideline for the individual groups in identifying the conditions and topics of future research programs. It certainly has driven the project layouts of ATLLAS end LAPCAT II on European level.

5. Deliverables

D2.0.1	Reference vehicle and trajectory definition for TBCC	REL
D2.1.1	TBCC thermodynamic cycle & propulsion system analysis	REL
D2.1.2	TBCC propulsion & configuration relevance to Mach 5 transport	REL
D2.1.3	Assessment of critical technologies for TBCC	REL
D2.1.4	Cost analysis report	REL
D2.1.5	Atmospheric Effects of LAPCAT vehicles	REL
D2.2.1	Preliminary Definition of Flight Vehicles for M_{cruise}=4 and M_{cruise}=8	DLR
D2.2.2	Update of Flight Vehicle Designs	DLR
D2.2.3	TBCC propulsion system analysis and thermodynamic cycle calculation	DLR
D2.2.4	TBCC propulsion system architecture and mass assessment	DLR
D2.2.5	Detailed Air Intake Analysis and Optimisation	CENAERO
D2.2.6	Assessment of critical technologies for TBCC	DLR
D2.3.1	Conceptual Design of a Dorsal-Type Mach 8 Vehicle: LAPCAT-MR1	ESTEC
D3.1.1	Heat exchanger design report	REL
D3.1.2	Heat exchanger manufacturing process definition	REL
D3.1.3	Heat exchanger test report	REL
D3.2.1	Helium turbine & compressor general lay-out	REL
D3.2.2	Layout of prototype He-turbine: aerodesign, performance and stress analysis	VKI
D3.2.3	Air model aerodynamic design & optimisation	CENAERO
D3.2.4	RIG scheme/detailed drawings + instrumentation diagrams	REL
D3.2.5	RIG + turbine blades: hardware	REL
D3.2.6	RIG/Turbine design performance measurement: test plan, measurement & analysis	REL
D4.0.1	Reference vehicle and trajectory assumed for RBCC	EADS
D4.1.1	RBCC propulsion system sizing models description	SNECMA
D4.1.2	RBCC propulsion system architecture trade-off	SNECMA
D4.1.3	RBCC propulsion system preliminary definition	SNECMA
D4.2.1	Propulsion System Architecture and RBCC Modelling Approach	EADS
D4.2.2	Propulsion Mass Assessment	DLR
D4.2.3	Vehicle Performance Assessment	EADS
D5.1.1	Detailed description of operating conditions	DLR
D5.1.2	Detailed description of test cases	DLR
D5.2.1	Description of model geometry, test plan, operating conditions	DLR
D5.2.2	Measurement plan & performance of the measurements	DLR
D5.2.3	Establishment of scaling laws	DLR
D5.2.4	Data assessment and comparison with CFD-results	DLR
D5.2.5	Scaling and optimization of injection, mixing and combustion for a generic scramjet combustion chamber	ESTEC
D5.3.1	Characterisation of a Double-Diaphragm Shock Tube and Hydrocarbon Spray Disintegration Experiments	ITLR
D5.3.2	Assessment of droplet evaporation models	ITLR
D5.3.3	Data for subcritical range	ITLR
D5.3.4	Data from near- & supercritical range	ITLR
D5.3.5	Final report	ITLR
D5.4.1	Definition, fabrication and operation of an injector head	DLR
D5.4.2	LOX/Methane combustion model	DLR
D5.4.3	Modified and adapted tools for CARS spectra evaluation	DLR
D5.4.4	Results on LOX/HC ignition and combustion	DLR
D6.1.1	Definition of Rocket Thrust Chamber and Fuel Characterization	EADS
D6.1.2	High-Pressure LOX/HC Combustion Modelling	EADS
D6.2.1	Development plan for 3D CFD combustion tool	CIRA
D6.2.2	Combustion model development	CIRA
D6.2.3	CFD-solver with validation test-cases	CIRA
D6.2.4	Final report	CIRA
D6.3.1	Definition of Ramjet Engine and Combustion Modelling	EADS
D6.3.2	Combined Rocket-Ramjet Combustion Modelling	EADS
D6.4.1	Development plan for supersonic/hypersonic reactive 3D-CFD tools	CIRA
D6.4.2	Combustion model development	CIRA

D6.4.3	C3NS-DB Solver for Supersonic Combustion: Validation and Preliminary Results	CIRA
D6.4.4	C3NS Solver for Supersonic Combustion Simulations: Final Report	CIRA
D6.4.5	CFD investigations of the Hyshot Generic Supersonic Combustion Experiment	ESTEC
D6.5.1	Extension of TAU-code with finite rate supersonic combustion modelling	DLR
D6.5.2	Survey and implementation of turbulent supersonic combustion models	DLR
D6.5.3	CFD Modelling of Scramjet Combustors using the DLR TAU Code - Code Validation: HyShot II Configuration in HEG -	DLR
D6.6.1	Comparison of Hydrogen Reaction Mechanisms for Sub- and Supersonic Flow	DLR
D6.6.2	Mixing enhancement and flame stabilization in practical scramjet combustors	DLR
D6.6.3	Numerical Investigations of the HyShot Supersonic Combustion Configuration	DLR
D6.6.4	Study of a multi-variate-β-PDF for species distributions and model improvement	DLR
D6.7.1	A Novel SGS Model for LES of Supersonic Combustion	DMA
D6.7.2	Numerical prediction of supersonic combustor and comparison with experimental measurements	DMA
D6.7.3	Cooling and combustion characteristics of selected LHC fuels using endothermic cracking/reforming	DMA
D7.1.1	Description of intake design methodology	DLR
D7.1.2	Experimental optimisation of intake and sensitivity analysis of perturbations on intake performance in H2K	DLR
D7.1.3	Numerical verification of intake design and sensitivity study	DLR
D7.1.4	Redesign of the LAPCAT-M8 Vehicle Intake	ESTEC
D7.2.1	Description of generic windtunnel model and measurement campaign	DLR
D7.2.2	Description of experimental parametric study	DLR
D7.2.3	Numerical verification of Nozzle-Base-External flow interaction	DLR
D7.3.1	Description of nozzle contour	DLR
D7.3.2	Implementation of advanced turbulence models	DLR
D7.3.3	Numerical investigation of nozzle flow	DLR
D7.4.1	Evaluation of LES for compressible turbulent & transitional flows	SOTON
D7.4.2	LES of shock-wave/boundary-layer interactions in intake flow model problems	SOTON
D7.4.3	Large Eddy Simulation of a Model Scramjet Intake	SOTON
D7.5.1	Transition strip study	UOXF

Note: Deliverables listed above are not intrinsically open for partners outside of the consortium

6. Dissemination of knowledge[1]

Overview table

Nr	Partner	Title	Authors	Conference, Journal, Public Internal reports, web-site…	Date	Location	Status
1	DLR	Comparative Study on Options for High-Speed Intercontinental Passenger Transports: Air-Breathing- vs. Rocket-Propelled	Martin Sippel, Josef Klevanski, J. Steelant	IAF 2005, paper # IAC-05-D2.4.09	17-22/10/2005	Fukuoka, Japan	Actual
2	ESA	www.esa.int/techresources/lapcat	-	web-site	23/11/2005	ESA	Actual
3	ESA	LAPCAT: Vehicle and Propulsion Aspects for Sustained Supersonic Flight	J. Steelant	Aeronautics Days 2006	19-21/06/2006	Vienna (A)	Actual
4	ESA	Comparison of Supersonic Combustion Tests with Shock Tunnels, Flight and CFD	J. Steelant, A. Mack, K. Hannemann, A. Gardner	42nd AIAA/ASME/SAE/ASEE Joint Propulsion Conference & Exhibit	9-12/07/2006	Sacramento, California	Actual
5	ESA	LAPCAT: an EC Funded Project on Sustained Hypersonic Flight	J. Steelant	IAF 2006	2-6/10/2006	Valencia (E)	Actual
6	ESA	Mixing and Combustion Enhancement in a Generic Scramjet Combustion Chamber	A. Mack, J. Steelant, K. Hannemann, S. Karl, J. Odam	14th AIAA/AHI Space Planes and Hypersonic Systems and Technologies Conference	6-9/11/2006	Canberra (Aus)	Actual

[1] ***Knowledge:*** means the results, including information, whether or not they can be protected, arising from the *project* governed by this *contract*, as well as copyrights or rights pertaining to such results following applications for, or the issue of patents, designs, plant varieties, supplementary protection certificates or similar forms of protection (Article II.1.14 of the contract)

Nr	Partner	Title	Authors	Conference, Journal, Public Internal reports, web-site…	Date	Location	Status
7	DLR	Preliminary Definition of the Supersonic and Hypersonic Airliner Configurations in LAPCAT	Martin Sippel, Josef Klevanski,	14th AIAA/AHI Space Planes and Hypersonic Systems and Technologies Conference	6-9/11/2006	Canberra (Aus)	Actual
8	DLR	Research on TBCC Propulsion for a Mach 4.5 Supersonic Cruise Airliner	Martin Sippel	14th AIAA/AHI Space Planes and Hypersonic Systems and Technologies Conference	6-9/11/2006	Canberra (Aus)	Actual
9	DMA	LES Modelling of Scramjet Combustion	A Ingenito, M.G. De Flora, E. Giacomazzi, C. Bruno, J. Steelant	44th AIAA Aerospace Sciences Meeting and Exhibit	09-12/01/2006	Reno, Nevada	Actual
10	DMA	A Novel Model of Turbulent Supersonic Combustion: Development and Validation	A Ingenito, M.G. De Flora, E. Giacomazzi, C. Bruno, J. Steelant	42nd AIAA/ASME/SAE/ASEE Joint Propulsion Conference & Exhibit	9-12/07/2006	Sacramento, California	Actual
11	DMA	Turbulent Supersonic Combustion: Modelling and Simulations	A Ingenito, M.G. De Flora, E. Giacomazzi, C. Bruno, J. Steelant	14th AIAA/AHI Space Planes and Hypersonic Systems and Technologies Conference	6-9/11/2006	Canberra (Aus)	Actual
12	DMA	Advance in supersonic combustion modelling	A Ingenito, C. Bruno, J. Steelant	EUCASS 2007	1-6/07/2007	Brussels, Belgium	Actual
13	DMA	Supersonic mixing and combustion	A Ingenito, C. Bruno	EUCASS Book Series, ADVANCES IN AEROSPACE SCIENCES, paper 5_08_02	Jul-07	Brussels, Belgium	Actual
14	DMA	Mixing and flame anchoring in a supersonic combustor	A Ingenito, C. Bruno	43rd AIAA/ASME/SAE/ASEE Joint Propulsion Conference	8-11/09/2007	Cincinnati OH	Actual
15	DMA	Effect of the Turbulent Schmit Number on Supersonic Regime	A Ingenito, C. Bruno	ISABE 2007	2-7/09/2007	Beijing (China)	Actual
16	DMA	Effect of the Turbulent Schmidt Number on Supersonic Regime	A Ingenito, C. Bruno	46th AIAA Aerospace Sciences Meeting and Exhibit	7-11 January 2008	Reno, NV	Actual

Nr	Partner	Title	Authors	Conference, Journal, Public Internal reports, web-site…	Date	Location	Status
17	VKI-REL-CENAERO	Counter-rotating turbine design for aeronautical applications	Paniagua G., Szokol S., Kato H., Manzini G., Varvill R.	ISABE 2007	2-7/09/2007	Beijing (China)	Actual
18	DLR	CFD Analysis of the HyShot Supersonic Combustion Flight Experiment Configuration	S. Karl, K. Hannemann, J. Steelant, A. Mack	14th AIAA/AHI Space Planes and Hypersonic Systems and Technologies Conference	6-9/11/2006	Canberra (Aus)	Actual
19	ITLR	Analysis of hydrocarbon jet disintegration experiments under subcritical conditions	I. Stotz, G. Lamanna, B. Weigand	ISSW06	15-20/07/2007	Göttingen (Germany)	Actual
20	DLR-CENAERO	Preliminary Definition and CFD Analysis of a TBCC Propulsion System for a Mach 4.5 Supersonic Cruise Airliner	M. Sippel, K. Okai, H. Kato, A. Kumar	ISABE 2007	2-7/09/2008	Beijing (China)	Actual
21	ESA	LAPCAT: a Technical Feasibility Study on Sustained Hypersonic Flight	J. Steelant	ISABE 2007	2-7/09/2008	Beijing (China)	Actual
22	SOTON	LES of Shock-wave/Boundary Layer Interactions in Hypersonic Inlet Compression Ramps	L. Krishnan, N. Sandham, J.Steelant	ISABE 2007	2-7/09/2008	Beijing (China)	Actual
23	CIRA	Injection, Mixing and Combustion Modelling in High-Pressure Lox/Methane Rocket Thrust Chambers	Cutrone L., Bonifacio S., Ranuzzi G., Battista F. and Steelant J.	15th AIAA International Space Planes and Hypersonic Systems and Technologies Conference	May-08	Dayton (USA)	Planned
24	ESA	Sensitivity Analysis for the HyShot Generic Supersonic Combustion Configuration using CFD	A. Mack, J. Steelant, J. Martinez-Schramm, K. Hannemann	ISABE 2007	2-7/09/2007	Beijing (China)	Actual
25	ITLR	Design of a double diaphragm shock tube for accurate fluid disintegration studies	I. Stotz, G. Lamanna, B. Weigand, J. Steelant	Rev. Sci. Instruments or Shock Waves	Apr-08		Planned/Submitted

Nr	Partner	Title	Authors	Conference, Journal, Public Internal reports, web-site…	Date	Location	Status
26	ITLR	Droplet vaporization at high pressure: A review and model evaluation	G. Lamanna, I. Stotz, A. Vögler, B. Weigand, J. Steelant	PECS	Sep-08		Planned
27	SOTON	Laminar-to-turbulent transition in a shock-induced separation bubble	L. Krishnan, N. Sandham, J.Steelant	Turbulence and Shear Flow Phenomena 2007	27-29/8/07	Munich	Actual
28	CIRA	SPREAD: a Scramjet PREliminary Aerothermodynamic Design Code	S.Bonifacio, S.Borreca, G.Ranuzzi, V.Salvatore	14th AIAA/AHI Space Planes and Hypersonic Systems and Technologies Conference	6-9/11/2006	Canberra (Aus)	Actual
29	CIRA	Supersonic Combustion Models Development for Advanced Propulsion Concepts	Battista F.,Cutrone L., Ranuzzi G., Borreca S..	15th AIAA International Space Planes and Hypersonic Systems and Technologies Conference	May-08	Dayton (USA)	Actual
30	CIRA	Simulation of Supercritical High Pressure Combustion for Advanced Propulsion Concepts	Battista F.,Cutrone L., Ranuzzi G., Borreca S..	15th AIAA International Space Planes and Hypersonic Systems and Technologies Conference	May-08	Dayton (USA)	Actual
31	DLR	Component Analysis of TBCC Propulsion for a Mach 4.5 Supersonic Cruise Airliner	K. Okai, M. Sippel	EUCASS 2007	1-6/07/2007	Brussels, Belgium	Actual
32	DLR	Selected Supersonic Combustion Activities at DLR within the European LAPCAT Project	O.J. Haidn, H. Ciezki, K. Hannemann, S. Karl	EUCASS 2007	1-6/07/2007	Brussels, Belgium	Actual
33	ESA	An European Project on Advanced Propulsion Concepts for Sustained Hypersonic Flight	J. Steelant	EUCASS 2007	1-6/07/2007	Brussels, Belgium	Actual
34	ESA	Impact of Intake Boundary Layer Turbulence on the Combustion Behaviour in a Scramjet	A. Mack, J. Steelant, V. Togiti and J. Longo	EUCASS 2007	1-6/07/2007	Brussels, Belgium	Actual
35	REL - VKI	The scimitar precooled Mach 5 engine	Jivraj F., Varvill R., Bond, A., Paniagua, G.	EUCASS 2007	1-6/07/2007	Brussels, Belgium	Actual

Nr	Partner	Title	Authors	Conference, Journal, Public Internal reports, web-site…	Date	Location	Status
36	VKI-ULB	Development of an analysis tool for combined propulsion cycles	Herbiet J.F., Paniagua G., Hendrick P.	EUCASS 2007	1-6/07/2007	Brussels, Belgium	Actual
37	REL-VKI-CENAERO	Design and Testing of the Contra-rotating Turbine for the SCIMITAR Precooled Engine	Varvill R., Paniagua G., Kato H., Thatcher M.	59th International Astronautical Congress	Sep-08	Glasgow, UK	Planned
38	DLR	Multi-Variate Assumed PDF Modeling of Turbulent Sub- and Supersonic Combustion	P. Gerlinger, F. Schneider, M. Aigner	ISABE 2007	2-7/09/2007	Beijing (China)	Actual
39	DLR	Numerical Investigation of Mixing Enhancement by Lobed Strut Injectors in Turbulent Reactive Supersonic Flow	M. Kindler, P. Gerlinger, M. Aigner	ISABE 2007	2-7/09/2007	Beijing (China)	Actual
40	CIRA	A CFD Method for Simulation of Mixing and Combustion in High Pressure Lox/Methane Rocket Engines	Cutrone L., Battista F., Ranuzzi G., Bonifacio S., Steelant J..	46th AIAA Aerospace Sciences Meeting and Exhibit	Jan-08	Reno (USA)	Actual
41	CIRA	A CFD Method for Simulation of Mixing and Combustion in High Pressure Lox/Methane Rocket Engines	Cutrone L., Battista F., Ranuzzi G., Bonifacio S., Steelant J..	AIAA Journal of Spacecraft and Rockets	May-08	Published	Planned
42	ITLR	Shock tube study on hydrocarbon free jets at elevated pressures and temperatures	I. Stotz, G. Lamanna, B. Weigand, J. Steelant	15th AIAA International Space Planes and Hypersonic Systems and Technologies Conference	May-08	Dayton (USA)	Actual
43	ITLR	High-speed visualization of liquid jet disintegration	G. Lamanna, I. Stotz, B. Weigand, J. Steelant	ILASS 2008	Sep-08	Como Lake (I)	Actual

Nr	Partner	Title	Authors	Conference, Journal, Public Internal reports, web-site…	Date	Location	Status
44	ITLR	Experimental characterization of hydrocarbon jet disintegration at critical conditions	I. Stotz, G. Lamanna, B. Weigand, J. Steelant	Atomization & Sprays	Jun-08	Published	Actual
45	DLR	A CFD study on Interaction of the Single Expansion Ramp Nozzle flow and the External Flow	V. Togiti, P. Gruhn, J. Longo	59th International Astronautical Congress	29/09-03/10/2008	Glasgow, UK	Actual
46	REL	REL website LAPCAT section. 103,000 website hits 3 February to 4 March 2008. Europe 30,000. Japan 28,000. USA 22,000. Others 23,000.	-	web-site	23/11/2005	REL	Actual
47	REL	Worldwide publicity from 5 February: 8 live radio interviews, 8 TV interviews, 5 known other TV items, 25 known magazine articles, unknown (but large) number of newspaper and web articles.	-	General Media	02/2008	REL	Actual
48	DLR	Reduced Chemical Model for High Presssure Methane Combustion with PAH Formation	N.A. Slavinskaya, O.J. Haidn	46th AIAA Aerospace Sciences Meeting Reno 2008	7-10/01/2008	Reno, USA	Actual
49	DLR	Reduced Chemical Mechanisml for Methane Combustion	N.A. Slavinskaya, O.J. Haidn	EUCASS 2007	1-6/07/2007	Brussels, Belgium	Actual
50	DLR	Ignition of a gaseous Methane/Oxygen Coaxial Jet	C. Pauly, J. Sender, M. Oschwald	EUCASS 2007	1-6/07/2007	Brussels, Belgium	Actual
51	ITLR	Experimental study of hydrocarbon jet disintegration at subcritical and supercritical conditions	G. Lamanna, I. Stotz, B. Weigand, J. Steelant	Sixth European Symposium on Aerothermodynamics for Space Vehicles	Nov-08	Versailles (F)	Actual
52	DLR	CFD Analysis of the HyShot II Scramjet Experiments in the HEG Shock Tunnel	S. Karl , K. Hannemann, A. Mack, J. Steelant	15th AIAA International Space Planes and Hypersonic Systems and	May-08	Dayton (USA)	Actual

Nr	Partner	Title	Authors	Conference, Journal, Public Internal reports, web-site…	Date	Location	Status
				Technologies Conference			
53	DLR	Ground Testing of the HyShot II Scramjet Configuration in HEG	J. Martinez Schramm, S. Karl, K. Hannemann, J. Steelant	15th AIAA International Space Planes and Hypersonic Systems and Technologies Conference	May-08	Dayton (USA)	Actual
54	ESTEC	Achievements Obtained for Sustained Hypersonic Flight within the LAPCAT project	J. Steelant	15th AIAA International Space Planes and Hypersonic Systems and Technologies Conference	May-08	Dayton (USA)	Actual
55	ESTEC	Aerodynamic and Thermal Loads at High-Speed Flows	J. Steelant	ECCOMAS CFD 2008	July 2008	Venice (I)	Actual
56	ESTEC	Impact of Intake Boundary Layer Turbulence on the Combustion Behaviour in a Scramjet	A. Mack and J. Steelant	Progress in Propulsion Physics, EUCASS advances in Aerospace Sciences Book Series; pp. 531-549, ISBN 978-2-7598-0411-5	2009		Published
57	DLR	Influence of Reaction Mechanisms, Grid Spacing and Inflow Conditions on the Numerical Simulation of Lifted Supersonic Flames	P. Gerlinger, K. Nold and M. Aigner	Int. J. for Numerical Methods in Fluids	April 2010		Published

Section 3 - Publishable results

The consortium is not yet ready to publicise and has not taken the appropriate measures to protect their IPR.